THE PHARMACOLOGY, PHARMACOKINETICS AND METABOLISM OF A NOVEL NONSTEROIDAL SELECTIVE ANDROGEN RECEPTOR MODULATOR.

DISSERTATION

Presented in Partial Fulfillment of the Requirements for the Degree Doctor of Philosophy in the Graduate School of The Ohio State University

By

Minoli A. Perera, Pharm.D.

* * * * * *

The Ohio State University

2003

Dissertation Committee:

Professor Kenneth Chan, Adviser

Professor William Hayton

Professor Robert Lee

Professor Duxin Sun

Professor Fredika Robertson

Approved by

_____

Adviser

College of Pharmacy

ABSTRACT

Testosterone is an important endogenous male hormone and used exogenously to treat a wide variety of disorders. However, there are many disadvantages to testosterone therapy, namely nonselective action, low oral bioavailability, and an unfavorable side effects profile. This has led to the investigation for compounds that bypass these obstacles. These compounds are known as selective androgen receptor modulators (SARMs).

During *in vitro* studies in our laboratory, we discovered modifications to the structures of the known nonsteroidal antiandrogens, bicalutamide, produced androgen agonist activity. We used these preliminary finding to synthesize a series of bicalutamide analogs to determine if they possessed *in vitro* agonist activity. These studies identified the chemical modifications that increase binding to the androgen receptor (AR) and AR-mediated transcriptional activation. In addition, *in vivo* pharmacologic studies were conducted on compounds showing the most promising *in vitro* results. From this study we discovered the first nonsteroidal anabolic SARM. These findings established the structure-activity relationships (SARs), which lead to the development the lead compound, S-4.

Pharmacokinetic studies of oral and intravenous doses were conducted in beagle dogs to determine the oral bioavailability and pharmacokinetic parameters associated with S-4. These studies showed that S-4 had a shorter half-life than bicalutamide (4 hours versus to 7 days), with a moderate to large volume of distribution (1.4 L/kg). In addition, S-4 showed dose dependent oral bioavailability, with the highest bioavailability of 91% seen following 0.1 mg/kg dose.

Earlier investigations of compounds in this series showed that the AR agonist, R-1 was metabolically converted to an AR antagonist through oxidation of the sulfur atom. In order to preserve the agonistic effects of these compounds, an oxygen atom was substituted for the sulfur atom on the B ring of the molecule. The metabolism and disposition of S-4 was studied to determine what metabolites were produced. A number of phase I and phase II metabolites were also identified in the urine and feces of dogs and rats on the basis of mass spectrometry. A mass balance and disposition study was conducted using [C^{14}] S-4. The metabolites were quantified urine and feces. Total recovery of radioactivity was 97% and 83% after the 24 and 48-hours studies respectively. These studies showed that S-4 was extensively metabolized and excreted in both the urine and feces. The major metabolite of S-4 was the hydrolysis product found in the urine, which accounted for 25% of injected doses. In addition a large portion of the dose, approximately 32% was seen as parent compound in the feces. This may be due to biliary excretion of the glucuronide conjugates of S-4 or the parent drug itself.

Dedicated to my parents and family, friends, and Eric

ACKNOWLEDGMENTS

I wish to thank my adviser, Dr. Kenneth Chan, for all his encouragement, and intellectual support. He allowed the scientific and scholarly freedom that pushed this project to its fruition.

I also wish to thank Drs. Duane Miller and James Dalton, for their unwavering support both intellectually and scientifically. Your enthusiasm for "small victories" and overall vision has been inspiring.

This work was supported by grants from the following organizations: The University of Tennessee, College of Pharmacy, and the National Institutes of Health (1 RO1 DK59800), American Foundation for Pharmaceutical Education (AFPE), and GTx., Inc.

VITA

January 26, 1976 .....Born - Columbo, Sri Lanka

May 1993 .....B.S. Biology, Christian Brothers University.

June 2001 .....Pharm.D., University of Tennessee

2001- present .....Research Associate, The Ohio State University

PUBLICATION

1. Perera MA, Yin D, Chung K, Chan KK, Miller DD and Dalton JT. Metabolism of a Novel Androgen Receptor Modulator. American Association of Pharmaceutical Scientists, Salt Lake City, Utah. October 2003.

2. Yin D, He Y, Perera MA, Hong SS, Marhefka C, Stourman N, Kirkovsky L, Miller DD, and Dalton JT. Key Structural Features of Nonsteroidal Ligands for Binding and Activation of the Androgen Receptor. Molecular Pharmacology 63 (2003) 211-223.

3. He Y, Yin D, Perera MA, Kirkovsky L, Stourman N, Dalton JT and Miller DD. Novel Nonsteroidal Ligands with High Affinity and Potent Functional Activity for the Human Androgen Receptor. European Journal of Medicinal Chemistry 37 (2002) 619-637.

4. Perera MA, Yin D, Chung K, Miller DD, and Dalton JT. Pharmacokinetics and Allometric Scaling of Andarine. American Association of Pharmaceutical Scientists, Toronto, Canada November 2002 .

5. Perera MA, Yin D, Chung K, Miller DD, and Dalton JT. Pharmacokinetics of Androxolutamide (GTx-007) in beagle dogs. The Endocrine Society, San Francisco, June 2002

6. Veverka K, Perera MA, Yin D, Gao W, Xu H, Kearbey JD, Chung K, Steiner MS, Miller DD, and Dalton JT. Preclinical Pharmacology and Pharmacokinetics of GTx-007, A Novel Selective Androgen Receptor Modulator. Society for Basic Urological Research, Tucson, AZ, December 2001

7. Dalton JT, Yin D, Perera MA, Gao W, Xu H, Kearbey JD, Chung K, and Miller DD. Preclinical Pharmacology and Pharmacokinetics of a Selective Androgen Receptor Modulator. International Society for Study of Xenobiotics. Drug Metabolism Reviews, 33(supplement 1): #222, 2001.

8. Reiner A, Perera MA, Paullus R, Medina L. Immunohistochemical localization of DARPP32 in striatal projection neurons and striatal interneurons in pigeons. Journal of Chemistry and Neuroanatomy 16 (1998) 17-33.

FIELD OF STUDY

Major Field: Pharmacy

TABLE OF CONTENTS

LIST OF TABLES

LIST OF FIGURES

LIST OF ABBREVIATIONS

Ac	Acetamide
ANOVA	Analysis of variance
APCI	Atmospheric pressure chemical ionization
AR	Androgen receptor
ARE	Androgen response element
AUC	Area under the curve
AUMC	Area under the moment curve
BMD	Bone mineral density
BPH	Benign prostatic hypertrophy
CL	Clearance
C_{max}	Maximum plasma concentration
Da.	Dalton
DHT	Dihydrotestosterone
ESI	Electrospray ionization
F	Oral bioavailability
FSH	Follicle stimulating hormone
g	Times gravity
HAP	Hydroxyapatite
GnRH	Gonadotropin releasing hormone

^{3}H-MIB	[17α-methyl-^{3}H] Mibolerone
HPLC	High pressure liquid chromatography
Hsp90	Heat-shock protein 90
IV	Intravenous
Ki	Equilibrium dissociation constant
LBD	Ligand binding domain
LC/MS	Liquid chromatography/ Mass Spectrometry
LH	Leutinizing hormone
$[M-H]^{-}$	Negative molecular ion
MIB	Mibolerone
MRT	Mean residence time
m/z	Mass to charge ratio
NAT	N-acetyltransferase
PEG	Polyethylene glycol
PO	Oral
RBA	Relative binding affinity
SAR	Structure-activity relationship
SARM	Selective androgen receptor modulator
SERM	Selective estrogen receptor modulators
SHBG	Sex hormone binding globulin
$T_{1/2}$	Plasma half-life
TFAc	Triflouroacetamide
T_{max}	Time of maximum plasma concentration

TP	Testosterone propionate
V_{ss}	Volume of distribution at equilibrium

CHAPTER 1

BACKGROUND INFORMATION

1.1. Testosterone

The sex hormones play a wide variety of roles in both men and women. Testosterone is the endogenous ligand for the androgen receptor (AR). It is important in the normal development of the male reproductive system as well as many non-reproductive tissues. The actions of testosterone on these tissues can be categorized as either anabolic or androgenic. Androgenic activity is defined as the pharmacologic response of reproductive tissues, such as prostate, seminal vesicles, and spermatogenesis. Anabolic activity includes the growth and maintenance of bone, muscle, and erythropoiesis[1].

Testosterone is secreted by Leydic cells in the testes with a minor fraction of testosterone precursors produced in the adrenal grand. Pulsatile release of gonadotropin releasing hormone (GnRH) from the hypothalamus causes the release of leutinizing hormone (LH) from the pituitary gland, which regulates the release of testosterone. Down regulation and desensitization of AR is seen following the continual release of LH or GnRH[2]. Therefore, the pulsatile release of testosterone is critical to normal androgen response. Testosterone also acts via the hypothalamus to block the release of GnRH,

while inhibin B, released from the seminiferous tubules after testosterone stimulation, blocks pituitary release of follicle stimulating hormone (FSH)[3]. Figure 1.1 shows the different tissues in which testosterone exerts its physiological effects. Testosterone is then metabolized in the liver by oxidation, reduction, or conjugation with glucuronide or sulfate. These metabolites are excreted in the urine. Because of its high first-pass metabolism testosterone is not administered orally.

The major active metabolite of testosterone is dihydrotestosterone (DHT), which is produced by the reduction of testosterone via the enzyme 5α-reductase. There are 2 5α-reductase isoforms that are responsible for this conversion[3]. Type 1 5α-reductase is found mainly in the liver and skin, while type 2 5α-reductase is found in the prostate. In situ hybridization studies showed that type 2 5α-reductase is distributed in the stromal cells and basal epithelium of the prostate[4]. DHT has higher binding affinity for the AR than testosterone[5], which allows lower tissue concentrations of DHT to elicit an androgenic response. DHT is the main androgen found in male reproductive tissues[6] and is therefore thought to control the androgen effects seen in tissues expressing 5α-reductase.

1.2. Androgen Receptor

The AR is a member of the nuclear receptor super family. Other receptors included in this class are steroids, retinoids, vitamin D and thyroid hormones[7]. The AR genome located in the Xq11-q12 sites on the X chromosome, is composed of 8 exons, and encodes a protein of approximately 110 kDa, spanning 90 kilobases [7-9]. Like many nuclear receptors, AR is comprised of 4 regions: NH_2-terminus, DNA binding domain,

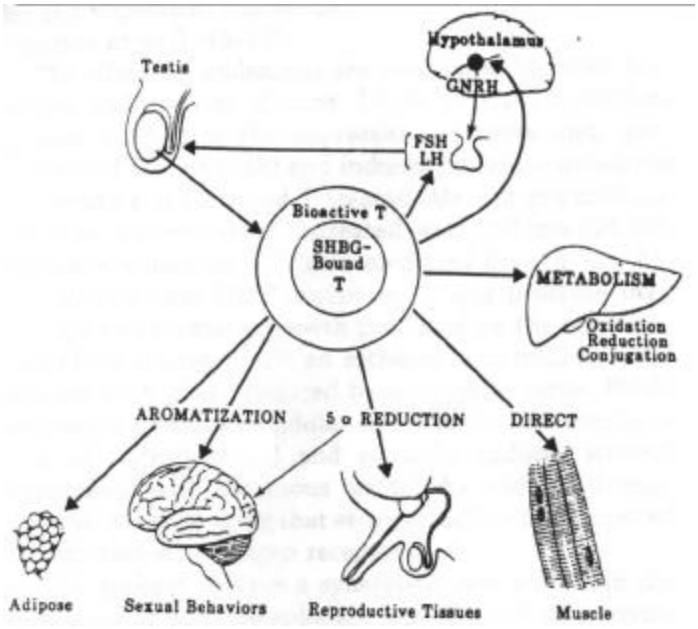

Figure 1.1. Tissues Effects of Testosterone.

Testosterone is bound to the plasma protein, sex hormone binding globulin (SHBG). Only unbound testosterone is pharmacologically active. GNRH and LH from the hypothalamus and pituitary respectively stimulate testosterone production in the testes. Testosterone can be aromatized to estrogen in neural and adipose tissue. It can be reduced by 5α reductase to 5α-dihydrotestosterone (DHT). It exerts a direct affect on the muscle and is highly metabolized in the liver. Adapted from reference 26.

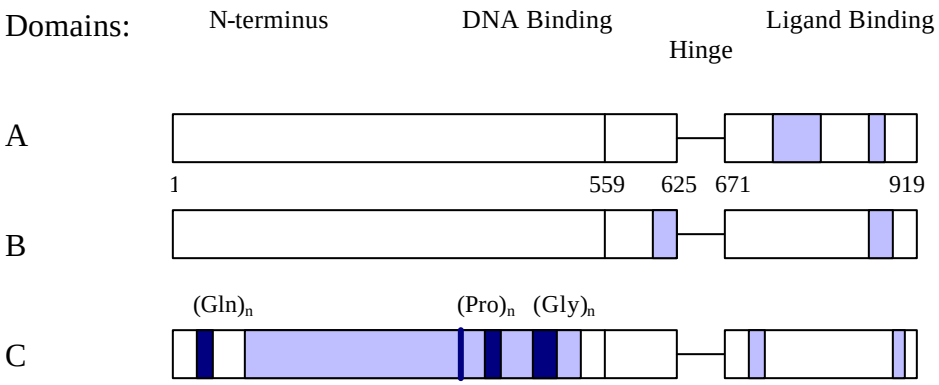

Figure 1.2. Androgen Receptor Domains

Stippled sections represent the following areas within the Androgen Receptor protein: A) Hydrophobic amino acid comprising the proposed ligand binding pocket (735 to 787 and 855 to 865). B) Regions involved in homodimerization. C) Transcriptional activation domains. Three polymeric regions are indicated as solid shaded areas. Adapted from reference 10.

hinge region, and ligand binding domain (LBD) (Figure 1.2). Within the N-terminus there are three polymeric regions. The region of polyglutamine repeats is important in transcriptional activation. Longer than average repeats (n>28) result in decreased ligand binding[10]. The LBD, in the absence of ligand, inhibits the transcriptional activation of the NH_2-terminus. Deletion of the LBD leads to a constitutively active receptor[7,8]. The AR, bound to heat-shock protein 90 (Hsp90), is located in the cytoplasm when unbound to ligand, but translocates once ligand is bound[9]. It is thought that ligand binding causes dissociation of the AR from the multi-protein complex that sequesters the AR in the cell cytoplasm and the receptor-ligand complex then homodimerizes[11]. After homodimerization the receptor-ligand complex is escorted into the nucleus by importins. This ligand-mediated movement can be seen in a variety of transfected cell lines, such as COS-1, CV-1, and HeLa[7]. Once inside the nucleus the homodimer binds to the target DNA sequence known as the androgen response element (ARE). Many coregulators (SRC-1, TIF-2) associate with the receptor-ligand complex and regulate the transcriptional activation of target DNA sequences. These interactions lead to the up or down-regulation of proteins involved in the physiological responses to testosterone (Figure 1.3).

The three-dimensional structure of the AR was determined by X-ray crystallography studies using the synthetic androgen R1881 and DHT[12,13]. Like many of the steroid receptors, the AR ligand binding site is composed of hydrophobic amino acids which interact with the steroid backbone of testosterone. This may explain the promiscuity of the AR, given that the hydrophobic interactions are not highly specific.

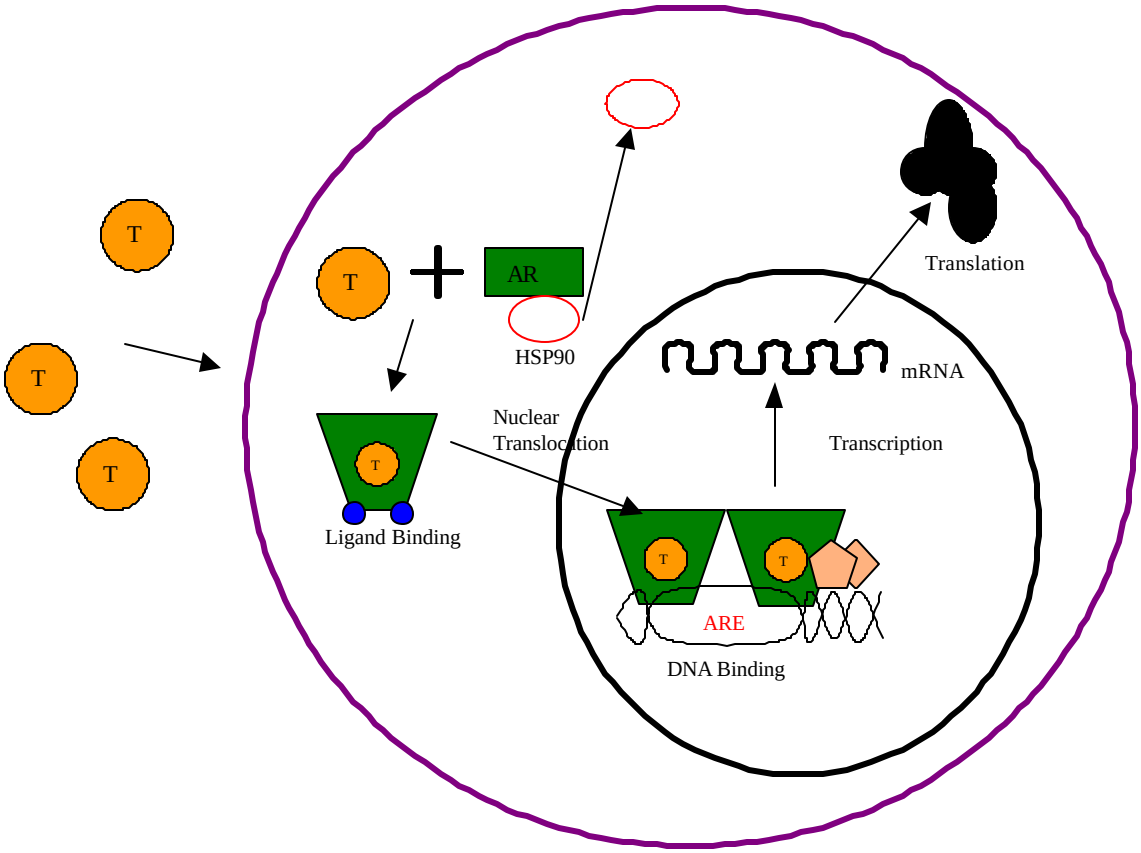

Figure 1.3. The Molecular Events Involved in Androgen Effects.

Testosterone (orange circles) enters the target cell and binds to the AR. This causes dissociation of HSP90 from the AR and phosphorylation (blue circle represent phosphate groups). The receptor-ligand complex is translocated into the nucleus where homodimerizes, interacts with transcriptional coregulators, and binds to the ARE (up-stream of the target gene sequence). The interaction of the receptor dimer with the target gene regulates transcription.

Therefore, AR can bind to other steroids, such as estrodiol-17β and progesterone[7]. Recent studies, using multimolecular dynamics simulations, showed the presence of an additional pocket within the LBD of AR, located below carbon 15 on the testosterone molecule bound within the LBD[14]. These results suggest that the X-ray crystal structure of the AR may not be accurate.

1.3. Physiological Role of Testosterone

Testosterone exerts control over many reproductive tissues. Within the testes, testosterone is responsible for spermatogenesis by the Sertoli cells. Sertoli cells have two major functions: to enable and coordinate germ cell production and to determine adult testis size and sperm number[15]. In addition to LH and FSH control of testosterone production, FSH also controls spermatogenesis, which is required for the full development of a normal number of germ cells[16]. The testes produce a majority of the testosterone found in males. Because of the negative feedback inhibition of LH and FSH caused by testosterone, exogenous androgens can decrease sperm production. The seminal vesicles are also an androgen-dependent tissue. Studies in rats treated with androgens showed an increase in seminal vesicle secretory activity and weight. In addition, seminal vesicles possess 5α-reductase activity[17], though it is thought that the majority of androgen-dependent effects on the seminal vesicles are mediated by testosterone.

Prostate growth is stimulated by DHT, which is the principal intracellular androgen in that tissue. The importance of DHT to prostate growth and maintenance is clearly seen in individuals that are 5α-reductase deficient. These individuals show

absence of prostate growth even though they have normal circulating testosterone levels[18]. In addition, studies in rats showed that treatment with inhibitors of 5α-reductase produced a significant reduction in prostate size[19]. Over growth of the prostate, known as benign prostatic hypertrophy (BPH), can lead to rectal or urethral obstruction. DHT again plays an important role in BPH. Studies in both man and dog showed that BPH tissue accumulates androgen to a greater extent than normal prostate tissue, leading to higher DHT levels within the tissue [20].

Testosterone also plays a vital role in non-reproductive tissues such as bone and muscle. The mechanism by which androgens exert their effects in skeletal muscle is still unclear. Skeletal muscle and levator ani muscle in rats express AR, with the levator ani muscle having a higher level of cytosolic AR compared to other muscles[21]. Anabolic activity in muscle causes hypertrophy (increase in cell size) of the muscle, rather than hyperplasia (increase in cell number)[22]. With castration, muscle mass in rats is reduced, but with administration of testosterone muscle mass is restored to that of intact controls. One of the major biochemical differences between muscle and reproductive tissue is the relatively low level of 5α-reductase in muscle[23]. This may prove to be clinically significant when attempting to separate anabolic and androgenic activity of compounds.

Estrogens play an important role in preventing osteoporosis, especially in postmenopausal women. However, androgen may also affect bone formation. Studies in hypogonadal men showed an increase in bone mineral density (BMD) with testosterone treatment[24]. There is also a direct relationship between bone mass and the decrease in testosterone with age[25]. Bone is a dynamic tissue, which is completely regenerated every ten years. Bone mass is determined by the rate of formation by osteoblasts and rate of

degradation by osteoclasts. Bone remodeling consists of cycles of these two elements. The rate of remodeling depends on the number of cycles the bone goes through. Androgens decrease the bone remodeling rate by attenuating the birth rate of osteoblasts and osteoclasts[25,26]. AR can be found in osteoblasts, but not osteoclasts[27]. Therefore androgen effects in osteoclasts are thought to be indirect. *In vivo* studies in young castrated rats showed increased trabecular bone loss and decreased periosteal bone formation. In aging castrated rats, there is a decrease in cortical bone thickness and trabecular bone[28]. These changes are due to the increases in osteoclast-covered bone surface.

General assumptions on testosterone's effects on erythropoiesis have been observed in pubescent boys showing an increase in hemoglobin with an increase in testosterone[29]. Studies in rats showed the administration of testosterone to polycythemic rats increases erythropoietin production[30]. Testosterone exerts this effect by stimulation of stem cells in bone marrow, which leads to the proliferation of blood cell lines[22]. Testosterone may also increase the erythropoietin production by the kidneys[31].

1.4. Therapeutic Uses of Testosterone

Currently the primary uses of testosterone are the treatment of reproductive disorders such as male hypogonadism. As mentioned before, exogenous testosterone decreases spermatogenesis; therefore, androgens in combination with progestin or estrogen are being examined as potential approaches for male contraception[32]. Given the variety of effects of testosterone, there are many other non-reproductive uses in which testosterone has shown benefit. A study on surgically menopausal women showed that treatment with

estrogen/androgen combination therapy increased hip and spine bone mineral density more than estrogen alone[31]. Because of the anabolic effects seen with testosterone, it has been used in combating muscle wasting syndrome associated with AIDS and end stage cancer[33]. The administration of testosterone to these patients is mainly for its affects on disease associated morbidity rather than for treatment of the underlying disease. Testosterone can also be used in anemias associated with chronic kidney or bone marrow failure, because of its affects on erythropoiesis[25,33]. This therapy is most affective when coupled with anti-thymocyte globulin therapy[33].

1.5. Ligands for the Androgen Receptor

Ligands for the AR can be categorized by structure (steroidal or nonsteroidal) and function (agonist or antagonist). Steroidal agonists, such as testosterone and its derivatives, are used for androgen replacement[34,22]. Steroidal antagonists, such as megestrol acetate and cyproterone acetate, are used to block the effect of androgens in disorders such as prostatic cancer[35]. Steroidal androgen antagonists interfere with the binding of androgen to the AR, as well as inhibiting the negative feedback release of LH and FSH. Through these mechanisms, they counteract the effect of androgens at both the testicular and adrenal levels. Because of this complete blockade, many patients that use steroidal antiandrogens experience loss of libido and potency[35,37]. No steroidal antiandrogen has purely antiandrogenic activity and many can bind several other steroid receptors, such as the estrogen and progesterone receptors. This cross reactivity with other steroid receptors is thought to account for many androgen-related side effects.

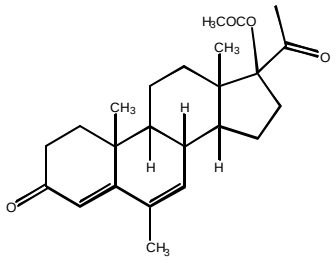

Megestrol Acetate

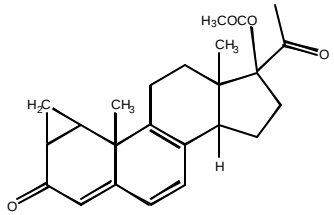

Cyproterone Acetate

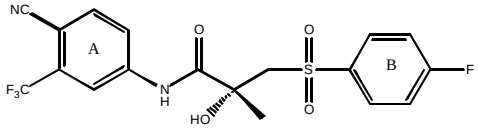

Bicalutamide

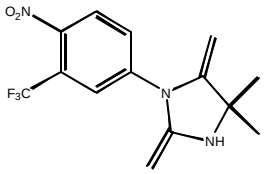

Nilutamide

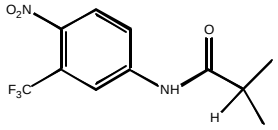

Flutamide

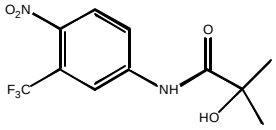

Hydroxyflutamide

Figure 1.4. Steroidal and Nonsteroidal Antiandrogens

Nonsteroidal structures were investigated to overcome many of the disadvantages of steroidal antiandrogen therapy. Neri *et al*. discovered flutamide, an androgen antagonist, in 1972[36] (Figure 1.3). It was the first nonsteroidal ligand for the AR used in large-scale clinical trials. Flutamide acts by blocking the binding of endogenous androgen to the AR, as well as inhibiting the translocation of ligand-bound receptor into the nucleus. Pharmacokinetics studies showed that flutamide was rapidly absorbed from the gastrointestinal tract and eliminated via hepatic metabolism, with a plasma half life of around 5 to 6 hours. The relatively short half-life of flutamide requires that it be dosed three times a day[37]. Metabolic studies showed that flutamide was extensively metabolized to 2-hydroxy-fultamide, which is the active metabolite of the drug[35]. The antiandrogenic effects of flutamide and its effects on the negative feedback mechanism of testosterone in the hypothalamus-pituitary axis, led to increases in LH and FSH levels and gynecomastia (i.e., breast pain) in patients[38]. Nilutamide was the next aniline derivative developed as a nonsteroidal antiandrogen. Nilutamide (Figure 1.4) has the same mechanism of action as flutamide, though it is also thought to inhibit an important enzyme pathway in testosterone biosynthesis[37]. As with flutamide, patients experience gynecomastia, as well as delayed adaptation to darkness[39].

To bypass some of the disadvantages seen with the other nonsteroidal antiandrogens, a "pure" antiandrogen, bicalutamide, was developed by Tucker *et al*[40]. Bicalutamide (Figure 1.4) is rapidly absorbed from the gastrointestinal tract, but has a long half life of 5 to 10 days. This permitted once daily dosing during clinical use of the drug. Bicalutamide is specific for the AR, thereby eliminating side effects caused by cross-reactivity with other receptors[35]. In addition, bicalutamide has a 5 to 10 times

higher potency as compared to flutamide, and a 2 to 4 times greater AR binding affinity than hydroxyflutamide in wild-type rat and human AR[41]. Bicalutamide is a chiral compound, with pharmacological activity residing in the R-enantiomer. Studies by Mukherjee *et al*. showed that the S-enantiomer of bicalutamide had a 30 times lower binding affinity as compared to the R-enantiomer, with the racemic mixture showing 2 times lower binding affinity as expected[42].

1.6. Structure Activity Relationships for the Androgen Receptor

With the development of nonsteroidal antiandrogens, structure-activity relationships (SARs) were formed which correlated functional groups with their binding affinity for the AR. Derivatives of flutamide showed that compounds with the highest binding affinities had two electron withdrawing groups on the aromatic ring separated from the tertiary carbinol by an amide linker. In addition, other factors, such as a hydrogen bond donator and a fixed conformational structure, were essential for high binding affinity (Figure 1.5 A. and B.)[10,43]. With the bicalutamide derivatives, higher binding affinities were seen with a cyano or nitro group on the 4'-position of the A ring, and a trifluoromethyl or chloro group on the 3'-position of the A ring. Proposed intramolecular hydrogen bonding within the bicalutamide molecule is shown in Figure 1.5 C. As with hydroxyflutamide, the hydroxyl group on the chiral carbon was important in AR binding. This hydroxyl group is thought to interact with an asparagine residue within the AR binding pocket (Asn^{705})[44]. It was interesting to note that Tucker *et al,* found partial agonist activity when a 2-trifluoromethyl group was added[40]. These SARs

A.

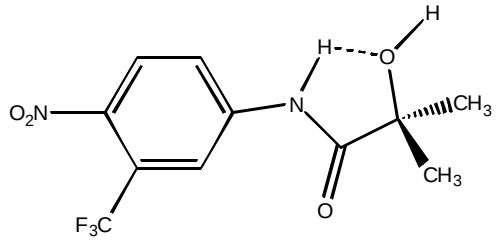

B.

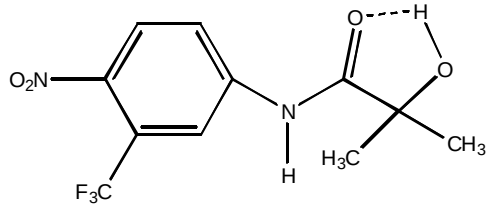

C.

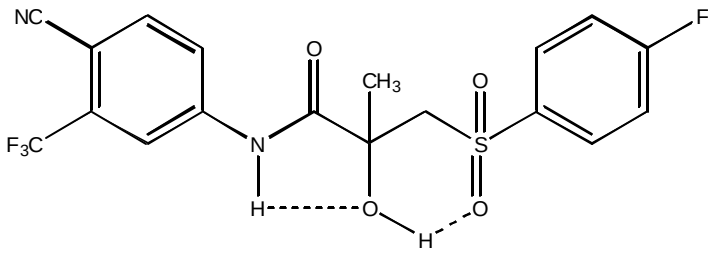

Figure 1.5. Hydrogen bonding of hydroxyflutamide and bicalutamide.

A. Favored confirmation for hydroxyflutamide. The planar geometry of the molecule is thought to be important in AR binding.
B. Alternative intramolecular hydrogen bonding of hydroxyflutamide.
C. Intramolecular hydrogen bonding thought to occur within the bicalutamide molecule. This conformation is favored in nonpolar solvents. In the aqueous environment of the AR, the hydrogen bond to the sulfonyl is disrupted and the hydroxyl group is thought to interact with the AR.

Adapted from reference 10.

can provide important clues to the factors that influence the binding of nonsteroidal ligands to the AR.

1.7. Selective Androgen Receptor Modulators

Testosterone, an endogenous ligand for the AR, is important in the normal development and maintenance of the male reproductive system. It is also involved in diverse physiological roles of several different organ systems such as muscle and bone. Exogenous testosterone is used to treat many disorders such as hypogonadism, osteoporosis, and primary anemias. However, there are many problems associated with testosterone therapy. Firstly, testosterone is primarily used as injectable solutions and transdermal patches. While 17α-alkylated androgens are orally bioavailable, they are associated with hepatic toxicity and changes in lipoprotein levels, and are therefore not a viable form of therapy[45]. Secondly, testosterone injections produce large fluctuations in testosterone plasma concentrations, which may lead to adverse affects. The normal physiologic level of testosterone in man shows a diurnal pattern, with a peak at 6 to 8 am and a nadir at 6 to 8 pm[46]. While transdermal patches reduce the fluctuation in the concentration-time profile, they are associated with skin irritation and do not mimic the normal diurnal variation[47]. In addition, anabolic steroids have the potential for hepatoxicity, blood pressure effects, and gynecomastia[31,47]. Thirdly, current steroidal preparations demonstrate equal anabolic and androgenic activity (i.e., they are non-tissue selective). The non-selective nature of testosterone and its derivatives, poor pharmacokinetic properties, and toxicities led to the search for androgens with improved properties.

Selective androgen receptor modulators (SARMs) were developed to address these deficiencies. The ideal SARM would have a minimum of side effects, good oral bioavailability, and a favorable pharmacokinetic profile (i.e., linear kinetics, half-life conducive to once-a-day dosing). Much like selective estrogen receptor modulators (SERMs), the SARM can be designed to be tissue specific. This would, for example, allow the drug to act as an androgen in muscle (anabolic) while having little to no effect on other organs (androgenic). Such a drug could be beneficial in disorders such as andropause, osteoporosis, or BPH, and avoid the concerns related to the role of testosterone in prostate cancer.

1.8. Andropause

Andropause, also known as androgen decline in the aging male (ADAM), is a relatively new clinical diagnosis, for the myriad of physiological effects that occur naturally as men age. There is a slow, but continuous decrease (110 ng/dL every decade)[45] in testosterone levels with age, with a greater decrease seen in free testosterone levels due to increased sex hormone binding globulin. Sixty percent of men over the age of 65 have free testosterone levels that are significantly lower than men aged 30 to 35[46,48,49]. The reduction of testosterone is a result of primary testicular and secondary hypogonadal dysfunction[49]. Studies also showed that the normal circadian rhythm seen with testosterone is blunted in the aging male[50]. This is caused by the disruption of the pulsatile release of LH and FSH.

The decrease in hormone level leads to a variety of effects. Sexual activity decreases while sexual dysfunction increases as men age. Epidemiological evidence has

linked free testosterone levels to sexual activity[51]. While erectile dysfunction is linked to impaired penile nitric oxide release, animal studies showed that the presence of nitric oxide synthase was dependent on serum testosterone concentrations[52]. Recent studies showed that concomitant treatment with phosphodiesterase-5 inhibitors and androgens improve sexual function[45,53]. Young hypogonadal men have decreased muscle mass and strength[24]. Several studies have shown positive effects on these functions with testosterone replacement therapy[54]. These results correlate well with studies showing a decrease in muscle mass and increase in fat mass, in particular abdominal fat, with age[55]. Testosterone treatment in elderly men decreases abdominal fat and increases muscle mass[55]. While muscle mass is correlated with serum and free testosterone, data on muscle strength is inconclusive. It is unclear if BMD in aging men is attributed to free testosterone levels alone or to conversion of testosterone by aromatase to estradiol[56,57]. Studies in androgen-deficient older men show an increase in BMD with testosterone treatment, but no correlation was made to fracture rate[58]. Several studies in young hypogonadal and healthy men demonstrated that testosterone treatment improves cognition[24,59]. This led to the investigation of testosterone treatment in older men with decreased serum testosterone. Short-term treatment with testosterone improved cognition, but a clear association with testosterone as opposed to testosterone aromatized to estradiol could not be made[60].

Although testosterone remains the only treatment for andropause, many concerns remain about its safety in older men. The unpredictable effects of testosterone on the prostate gland are one of the primary concerns with testosterone treatment. While many studies in elderly men have shown no significant change in prostate volume, or symptoms

of urinary obstruction with treatment[61], a modest irreversible increase in prostate specific antigen (PSA), a marker of BPH and prostate cancer, is seen[62]. Few long-term studies have been conducted on elderly men; therefore determination of treatment, dose and possible adverse effect to prostate and atherosclerosis remains to be determined.

1.9. Overview of Dissertation

The objective of this dissertation was to identify potential SARMs *in vitro* and determine their pharmacologic and pharmacokinetic properties *in vivo.* This involved determination of AR binding activity and *in vitro* functional activity, evaluation of pharmacological properties, and identification of pharmacokinetic parameters and metabolic profiles. These studies are discussed in Chapters 2 through 4 of this dissertation. The evaluation of the impact of this work and future research directions are discussed in Chapter 5. Each chapter contains a brief introduction of the relevant literature and purpose of the study, a section describing the methods, and a discussion of the findings. The data relevant to each chapter are included in a separate appendix at the end of the document. Tables and figures relevant to these chapters are included within each chapter.

This project was conducted as a collaboration between Dr. James Dalton in the Division of Pharmaceutics at The Ohio State University and Dr. Duane Miller, in the Department of Pharmaceutical Sciences at the University of Tennessee. A series of bicalutamide and hydroxyflutamide analogs was created to investigate affinity labeling of the AR. Fortuitously, some of these compounds showed agonist activity during *in vitro* AR binding assays and cell culture studies for transcriptional activation. This led to the

development of structure-activity relationships, which were used to create more potent androgen agonists. In Chapter 2 we describe the *in vitro* assay of a series of bicalutamide analogs used to determine AR activity, under the hypothesis that by using SARs we could develop AR agonists with high potencies and efficacies. The results of these studies showed that many of the compounds bound reversibly to the AR and different functional groups within the molecule affected the potency and efficacy of the compound. Those compounds that showed promising *in vitro* results were moved on to the immature castrated rat model. In addition, this chapter also describes the *in vivo* pharmacological activity studies to determine agonist activity. The results of this study showed that two compounds not only showed agonist activity *in vivo*, but also selectively affected anabolic tissue (i.e. muscle). This was the first anabolic SARM discovered. Another bicalutamide analog, R-1, was developed that contained high binding affinity and AR mediated transcriptional activation, but did not contain *in vivo* pharmacological activity[63]. To rectify the discrepancy between *in vivo* and *in vitro* assays, pharmacokinetic studies were conducted. The result of these studies showed that the AR agonists were converted to antagonists in rats by metabolic modification. In Chapter 3, we discuss the pharmacokinetics of the lead compound S-4, which was developed to overcome some unfavorable properties of R-1. These studies showed that S-4 is rapidly absorbed and highly bioavailable after oral doses, which are capable of maximal pharmacologic activity. Further, S-4 demonstrated a low plasma clearance (CL) indicative of low hepatic extraction and a moderate Vss and half-life. In Chapter 4, we report the metabolic profile of S-4 in rats and beagle dogs and the final disposition of S-4 in rats. Given the metabolic conversion of R-1 to an AR antagonist, we hypothesized that substitution of an oxygen

atom for the reactive sulfur atom in the compound would reduce this conversion. The result of these studies showed that S-4 was highly metabolized, with the major metabolite being the hydrolysis product. A minor metabolite in dogs showed antagonist activity.

The hypotheses for these studies were as follows:

(i) *In vitro* studies could be used to identify novel androgen agonists. Since agonists bind to a receptor and elicit a cellular response, high affinity and transcriptional activity would be a major determinant of agonist activity.

(ii) Compounds that showed high binding affinities *in vitro* will display selective pharmacologic activity *in vivo*. Determining the *in vivo* androgenic activity of a series of compounds would help correlate *in vitro* and *in vivo* studies. In addition, determining the anabolic versus androgen activity of a potential SARM is key in the development of the compound.

(iii) Using known SARs and pharmacological data, a selective androgenic compound could be synthesized that is orally bioavailable and possesses pharmacokinetic and metabolic profiles that allow adequate tissue concentrations to elicit a response. Pharmacokinetic studies will determine the compound's utility, considering that a compound's pharmacologic activity and body's exposure to the compound determine its therapeutic efficacy. Metabolic studies would identify possible conversion of the compound to an antagonist and help in developing strategies to prevent this conversion. Final disposition studies will quantify the amount of each metabolite and help determine if it is pharmacologically relevant.

These studies demonstrated that by using SAR for the AR, a potent, selective compound can be developed that can be used as an alternative to testosterone therapy. S-4 is the first anabolic SARM developed thus far.

CHAPTER 2

IN VITRO AND *IN VIVO* PHARMACOLOGY OF NONSTEROIDAL ANDROGEN RECEPTOR LIGANDS

2.1. Introduction

Nonsteroidal androgen antagonists are used clinically for the treatment of prostate cancer. The toluidide androgen antagonists, such as flutamide or nilutamide, possessed short plasma half lives requiring multiple daily dosing. Bicalutamide was developed as a preferentially selective antiandrogen to overcome some of the disadvantages seen with flutamide and nilutamide. Bicalutamide has a long half life, permitting once-a-day dosing, and demonstrates higher potency and efficacy than other nonsteroidal antiandrogens. Tucker *et al*.[38] were the first to investigate the novel chemical structure of bicalutamide, while conducting investigations on AR antagonists. Structure activity relationships (SAR) were developed by investigating the requirements for AR binding. Using this SAR information, our laboratory developed a series of chiral nonsteroidal chemoaffinity ligands for the AR as tools to characterize the structure and function of this important protein[42]. During these studies we identified a series of compounds that possessed agonist activity[64,70]. Initial studies focused on electrophilic ligands for the AR.

Fortuitously, compounds showing full agonist activity were documented[63]. The first series of compounds to show high AR binding affinity and stimulated AR-mediated transcriptional activation contained an electron-withdrawing group (e.g., chloroacetamide) at the para position of the B ring (Table 2.1). Concerns of irreversible binding of the chloroacetamide functional group to nucleophilic cellular components prompted the substitution of an acetoamido group at this position, which retained its agonistic activity. These findings demonstrated that key structural changes to a known antagonist structure could produce an AR agonist.

Bicalutamide is marketed and sold as a racemic mixture. Mukherjee *et al.*, showed that the R-isomer possessed higher binding affinity and more potently inhibited AR-mediated transcriptional activation than the S-isomer[42]. Using the SAR information acquired during the development of nonsteroidal antiandrogens and chemoaffinity ligands for the AR, our laboratory synthesized the R and S isomers of a novel series of potential nonsteroidal androgens. *In vitro* studies showed that the R isomers of bicalutamide analogs possessed significantly higher AR binding and transcriptional activation[41]. Subsequent studies, including those in this chapter, focused on predominantly R-isomers.

In vitro assays were used to efficiently identify potential AR agonists. These studies enable classification of individual compounds by binding affinity and AR-mediated transcriptional activation activity. Dihydrotestosterone (DHT), the most potent endogenous androgen, has a Ki (equilibrium dissociation constant) of 0.28 nM[42]. The dissociation constant for DHT was used as the reference of comparison to determine the binding affinity of these potential AR agonists.

AR-mediated transcriptional activation determined the potency and efficacy of the series of compounds tested. Full AR agonists were defined as those compounds that can induce transcriptional activation that is equal to or greater than that elicited by 1nM DHT. Those compounds that fall below this range are considered to be either partial agonists or antagonists.

Although *in vitro* assays are useful in identifying possible androgen agonists, the true value of a compound can only be discerned by *in vivo* pharmacologic experiments. *In vitro* assays have the advantages of high throughput, high sensitivity and specificity. However, they do not take into account pharmacokinetic properties of the drug, such as absorption, distribution, metabolism, and elimination. On the other hand, *in vivo* assays reflect the pharmacology of the compound in entire system as opposed to a specific endpoint. The pharmacological activity of the bicalutamide analogs was examined in an immature rat model based on the Hershberger assay[67]. Immature rats, at approximately 6 weeks, were used in this assay because younger rats show greater sensitivity to organ-related changes caused by testosterone depletion. In addition, testosterone-mediated organ re-growth is greater in immature animals[67,68].

Androgen sensitive tissues were assayed to determine the andogenic activity of the test compounds. Maintenance of accessory sex organ weight requires androgen supplementation. Kim *et al*. showed that with doses of less than 0.2 mg/kg of testosterone, there was a significant increase in prostate and seminal vesicle weight after castration, with maximal response seen at doses of 1.6 mg/kg[69]. In this study, doses at 1 mg/day of testosterone propionate were used to restore organ weight and for comparison of the pharmacology activity of our compounds.

The prostate and seminal vesicles were chosen as markers of androgenic activity. The prostate is composed of three types of tissue: glandular epithelium, stromal epithelium and basal epithelium[70]. With testosterone depletion, the prostate quickly involutes, with the majority of volume lost from the glandular epithelial cells, since these are the only cells within the prostate that are androgen sensitive[36]. The seminal vesicles are also androgen dependent. While 5α reductase activity is present in the seminal vesicles, studies in isolated seminal vesicle epithelium showed that testosterone, not DHT, maintained seminal vesicle wet weight[16].

The levator ani muscle is used as a marker of anabolic activity. Muscle tissue has androgen receptors, while it lacks 5α reductase activity[22]. The levator ani muscle was chosen for is relatively high androgen receptor content as compared to other muscles and it's relatively low exercise induced increase in weight[21].

This chapter describes the result from *in vitro* and *in vivo* studies involving a series of bicalutamide analogs. These studies determined the pharmacologic activity and selectivity (anabolic versus androgenic activity) of these potential androgen agonists and will assist in the development of SARs.

2.2. Materials and Methods

2.2.1 Chemicals

Compounds R-1 through R-8 (Table 2.1) were synthesized in Dr. Duane Miller's laboratory at the University of Tennessee, as previously described[71]. The purity of the synthesized compounds was analyzed by elemental analysis and mass spectrometry. [17α-methyl-^{3}H] Mibolerone (^{3}H-MIB) and unlabeled mibolerone (MIB) were purchased

from PerkinElmer Life Sciences (Boston, MA). Triamcinolone acetonide, phenylmethylsulfonyl fluoride (PMSF), Tris base, sodium molybdate, DHT, and polyethylene glycol 300 were purchased from Sigma-Aldrich (St. Louis, MO). Hydroxyapatite (HAP) was purchased from Bio-Rad Laboratories (Hercules, CA). EcoLite scintillation cocktail was purchased from ICN Pharmaceuticals (Costa Mesa, CA). Minimal essential medium (MEM), Dulbecco's modified eagle medium (DMEM), penicillin-streptomycin, trypsin-EDTA, and Lipofectamine reagent were purchased from Invitrogen (Carlsbad, CA). Fetal bovine serum was purchased from Atlanta Biological (Norcross, GA).

2.2.2 Buffers

Homogenization Buffer contained 50 mM Tris, 1 mM potassium phosphate, and 0.1 mM PMSF. Incubation Buffer contained 10 mM Tris, 1.5 mM EDTA, 0.25M sucrose, 10 mM sodium molybdate, and 1 mM PMSF at pH 7.4. Washing Buffer contained 50 mM Tris at pH 7.2. Beta-galactosidase buffer consisted of 200 mM sodium phosphate, 2 mM magnesium chloride, 100 mM B-mercaptoethanol, and 1.33 mg/ml ONGP. Luciferase assay buffer contained 25 mM glycylglycine, 15 mM magnesium chloride, and 5 mM ATP.

2.2.3 Preparation of Cytosolic AR

All studies were conducted under the auspices of an approved animal care protocol at the University of Tennessee. Cytosolic AR was prepared from the ventral prostate of castrated Sprague-Dawley rats. Male Sprague-Dawley rats weighing

approximately 250 g. were obtained from Harlan Bioscience (Indianapolis, IN), and were maintained on a 12 hours light/dark cycle with free access to food and water. Animals were castrated and allowed 24 hours to recover. The ventral prostate of each animal was excised, all excess fat removed, and the tissue minced with scissors. An aliquot (1 mL) of homogenization buffer was added per 500 mg of prostate tissue. Prostate tissue was homogenized in a mechanical homogenizer (Model PRO 200, Pro Scientific, Monroe, CT). The homogenate was centrifuged at 114000 g for 1 hour. The cytosolic supernatant, containing the AR, was decanted and stored at -80°C.

2.2.4 Competitive AR Binding Assay

The binding affinities of synthesized compounds were determined by incubating AR with increasing concentrations (10^{-6} to 10 μM) of test compound in the presence of the high affinity AR ligand, ^{3}H-MIB (1 nM) for 18 hours at 4°C. Triamcinolone acetonide (1000 nM) was added to the incubate to prevent the binding of ^{3}H-MIB to the progesterone receptor. Nonspecific binding was determined by the addition of an excess of unlabeled MIB to the incubate. Separation of bound radioactive ligand at the end of the incubation was accomplished by the addition of an aliquot (1 mL) of a HAP suspension. The incubates were centrifuged at 1000 g for 10 minutes and then rinsed with washing buffer three times. An aliquot (1 mL) of ethanol was added to the suspension and vortexed periodically at room temperature for 1 hour. The HAP suspensions were centrifuged at 1000 g for 10 minutes and an aliquot (1 mL) of the ethanolic supernatant was added to 5 mL of scintillation cocktail. Radioactivity was counted in a Beckman LS6500 liquid scintillation counter (Beckman Instruments Inc.,

Irvine, CA). The inhibition curves were constructed using WinNonLin version 3.1 (Pharsight Corporation, Mountain View, CA).

2.2.5 Determination of AR Binding Affinity

Specific binding was determined by subtracting the nonspecific binding (binding of ^{3}H-MIB in the presence of excess unlabeled MIB) from total binding (binding of ^{3}H-MIB without excess unlabeled MIB). Inhibition curves were constructed for each ligand using the percentage of specific binding. The IC50 (concentration required to inhibit ^{3}H-MIB by 50%) was determined by the following equation[63]:

$$B = Bo * \left[1 - \frac{C}{IC50 + C}\right]$$

in which Bo was the specific binding of the radioactive ligand in the absence of test compound, B is the specific binding in the presence of test compound and C is the concentration of test compound. The Ki for each compound was calculated with the following equation[63]:

$$Ki = \frac{Kd * IC50}{Kd + L}$$

The Kd (equilibrium dissociation constant for ^{3}H-MIB) was determined using the same procedure with increasing concentrations of ^{3}H-MIB (0.01 to 10 nM) in AR containing cytosol. We determined that the minimum concentration required to saturate the AR was 1nM (L). This concentration of ^{3}H-MIB was therefore used for all competitive binding studies.

2.2.6 AR Mediated Transcriptional Activation Assay Method

AR-mediated transcriptional activation was determined in CV-1 (American Type and Culture Collection, Rockville, MD) monkey kidney cells co-transfected with the human AR and a luciferase reporter gene. One day prior to transfection, 5 x 10^5 cell/well were seeded into 6-well plates containing 3 mL of DMEM, supplemented with 10% fetal bovine serum (FBS) and 1% penicillin-streptomycin. Transient transfection of the plated cells was performed in serum-free media using Lipofectamine, with 100 ng human androgen receptor plasmid (pCMVhAR; generously provided by Dr. Donald J. Tindall, Mayo Clinic and Mayo Foundation, Rochester, MN), 2.5 µg luciferase reporter plasmid (pMMTV-Luc, generously provided by Dr. Ronald Evans at the Salk Institute, San Diego, CA), and 2.5 µg beta-galactosidase plasmid (pSV-β-galactosidase; Promega, Madison, WI) with 15 µL of Lipofectamine. After 10 hours, the cells were allowed to recover in DMEM supplemented with 0.02% FBS for 10 to 20 hours. Cells were then treated with various concentrations of test compounds, 1 nM DHT or vehicle for 48 hours. Test compounds were initially dissolved in ethanol and the resulting solutions serially diluted in DMEM to 1, 10, 50, 100, 500, and 1000 nM. The final concentration of ethanol was less than 0.1%. The drug-containing media was replaced with fresh drug every 24 hours within the 48-hour incubation. Following drug treatment, the cells were washed in potassium phosphate buffered saline. Cells were then lysed by the addition of 350 µL of Reporter Lysis Buffer (Promega, Madison, WI). Plates were rocked for 30 minutes at room temperature. Cells were then scraped and the lysate was centrifuged at 12,000 g for 2 minutes. Samples were prepared for measurement of luciferase activity by adding 100µL of lysate to 100 µL of luciferase assay buffer and vortexing. An aliquot

(100 μL) of 1 mM beetle luciferin (Promega, Madison, WI) was then added to each tube and the luminescence was read by an AutoLumate LB953 luminometer (Wallace Inc., Gaithersberg, MD). Beta-galactosidase activity was determined by adding 150 μL of lysate to 150 μL of beta-galactosidase assay buffer. The reaction was stopped by the addition of 0.7 mL of 1 M sodium bicarbonate. The optical density was measured on a UV spectrophotometer (Cary Model 1E, Varian Associates, Sunnyvale CA) at a wavelength of 420 nm. The transcriptional activity at each concentration was calculated as the ratio of luciferase activity to beta-galactosidase activity (normalization for cell number and transfection efficiency).

2.2.7 Animals

Male Sprague-Dawley rats weighing approximately 250 g were purchased from Harlan (Indianapolis IN). The animals were maintained on a 12-hour cycle of light and dark, and had free access to food and water unless otherwise stated. The animal protocol was reviewed and approved by the Institutional Laboratory Animal Care and Use Committee of University of Tennessee.

2.2.8 *In vivo* Pharmacologic Study Method

Immature Sprague Dawley rates were randomly divided into seven treatment groups with three animals per group. One day prior to treatment, groups 1 through 6 were anesthetized with ketamine/xylazine and castrated via an testicular incision. Animals were given 24 hours to recover after surgery. Animals in group 7 served as an intact control. All drugs given to the animals were freshly prepared by dissolving an

apporpriate amount of compound in ethanol and diluting to a final concentration of 1 mg/mL in PEG 300. The final concentration of ethanol was less than 5% of the dose. Groups 1 through 5 received subcutaneous injections of compounds R-5 through R-8 and testosterone propionate at doses of 100 µg/day for 14 days. Group 6 received daily injection of PEG 300 (vehicle control). After the treatment period, the animals were weighed, anesthetized and sacrificed. The following organs were excised cleaned of extraneous tissue and weighed: ventral prostate, seminal vesicles, levator ani muscle, and kideys. All organ weights were normalized to body weight. The ventral prostate and seminal vesicles were used as a index of androgenic activity. Levator ani muscle weight was used as an index of anabolic activity.

2.3. Results

2.3.1 *In vitro* AR binding Affinity Results

The binding affinity of potential AR ligands was determined by the competitive displacement of ^{3}H MIB from AR binding sites with increasing concentrations of the test compound. Figure 2.1 shows a binding curve representative of those seen in the study. Table 2.1 summarizes the results of the series of AR ligands tested.

Many compounds showed K_i values in the nanomolar range, with affinity greater than or comparable to R-bicalutamide (11± nM)[42]. The compounds tested had lower binding affinity than DHT (Ki = 0.28 nM). The 4-cyano and 4-nitro A- ring substituted analogs showed similar binding affinities (compare R-1 to R-5). However, previous

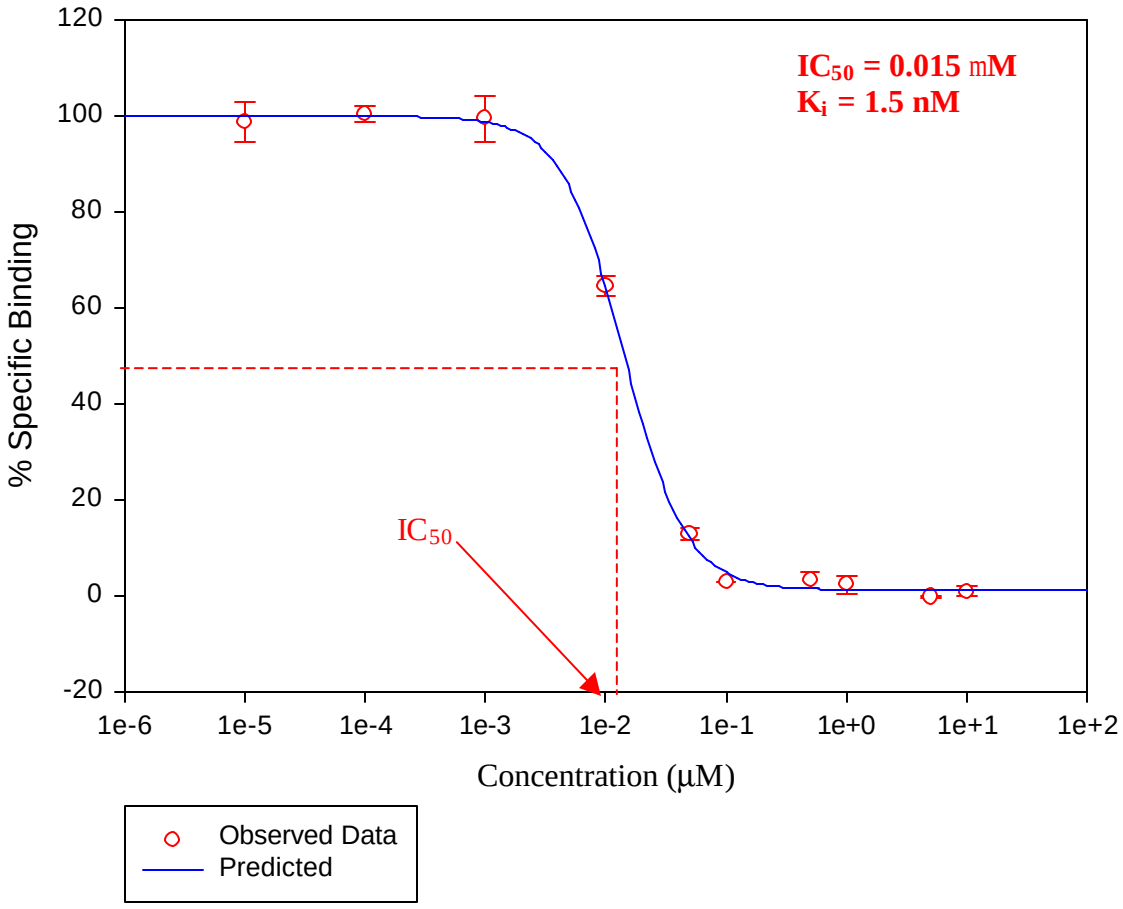

Figure 2.1. Representative Binding Curve

Increasing concentrations (10^{-6} to 10 µM) of R-2 in the presence of the high affinity AR ligand, ^{3}H-MIB (1 nM), were incubated with AR. Specifically bound ^{3}H-MIB was measured as described in section 2.2.4.

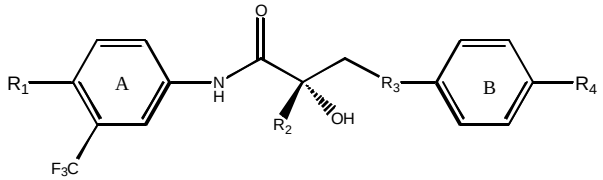

Compound	R_1	R_2	R_3	R_4	Ki (nM)	RBA (%)	Efficacy [a] (%)	Potency [b] (nM)
DHT					0.28 ± 0.02[c]	100	100	1[d]
R-Bicalutamide	NC	CH_3	S	F	11.0 ± 1.5[c]	ND	9.1	5000[d]
R-1	NC	CH_3	S	$NHCOCH_3$	2.1 ± 0.36	13	ND	ND
R-2	NO_2	CF_3	S	$NHCOCH_3$	1.5 ± 0.13	19	646	10
R-3	NC	CH_3	S	$NHCOCH_2CH_3$	9.3 ± 0.19	2.9	ND	ND
R-4	NC	CH_3	S	$N(COCH_2CH_3)_2$	46 ± 1.29	0.58	ND	ND
R-5	NO_2	CH_3	S	$NHCOCH_3$	3.0 ± 0.8	9.0	94	50
R-6	NO_2	CH_3	SO_2	$NHCOCH_3$	4.2 ± 0.37	6.4	57	>1000
R-7	NO_2	CH_3	S	$NHCOCF_3$	1.2 ± 0.18	23	278	10
R-8	NO_2	CH_3	SO_2	$NHCOCF_3$	2.8 ± 0.51	9.6	12	>1000
R-9	NO_2	CH_3	S	NO_2	20.3 ± 1.88[e]	ND	914	100
R-10	NO_2	CH_3	S	$NHCOCH_2Cl$	11.5 ± 0.33	6.2	100[e]	100[e]

a. The maximal percentage of transcriptional activation seen for each ligand.
b. The concentration that results in transcriptional activation equal to or greater than that observed with 1 nM DHT.
c. Previously reported in Mukherjee *et al*. Reference 42
d. Concentration that showed maximal transcriptional activation
e. Previously reported by Yin *et al*.
ND. Not determined

Table 2.1. Competitive Binding Affinity and Transcriptional Activation of Potential AR Ligands.

studies with hydroxy-flutamide analogs showed that the nitro substitution at the para position of the A ring significantly increased binding affinity[63]. These results agree with the previous studies showing that an electron deficient A ring may be important in AR binding[66].

To optimize binding, a variety of substituents were introduced on the para-position of the B ring. Compounds incorporating longer alkyl chains and tertiary amines at the para-position of the B-ring exhibited lower binding affinity, suggesting that steric hindrance at this position interfere with AR binding. It was noted that the addition of a trifluoroacetamide (TFAc) in place of the acetamide (Ac) at the R_4 position significantly increased binding affinity, as seen when comparing compounds R-5 to R-7 and comparing compounds R-6 to R-8. This may be due to the greater electronegative potential of the TFAc group as compared to the Ac. R-7 showed the greatest binding affinity of all the compounds tested. The addition of a chloroacetamide group (R-10) resulted in lower binding affinity than the Ac or TFAc groups. The addition of a nitro group at R_4 decreased the binding affinity (R-9), suggesting that the presence of a hydrogen bond acceptor or lack of the acetamide linkage at this position muted interaction with the AR.

To investigate the effect of the linker position (R_3) on AR binding, analogs with a sulfur or sulfonyl group at this position were examined. Results showed that the sulfide analogs (R-1, R-2, R-5, R-7) showed higher binding affinities than their corresponding sulfonyl analogs (R-6 and R-8). It is important to note that the pharmacological relevance of small (i.e. <1 nM) differences in Ki between compounds is unknown.

The effect of the substitution of a trifluoromethyl at position R_2 for the methyl group was also investigated (R-2). This compound was synthesized as a racemic mixture. This substitution further increased binding affinity, as seen when comparing R-2 to R-5.

2.3.2 *In Vitro* Transcriptional Activation Results

To determine the effects of these compounds on AR-mediated transcriptional activation, compounds were tested in a CV-1 monkey kidney cell culture transfected with human AR receptor plasmid, an androgen-sensitive luciferase reporter plasmid, and a plasmid for constitutive expression of beta galactosidease (used to correct for cell number and transfection efficiency). Transcriptional activity increased with increasing ligand concentration and then plateaued for all the compounds tested. Figure 2.2 shows the data observed after a typical transcriptional activation experiment. Table 2.1 shows the potency and efficacy of the compounds tested. Potency was defined as the lowest concentration that resulted in transcriptional activation equal to or greater than that observed with 1 nM DHT. Efficacy was defined as the maximal percentage of transcriptional activation seen for each ligand, at any concentration.

None of the compounds showed potencies equal to DHT (1 nM). However, many showed efficacy equal to or greater than DHT, such as R-2, R-5, and R-7. As seen in the binding affinity assay, sulfide analogs (R-2, R-5, R-7) showed higher potency and efficacy than their corresponding sulfonyl analogs (R-6 and R-8). These results concur with additional studies in our laboratory, which in fact showed that the sulfonyl analogs were AR antagonists in transcriptional activation studies[63]. The substitution of the TFAc

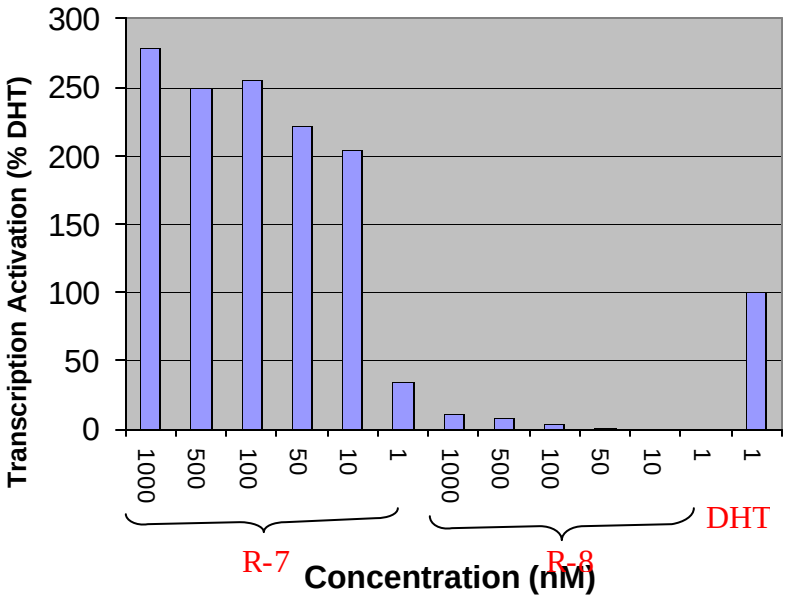

Figure 2.2. Representative Transcriptional Activation Graph

Increasing concentrations of compounds R-7 and R-8 were used in a cotransfection assay to determine *in vitro* functional activity. The graph shows transcriptional activation as a percentage of the transcriptional activation seen with 1 nM DHT. R-7 has a potency of 10 nM (The lowest concentration that resulted in transcriptional activation equal to or greater than that seen at 1 nM DHT) and efficacy of 278 % (maximum transcriptional activation seen). R-8 has a significantly lower potency and efficacy (>1000 nM and 13 % respectively).

group at the R_4 position increased both potency and efficacy (R-7), supporting the results of the previous binding studies. While the addition of the nitro group at the R_4 position (R-9) increased the efficacy of AR-mediated transcriptional activation, it showed lower potency than the Ac or TFAc substitution (compounds R-5 and R-7 respectively). Binding studies showed that this compound had a relatively low binding affinity. These results suggest that other factors such as hydrogen bonding may play an important role in AR binding.

It would seem that more electronegative atoms at the para position of the B-ring such as TFAc increased binding and functional activity. These groups are highly electron withdrawing and therefore may decrease the electron density of the ring, causing a favorable interaction within the receptor binding pocket. However the addition of the electron-withdrawing nitro group at the R_4 position decreased binding, while increasing efficacy in the transcriptional activation studies. Given that the TFAc and the nitro groups are both hydrogen bond acceptors, this may indicate the presence of a hydrogen bond donor within the lower binding pocket of the AR.

These data and other data in the laboratory suggest that compounds R-1, R-2, R-5, and R-7 should be further evaluated in an *in vivo* model. While compound R-2 showed promising results in all *in vitro* assays, difficult chemical synthesis precluded its inclusion in the *in vivo* pharmacologic studies.

2.3.3 *In vivo* Pharmacological Study Results

Competitive binding assays and transcriptional activation data help identify potential androgen agonists. However *in vivo* studies remain the "gold standard" for

assessing the pharmacologic activity of a compound. The pharmacologic activity of these compound were evaluated in a castrated immature rat model for 14 days.

Pharmacologic activity was investigated in 4 compounds (R-5, R-6, R-7, and R-8), positive control (TP), negative control (PEG 300), and intact control. The results of the pharmacological studies are summarized in Figure 2.3. No significant changes in body weight were observed during the study. Castration resulted in a significant reduction of ventral prostate, seminal vesicles and levator ani muscle weights (8%, 10%, and 40% of intact control, respectively), confirming the androgen responsive growth of these organs. Subcutaneous administrations of TP at a dose of 100 μg/day partially restored organ weight (120%, 110%, and 70% of intact control, respectively).

None of the compound tested showed significant increase in ventral prostate or seminal vesicle weight as compared to TP treated animals or intact controls. These findings suggest that these compounds lack androgenic activity. Compounds R-5 and R-7 showed a small but significant increase in levator ani weight (p-value < 0.05). These findings suggest that these compounds may possess anabolic activity. No change was seen in kidney weight with treatment or castration.

2.4. Discussion

A series of potential AR agonists were created by modifications to bicalutamide, a known androgen antagonist. Early work on AR binding affinity showed several key features necessary for binding of antagonist to the receptor: i) The A aromatic ring

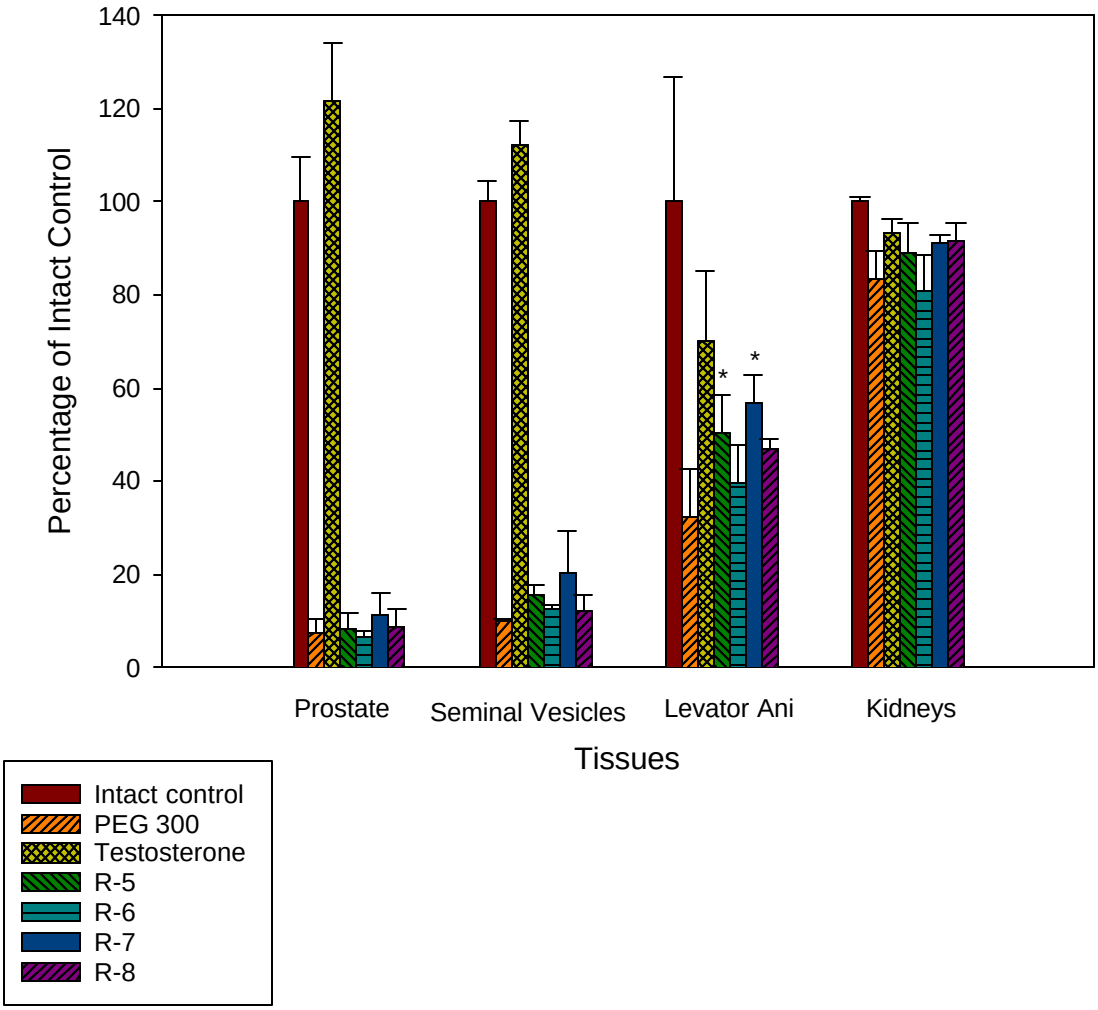

Figure 2.3. In Vivo Pharmacological Study Results of Androgen-Dependent Organ Weights.

Asterisks indicate compounds that were not significantly different from the testosterone treated group, and were significantly different from the vehicle control (p-value ≤ 0.05)

separated from the tertiary carbinol by an amide linker, ii) cyano or nitro group on the 4'-position of the A ring, and a trifluoromethyl of chloro group on the 3'-position of the A ring, and iii) a hydrogen bond donor and a fixed conformational structure (see Figure 1.4). Importantly, the studies described in this chapter identified other SARs that were key for agonist activity. In these studies, binding and AR-mediated transcriptional activation were generally enhanced by: i) less bulky substituents on the para position of the B ring, ii) a trifluoromethyl group on the chiral carbon (position R_2), iii) higher electron withdrawing and/or hydrogen bonding capacity of the substituent on the para position of the B ring, and iv) a sulfur, rather than a sulfonyl linker at the R_3 position.

Studies by Matias *et al.*[12] indicate that the ligand binding pocket for the human AR is made up of 18 to 19 amino acids, most of which are hydrophobic and interact with the steroidal backbone of testosterone. However, specific moieties are hydrophilic (Asn^{705}, Gln^{711}, Gln^{752}, and Thr^{877}) and can hydrogen bond with ligand in the receptor pocket. Using homology modeling, Poujol *et al*. showed bicalutamide docking within the LBD of the AR. It is interesting to note that the A ring of bicalutamide was positioned similarly to hydroxyflutamide (the trifluoromethyl group on the A ring positioned between two methionine residues). However, the aromatic ring containing the sulfonyl group pushed away helix 11 and 12, leading to inappropriate protein folding[10]. The folding of helix 12 over the LBD is thought to be crucial for homodimerization and transcriptional activation[65]. These findings correlated to the SAR we found in our *in vitro* studies, in which compounds containing a sulfonyl group showed lower binding affinity and only partial agonist or antagonist activity as compared to their sulfur analogs (R-8).

Poujol *et al*. showed that the bicalutamide molecule displayed a bent conformation within the AR binding pocket[44]. Homology modeling by Marhefka *et al.* found an unoccupied binding pocket under carbon 15 of testosterone bound to the LBD (Figure 2.4)[14]. This suggests that the substituent on the para position of the B ring may occupy and interact with amino acid residues in this pocket. Modification to the para-position of the B ring (R_4) produced the greatest changes in binding and transcriptional activation in our series of compounds. As we increased the size of the substituent from an acetamide to a propamide group, binding decreased. This was corroborated by the addition of two propamide groups at this position. These groups may be too bulky to fit within the lower binding pocket of the LBD and therefore decreased binding.

Highly electrophilic groups, such as TFAc, showed the highest binding affinity of the series of compounds studied, while the substitution of a nitro group significantly decreased the binding and potency, but greatly increased efficacy. The nitro group is a hydrogen bond acceptor while the TFAc can be both a hydrogen bond donor and acceptor. Therefore, both these interaction may be influential in AR binding. Further studies are needed to determine the exact nature of ligand binding within the lower binding pocket.

The hydroxyl group at the chiral carbon of bicalutamide, which is analogous to the 2-hydroxy group on hydroxyflutamide, is involved in hydrogen bonding with hydrophilic amino acids within the LBD[43]. This group is thought to hydrogen bond to the Asn^{705} residue, and mutation of this amino acid decreases the antagonist activity of hydroxyflutamide[44]. In addition, the chirality of the hydroxyl containing carbon is important in hydrogen bonding to the AR. The substitution of a trifluoromethyl group for

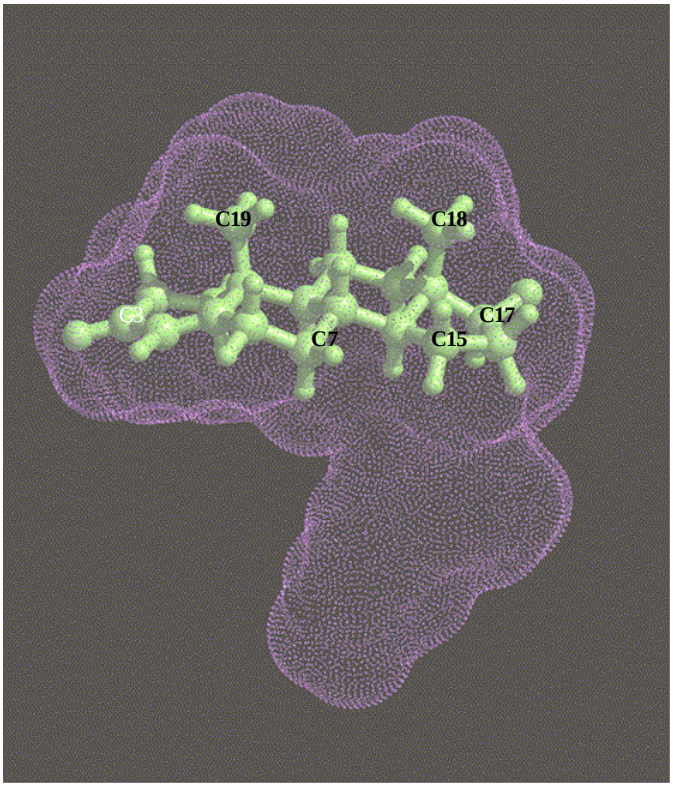

Figure 2.4. Binding of Testosterone to the Ligand Binding Domain of the AR.

A small binding pocket is located under C15 of testosterone bound to AR. The hydroxyl group on C17 may interact with Asn^{705} ; a group which is a crucial to binding of hydroxyflutamide to the AR. Adapted from reference 14.

the methyl group showed a significant improvement in binding, efficacy, and potency. This may be due to the electron-withdrawing properties of this group, increasing the hydrogen donor capacity of the hydroxyl group on the chiral carbon. These studies help to establish new SARs and determine which compounds should be further evaluated in *in vivo* pharmacological studies. Compounds R-1, R-2, R-5, and R-7 showed full *in vitro* agonist activity and high reversible binding.

Wet organ weights of androgen sensitive organs were measured after treatment with testosterone, vehicle or test compound treatments. While none of the compounds restored the organ weight back to that of intact controls, interesting result were seen when comparing testosterone control to the compounds tested. Testosterone treatment restored prostate, and seminal vesicles back to at least that of intact controls, while levator ani weight increased to 70% of intact control. None of the compounds tested showed a significant increase in prostate weight as compared to vehicle control, or testosterone and intact controls. Compounds R-5 and R-6 showed a significant difference in the seminal vesicles from vehicle control, but were also significantly different from testosterone and intact control. Therefore, no physiologically meaningful effect could be seen in seminal vesicles. Two compounds (R-5 and R-7) showed a significant increase in levator ani weight as compared to all controls. Although the test compounds did not restore organ weight back to that of intact controls, these increases were comparable to testosterone treatment ($p = 0.05$). A dose response study would help elucidate the extent of pharmacologic effect seen in these compounds.

The mechanism by which these compounds show selectivity is still unknown. Many factor such as pharmacokinetics, metabolism, *in vivo* drug disposition, or

coactivator/corepressor recruitment, could influence the selective anabolic nature seen in these compounds. It is important to note that there is only one AR isoform identified in humans. Therefore, subtype differences cannot explain the selective affect of these agents, as in the case of estrogens. In accessory sex organs, a majority of the androgenic activity of testosterone is mediated through DHT. Testosterone alone exerts the anabolic effect seen in the muscle, because of the lack of 5α-reductase in muscle tissue. The ability of the compound to recruit specific coactivators/corepressor within these tissue, may explain the anabolic activity seen.

These studies have established new SARs, which can now be used to redesign known SARM and improve their overall pharmacologic activity. In addition, these studies have identified the first non-steroidal anabolic SARM. Later chapters will discuss the impact of additional modification to this initial chemical structure to "fine-tune" its selective activity.

The data presented here is a subset of a much larger series of bicalutamide analogs that were investigated in our laboratory as possible SARMs. After the identification of R-5 and R-7 as possible anabolic SARMs, other *in vitro* and *in vivo* assays helped identify important SARs that led to the discovery of compound S-4. One such metabolic study showed that the R_4 substituent was rapidly cleaved to form an amine. Given that the TFAc group would provide a better leaving group than the Ac group, compound R-7 was not evaluated in further *in vivo* studies. Chapter 3 will discuss that decision to further modify compound R-5 to that of S-4 (Figure 3.2), for pharmacokinetic and metabolic studies. This novel compound was equipotent to DHT in restoration of levator ani muscle weight while having little effect on prostate and seminal

vesicles[72]. This became the lead compound in the investigations that are described in the following chapters.

CHAPTER 3

PHARMACOKINETICS OF S-4, A NOVEL NONSTEROIDAL ANDROGEN AGONIST

3.1. Introduction

After the *in vivo* studies conducted on R-5 and R-7, other members in the laboratory conducted studies on R-1, also known as acetothiolutamide. R-1 demonstrated high binding affinity (Ki = 2.1 nM) and full *in vitro* agonist activity. The identification of R-1 as an androgen agonist prompted the investigation into its pharmacologic activity. Male rats were castrated and then received a subcutaneous injection (1 mg/day) of R-1. After 14 days of drug treatment the animals were sacrificed and the prostate, seminal vesicles, and levator ani were weighed. R-1 has no effect on seminal vesicle weight, but increases levator ani weight. There was a small but significant increase in prostate weight; however, the magnitude of the increase was not considered to be pharmacologically significant. The absence of androgenic effect was further confirmed by the lack of increase in seminal vesicle weight. Although the increase in levator ani weight was indicative of anabolic activity, the magnitude of change was smaller than that of testosterone. These findings were unexpected, given that R-1 showed an *in vitro*

efficacy comparable to that of testosterone. Therefore, pharmacokinetic studies were conducted to determine if factors such as rapid clearance or low subcutaneous bioavailability affected the *in vivo* activity of the compound. The pharmacokinetic studies showed that R-1 was completely systemically available after subcutaneous administration. However, R-1 showed rapid elimination from plasma with a total clearance of 45 ml/min/kg and a plasma half-life ($T_{1/2}$) of less than 30 minutes. Since R-1 was rapidly cleared from the plasma, the concentration at the target tissue may have been too low to elicit a pharmacologic response. In addition to the pharmacologic and pharmacokinetic studies, the metabolic profile of R-1 was also evaluated. LC-MS was used to determine the urinary and fecal metabolites. Analysis showed that oxidation of the thio linkage at R_3 to a sulfone was a major metabolic pathway. This result raised a concern, since sulfone compounds (R-6 and R-8 in Table 2.1) showed low binding affinity and transcriptional activation in *in vitro* assays. When the sulfone analog of R-1 was assayed *in vitro*, it not only showed low binding, but it was also a partial androgen antagonist in the transcriptional cell culture assay. These findings therefore explain the discrepancies seen between *in vitro* and *in vivo* studies.

With the information that R-1 was metabolic converted from agonist to antagonist, structural modifications were made to R-1 in an attempt to protect the R_3 position of the molecule from oxidation. The thio group at position R_3 was replaced with a less metabolically labile oxygen atom. Additionally, the cyano group in the R_1 position was changed to a nitro because of the increased binding affinity observed in prior studies[66]. The resulting novel SARM was S-4 (Figure 3.2). The substitution of the oxygen for the sulfur atom at the R_3 position caused a change in sterochemical notation

according to the Cahn-Ingold-Perlog[72] notation, although there is no change in the absolute configuration. To examine if this molecular change resulted in any change in activity, *in vitro* binding and transcriptional activity assays were conducted. These studies showed that S-4 had a high binding affinity (Ki = 7 nM) and was a full androgen agonist in transcriptional studies. Dose response studies of S-4 in castrated rats showed that it had little effect on restoration of prostate or seminal vesicle weight as compared to testosterone treated control, however, it increased levator ani weight back to that of intact control, when subcutaneous doses of 0.3 mg/day were given (Figure 3.1).

The bioavailability of a new SARM is a key given that the lack of oral bioavailability is one of the disadvantages to testosterone therapy, which limits its use. While 17α-alkylated androgens are orally bioavailable, they are associated with hepatic toxicity and changes in lipoprotein levels, and are therefore not a viable form of therapy[45]. Therefore, an orally bioavailable SARM would permit easier dosing, decrease the incidence of adverse effect associated with the steroidal androgens, while specifically effects the target tissue. Thus, in this chapter we determined the oral bioavailability of S-4.

A dog model was chosen in these studies because of its ease of sampling, and well understood physiology. The overall gross physiology of the stomach and small intestines of dogs are similar to those of man[73]. There are some differences that should be taken into account when using dogs in pharmacokinetics studies. Dogs are poor acid secretors[73-76]. This may affect the oral absorption of drugs with pKa within the pH range of 3 to 7. It was found that the glomerular filtration rate and other urinary excretion parameters are similar to humans[76]. However, hepatic metabolism differs significantly

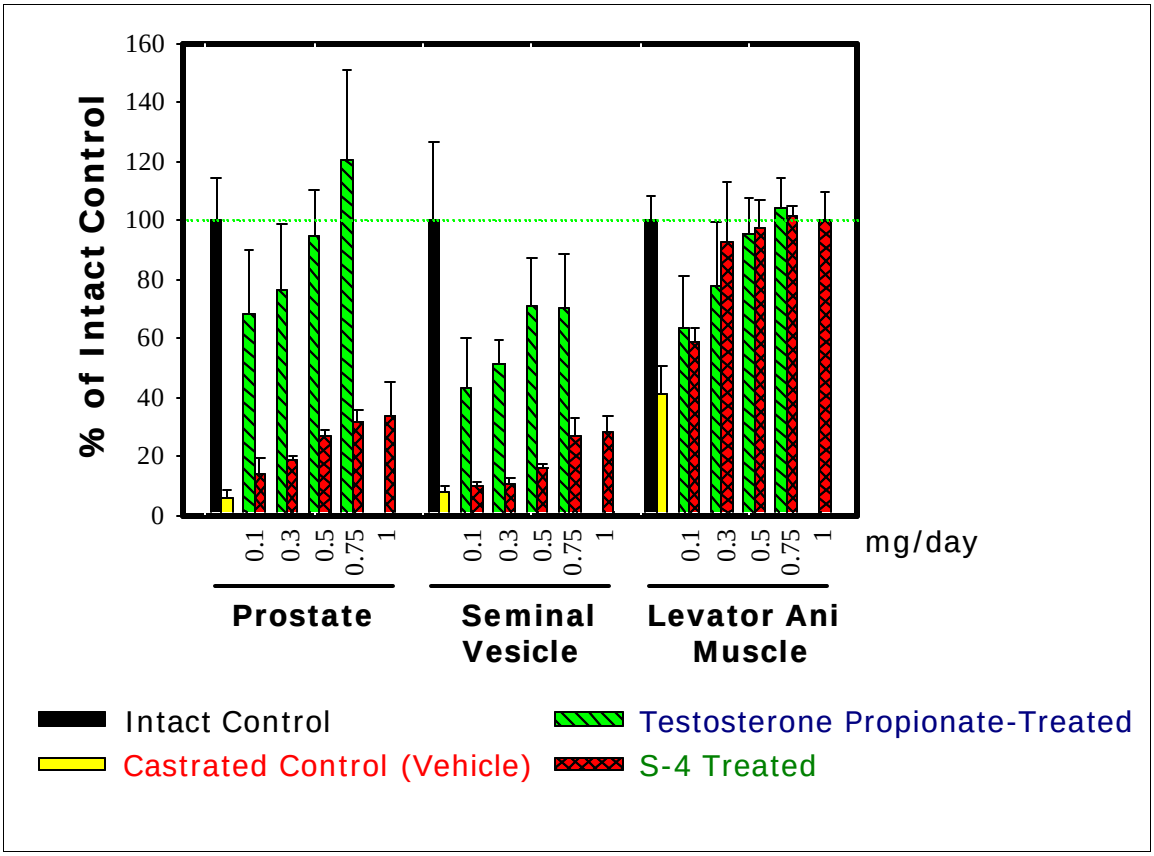

Figure 3.1. Pharmacological Response of S-4 in Rats.

Pharmacological studies of S-4 were conducted in an immature castrated rat model (see section 2.2.8). Seminal vesicles and prostate showed a small increase in wet organ weight as compared to castrated control. While statistically significant, these increases were not pharmacologically significant. S-4 restored the weight of the levator ani muscle back to that of intact and testosterone-treated controls. Adapted from reference 78.

from humans. An example of such a difference can be seen with CYP2B11, which comprises 20% of the total canine hepatic CYP450 content. Comparison of CYP2B11 with the homologues of this enzyme in other species showed marked differences in not only the rate of metabolism of testosterone, but also in the structure of the metabolites formed[77].

3.2. **Materials and Methods**

3.2.1 Chemicals:

Compounds S-4, S-5, and CM-II-87 (Figure 3.2) were synthesized as in Dr. Duane D. Miller's laboratory at the University of Tennessee, College of Pharmacy and as previously reported[71]. The purities of these were confirmed by elemental analysis and mass spectrometry. Polyethylene glycol (PEG) 300 (reagent grade) was purchased from Sigma Aldrich (St. Louis, MO). Ethyl alcohol, acetonitrile, and ethyl acetate were purchased from Fisher Scientific Company (Fair Lawn, NJ).

3.2.2 Animals

Three male and three female beagle dogs were procured from approved vendors through the College of Veterinary Medicine at The Ohio State University (OSU). The animals were 2 to 6 years old and weighed 11.4 to 14.7 kg. Dogs were individually housed in the Animal Care Facility at the College of Veterinary Medicine, and acclimated for at least one week before the study. The animals were maintained on a 12-hour cycle of light and dark, and had free access to food and water unless otherwise stated. The

A.

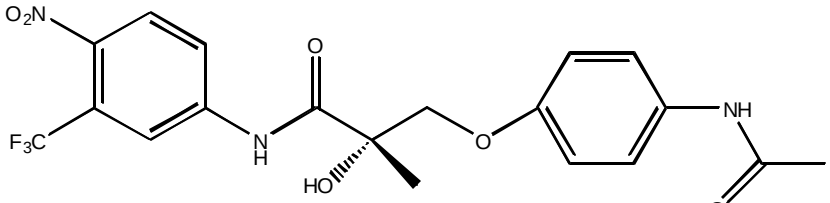

S-4

B.

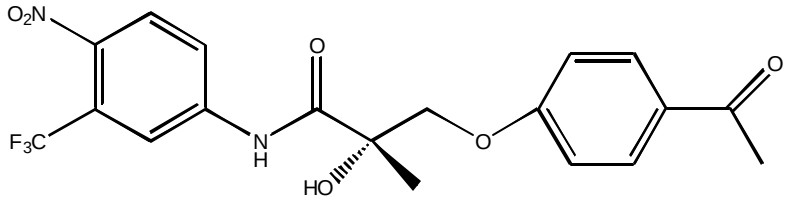

S-5

C.

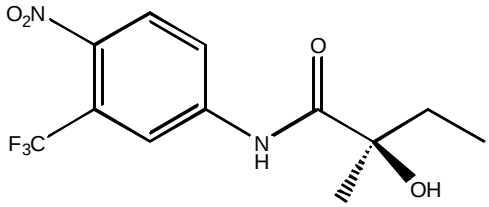

CM-II-87

Figure 3.2. Chemical structures of S-4 and S-5

A. S-4 has a Ki = 7nM and is a full agonist in AR mediated transcriptional activation studies. S-4 has a molecular mass of 441. HPLC and LC/MS assays were developed to quantify S-4 in plasma.
B. S-5 was used as the internal standard in the LC/MS assay because of its similar ionization properties as S-4
C. CM-II-87 was used as the internal standard in the HPLC assay.

animal protocol was reviewed and approved by the Institutional Laboratory Animal Care and Use Committee of OSU.

3.2.3 Plasma Protein Binding

The plasma protein binding of S-4 was determined in rat, dog, and human plasma by ultrafiltration method using centifugal filter devices with YMT membrane (Centrifree® Millipore, Bedford, MA). An aliquot (0.5 mL) of plasma was spiked with appropriate amounts to achieve final concentrations of S-4 of 1, 5, and 10 µg/mL. The plasma samples were incubated at 37 °C for 60 minutes. The plasma samples were then placed in centrifugational devices and centrifuged at 2000g, 25 °C for 20 minutes. Internal standard was added to each sample and extracted by the method stated in section 3.2.6. The concentration of S-4 was determined by HPLC as described in section 3.2.7. The amount of S-4 adsorbed onto the filtration device and membrane was determined by comparing S-4 concentration in deionized water before and after ultrafiltration. The percentage of S-4 bound to plasma proteins (PB%) was determined using the following equation:

$$PB\% = \left(1 - \left(A_{free} \Big/ \left(A_{total} - A_{adsorption}\right)\right)\right) * 100$$

where A_{total} and A_{free} were the total and free amounts of S-4 at equilibrium, and $A_{adsorption}$ was the amount of S-4 adsorbed to the filtration device and membrane at each concentration.

3.2.4 Pharmacokinetic Study #1

A four treatment, four period crossover design was used to determine the pharmacokinetics of S-4 in six beagle dogs. Dogs were randomly assigned to a treatment group with a one-week washout period after each dose. Intravenous (IV) bolus dose of 3 or 10 mg/kg, an oral (PO) solution dose of 10 mg/kg, or an oral capsule dose of 10 mg/kg administered in a packed gelatin capsule (size 0) were administered during this study. Each animal was weighed prior to dosing. Animals were placed in metabolism cages 18 hours prior to dosing and for up to 72 hours after the dose was administered. Animals were fasted for 18 hours prior to dosing and for 8 hours after the dose were administered. Animals were allowed water *ad libitum*. Oral and intravenous solutions were freshly prepared by aseptic methods. An appropriate quantity of S-4 was weighed and dissolved in ethanol and diluted to a final volume of 3 mL with PEG 300. Ethyl alcohol content did not exceed 5% of the final volume. Solutions were stored at 4°C and used within 24 hours. The gelatin capsule doses were prepared by weighing an appropriate amount of S-4 powder and loosely packing a size 0 gelatin capsule. Angiocatheters were placed in the right saphenous vein of the dog for blood collection. Intravenous doses were administered as bolus doses through the left saphenous vein. Oral doses were administered by gavage followed by a 10 mL water flush. Blood samples (5 mL) were collected into heparinized vacutainers prior to the dose and at 2, 5, 10, 15, 30, 60, 120, 240, 360, 480, 600, 1440, 2880, and 4320 minutes after IV doses and at 10, 30, 60, 90, 120, 180, 240, 300, 360, 480, 600, 1440, 2880, and 4320 minutes after PO doses. Blood samples were immediately centrifuged at 2000g for 10 minutes and the plasma collected and stored at –20°C until analysis.

3.2.5 Pharmacokinetics Study #2:

The lack of bioavailability (Section 3.3.2) at low doses of S-4 prompted a second pharmacokinetic study. A three treatment, three period crossover design was used to determine the bioavailability of S-4 in four beagle dogs weighing approximately 12 kg. Dogs were randomly assigned to a treatment group with a one-week wash-out period after each dose of either an intravenous (IV) dose of 1 mg/kg or an oral (PO) dose of 1 or 0.1 mg/kg. Each animal was weighed prior to dosing. Animals were placed in metabolism cages 18 hours prior to dosing and remained there until 24 hours after the dose was administered. Animals were fasted for 18 hours prior to dosing and 8 hours after the dose was administered. Animals were allowed water *ad libitum*. Oral and intravenous solutions were freshly prepared by aseptic methods. An appropriate quantity of S-4 was weighed and dissolved in ethanol and diluted to a final volume of 3 mL with PEG 300. Ethyl alcohol content did not exceed 5% of the final volume. Solutions were stored at 4°C and used within 24 hours. Angiocatheters were placed in the right saphenous vein of the dog for blood collection. Intravenous doses were administered as bolus doses through the left saphenous vein. Oral solution doses were administered by oral gavage followed by a 10 mL water flush. Blood samples (5 mL) were collected into heparinized vacutainers prior to the dose and at 2, 5, 10, 15, 30, 60, 120, 240, 360, 480, 600, and 1440 minutes after IV doses and at 10, 30, 60, 90, 120, 180, 240, 300, 360, 480, 600, and 1440 minutes after PO doses. Blood samples were immediately centrifuged at 2000g for 10 minutes and the plasma collected and stored at –20°C until analysis.

3.2.6 Sample Preparation

An aliquot (0.5 mL) of plasma was spiked with an internal standard (S-5 or CM-II-87, Figure 3.2) and mixed with two volumes of acetonitrile to precipitate plasma proteins. The samples were centrifuged at 2000g for 5 minutes, and the supernatants were removed and then mixed with 7 mL of ethyl acetate for 40 minutes on a shaker. The samples were then centrifuged at 2000g for 5 minutes to facilitate phase separation. The organic phase was collected and evaporated under a stream of nitrogen gas. The residue was reconstituted in 100µL of mobile phase. An aliquot (20 µL) was injected and analyzed by high pressure liquid chromatography (HPLC) or liquid chromatography/mass spectrometry (LC/MS).

3.2.7 HPLC Analysis Method

An aliquot (100 µL) of each sample was injected onto a Nova-pak® C_{18} column (3.9 mm X 150 mm, 4 µm particle size, Waters Corp., Milford, MA), and eluted with a mobile phase containing acetonitrile: water (35:65, v/v) at a flow rate of 1.0 mL/min. The UV absorbance of the eluents was monitored at 270 nm. The HPLC system consisted of a Waters Model 510 solvent pump, a Waters Model 717 autosampler, and a Waters Model 486 absorbance detector. Calibration standards were prepared in untreated dog plasma with S-4 concentrations ranging from 0.08 to 200 µg/mL. Standard curve samples were run in triplicate along with each sample run. The coefficients of variation of the assay, both intra-day and inter-day, were below 15% at all concentrations (Table 3.1).

S-4 Concentration μg/mL	Average Coefficients of Variation	
	Intra-day	Inter-day
0.08	6.4	4.5
0.2	8.5	7.7
0.4	7.3	14.2
2	4.6	6.5
4	3.5	8.8
10	3.2	6.7
16	5.2	8.4
20	3.4	7.8

Table 3.1. Validation for HPLC assay of S-4.

The coefficients of variation were determined between days and within days. The data above was produced from 9 separate runs, analyzed in triplicate.

3.2.8 LC/MS Analysis Method

Since it was anticipated that the second pharmacokinetic study would involve doses of S-4 that would produce plasma concentrations lower than the limit-of-quantitation of the HPLC assay (0.08 µg/mL), a separate LC/MS assay was developed. An aliquot (20 µL) of each sample was injected into a Zorbax® Phenyl column (2.1 mm X 50mm length, 3.5 µm particle size, Waters) and eluted with a gradient mobile phase consisting of water and methanol. At the beginning of each chromatographic run, the mobile phase consisted of 10% methanol and 90% water. The percentage of methanol was increased to 100% over 20 minutes and held at this concentration for 5 minutes at a flow rate of 0.300 mL/min. LC/MS analysis was performed on a ThermoFinnigan LCQ Deca Ion Trap System, which consisted of a Surveyor Pump, Surveyor Autosampler, Surveyor PDA coupled to a LCQ Deca Ion Trap mass detector using an atmospheric pressure chemical ionization (APCI) interface. Data acquisition was controlled by Xcaliber software. The un-split elute was introduced into the mass spectrometer APCI interface that was set at the following conditions: vaporization temperature 450°C, sheath gas (nitrogen) flow 660 mL/min, auxiliary gas (nitrogen) flow 60 mL/min, discharge current 10µA, capillary temperature 150°C, capillary voltage –19.00V, tube lens offset 35.00V, multipole 1 offset 2.25V, lens voltage 88 V, multipole 2 offset 16.5 V, multipole RF amplitude 510.0 V p-p, entrance lens voltage 30 V, and electron multiplier voltage –900.0 V All analyses were conducted in negative ion mode. The scan range for full-scan spectrometry analysis was from 100-2000 m/z. For MS^2 analysis, precursor ions were isolated with a width of 4 m/z and fragmented with a fragmentation voltage of 26 V. Calibration standards were prepared in untreated dog plasma with S-4 concentrations

ranging from 4 to 1,000 ng/ml. Standard curve samples were run in triplicate along with each sample run. The standard curves were linear with a coefficient of determination ≥ 0.997. Intra and inter day variabilities were <20% at all concentrations (Table 3.2).

3.2.9 Data Analysis

The plasma concentration-time profiles for each animal were analyzed by noncompartmental methods using WinNonlin (version 3.1, Pharsight, Mountain View, CA). The area under the concentration-time curve (AUC) was calculated using the trapezoidal rule with extrapolation to time infinity. The terminal elimination half-life ($T_{1/2}^{?}$) was calculated from $T_{1/2}^{?} = 0.693/?$, where ? is the terminal elimination rate constant. The plasma clearance (CL) was calculated as $CL = Dose_{iv}/AUC_{0-\infty, iv}$, where $Dose_{iv}$ and $AUC_{0-\infty, iv}$ were the intravenous dose and the corresponding area under the curve from time 0 to infinity, respectively. The apparent volume of distribution at equilibrium (V_{ss}) was calculated by:

$$V_{ss} = Dose * AUMC_{0-\infty,} / (AUC_{0-\infty})^2$$

where $AUMC_{0-\infty}$ was the area under the first moment of the plasma concentration-time curve extrapolated to infinity. The mean residence time (MRT) was calculated as:

$$MRT = AUMC_{0-\infty} / AUC_{0-\infty}$$

Oral bioavailability (F_{sc}) was calculated as:

$$F_{sc} = (AUC_{0-\infty, po} * Dose_{iv}) / (AUC_{0-\infty, iv} * Dose_{po})$$

where $Dose_{po}$ and $AUC_{0-\infty, po}$ were the oral dose and the corresponding area under the curve from time 0 to infinity, respectively.

S-4 Concentration (ng/mL)	Average Coefficients of Variation	
	Inter-day	Intra-day
4	10.5	13.2
10	9.8	14.4
20	19.6	11.2
40	7.5	9.1
200	17.6	8.4
400	8.7	8.1
1000	19.8	8.1

Table 3.2. Validation of LC/MS assay for S-4.

The coefficients of variation were determined between days and within days. The data above was produced from 4 separate run, analyzed in triplicate.

3.2.10 Statistical Analysis

Statistical analyses were performed using single factor ANOVA. P-values less than 0.05 were considered as statistically significant.

3.3. Results

3.3.1 Plasma Protein Binding

Plasma protein binding of S-4 in rats, dogs and humans were determined in order to gain insight into the pharmacokinetic determinants of its disposition. From these studies, it was determined that S-4 was highly bound to rat, dog and human plasma proteins (>99%). Binding was independent of plasma concentrations over the range of 1 to 10 µg/mL. Table 3.3 summarizes the results of these studies.

3.3.2 Results of Pharmacokinetic Study #1

Plasma concentrations after IV doses declined in a bi-exponential manner, and the drug concentration remained detectable for up to 600 minutes after the dose. Concentration-time profiles for S-4 after IV administration are shown in Figure 3.3. Pharmacokinetic parameters determined after the IV doses are presented in Table 3.4. The mean total clearance (CL) of S-4 after IV administration was 4.4 mL/min/kg. There was a significant difference in CL and $AUC_{0-\infty}$ in female dogs after a 3 mg/kg IV dose as compared to male dogs. However, these differences were not seen after the 10 mg/kg IV dose. In general the plasma concentrations in female dogs was higher than male dogs, but

Species	Concentration	PB%
Rat	10	99.4
	5	99.5
	1	ND
Dog	10	98.2
	5	98.9
	1	99.4
Human	10	97.9
	5	99.3
	1	99.6

ND No S-4 peak was detectable at this concentration

Table 3.3. Plasma Protein Binding of S-4

Plasma protein binding was calculated in three species (rat, dog, and human) at 10, 5, and 1 μg/mL. No concentration dependent plasma protein binding was seen. Average plasma protein binding was >99%.

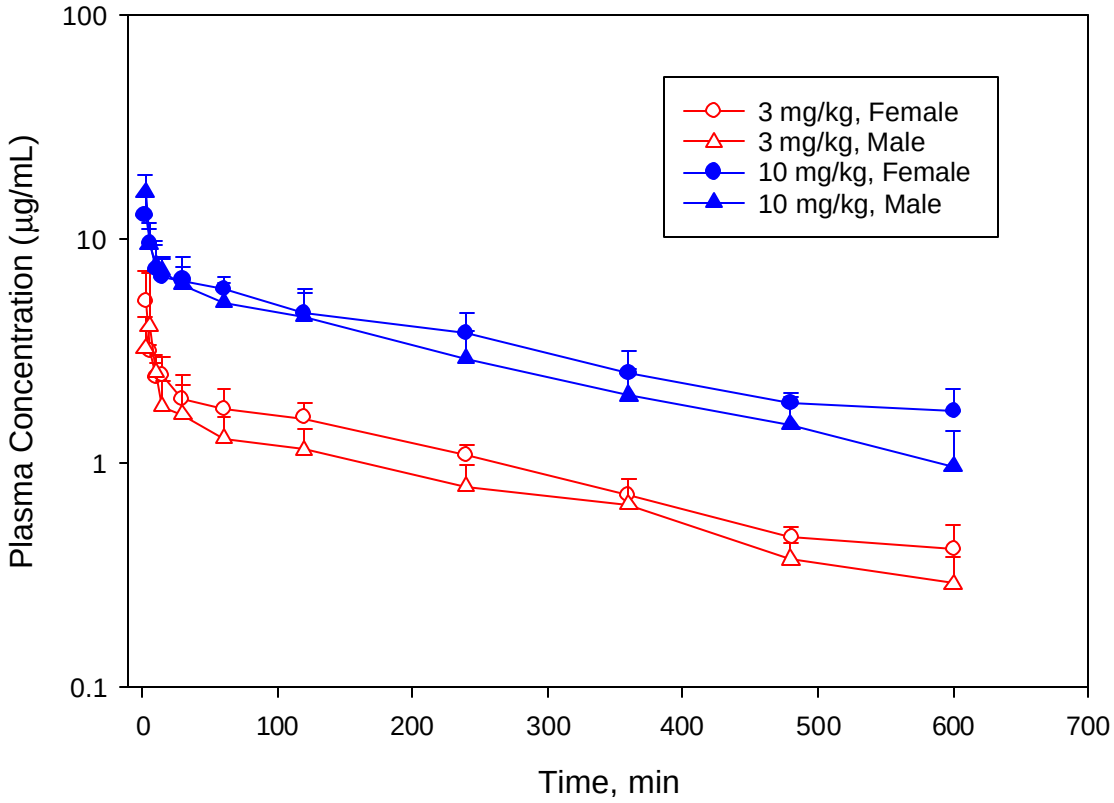

Figure 3.3. Concentration-Time Profiles of S-4 After IV Administration.

Plasma concentrations declined bi-exponentially after IV administration of S-4. Pharmacokinetic parameters were calculated for each animal individually. The concentration-time profiles show the average concentration and standard deviation at each point. Significant differences in CL and AUC were seen between genders after the 3 mg/kg dose. However these differences were not seen after the 10 mg/kg dose.

Parameter	Dose, mg/kg					
	3			10		
	Male (n=3)	Female (n =3)	All	Male (n=3)	Female (n =3)	All
$AUC_{0-\infty}$ (μg•min/mL)	571 ± 59	757 ± 92 *	664 ± 123	2352 ± 724	2642 ± 389	2497 ± 544
MRT (min)	308 ± 63	305 ± 31	306 ± 45	331 ± 63	364 ± 38	348 ± 50
$T_{1/2}^{\lambda}$ (min)	222 ± 45	203 ± 26	213 ± 34	238 ± 65	247 ± 14	242 ± 42
CL (mL/min/kg)	5.3 ± 0.6	4.0 ± 0.5 *	4.6 ± 0.9	4.5 ± 1.2	3.8 ± 0.6	4.2 ± 0.9
V_{ss} (L/kg)	1.6 ± 0.4	1.2 ± 0.1	1.4 ± 0.3	1.4 ± 0.3	1.4 ± 0.4	1.4 ± 0.3

* Statistically significant difference from the male (p=0.04)

Table 3.4. Plasma Concentration-Time profile after administration of an Oral Solution of S-4 at 10 mg/kg.

Significant differences in AUC and CL were seen between genders after the 3 mg/mg IV dose. These differences were not seen after the 10 mg/kg dose. Therefore, we concluded that no gender differences were seen, possibly due to the small number of animals used in this study.

these difference were not statistically different. Even though there were gender differences after the 3 mg/kg dose, we concluded that the elimination of S-4 was not gender-dependent because these difference were not seen at the higher dose. The mean terminal $T_{1/2}$ and Vss were 221 min and 1.4 L/kg, respectively. These parameters were not significantly different between the doses given, indicating no dose-dependent pharmacokinetics for S-4 within this range.

S-4 showed a rapid increase in plasma concentrations after PO administration, suggesting rapid absorption. Figure 3.4 shows the plasma concentration-time profile for S-4 following a 10 mg/kg oral solution dose of S-4. Table 3.5 summarizes the pharmacokinetic parameters of S-4, following the 10 mg/kg PO dose in male and female dogs. The mean elimination $T_{1/2}$ was 234 min with a C_{max} of 2.5 μg/mL at a T_{max} of 110 min (T_{max} varied from 30 to 180 min between individual animals). The mean oral clearance (CL/F) after PO administration was 12.1 mL/min/kg, with an oral bioavailability of 38%. In general, plasma concentrations in females were higher than those in males. This can be seen in the increase MRT and $AUC_{0-\infty}$ values. However, these differences were not statistically significant, given the low number of animals in the study or the high inter-individual variability. Thus, no statistically significant gender-related differences in pharmacokinetics parameters were seen after the 10 mg/kg oral dose.

S-4 was also administered as a packed gelatin capsule. Figure 3.5 shows the plasma concentration-time profile for individual animals, since some time points were below the limit of quantitation for the HPLC assay. Table 3.6 presents the pharmacokinetic parameters after administration of the capsule dose. Given only two

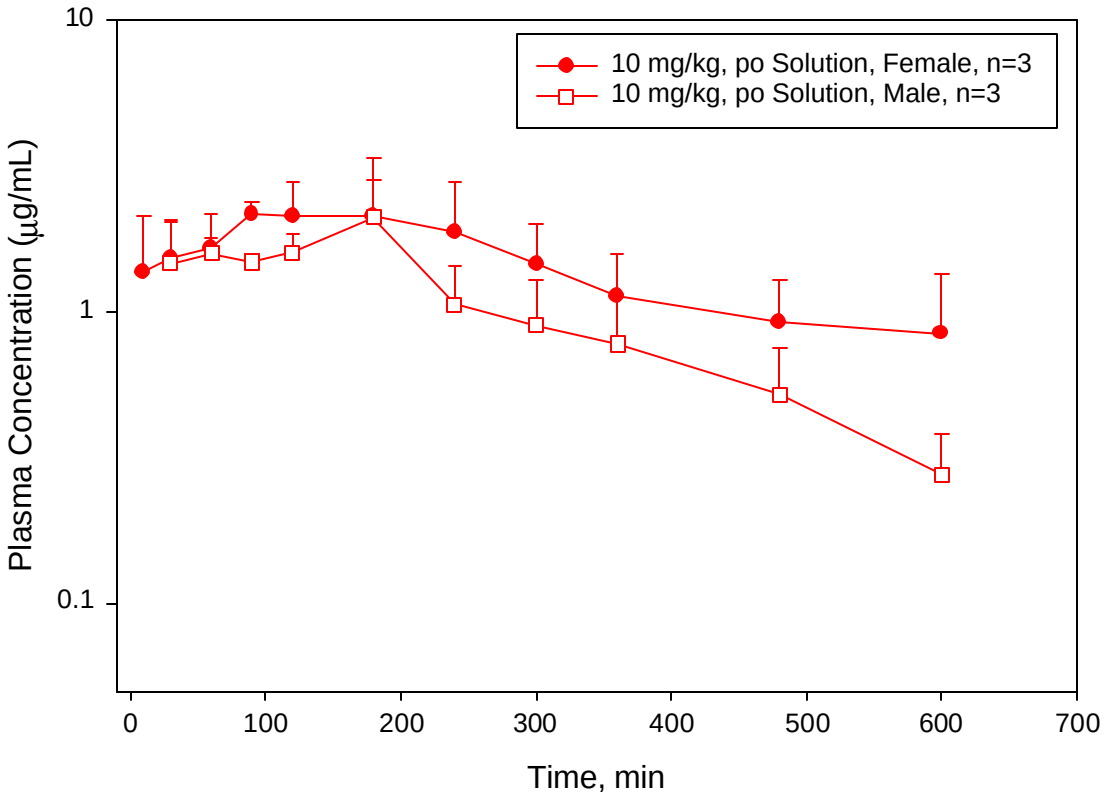

Figure 3.4. Plasma Concentration-Time profile after administration of an Oral Solution of S-4 at 10 mg/kg.

Plasma concentrations increased to a C_{max} of 2.5 µg/mL at a T_{max} of 110 min. No significant difference was found between genders. S-4 had a bioavailability of 38% after the 10 mg/kg oral solution dose.

Parameters	10 mg/kg Solution		
	Male (n=3)	Female (n=3)	All
T_{max} (min)	110 ± 75	110 ± 62	110 ± 62
C_{max} (µg/mL)	2.5 ± 0.9	2.5 ± 0.4	2.5 ± 0.6
$AUC_{0-\infty}$ (µg•min/mL)	733 ± 274	1147 ± 339	940 ± 357
MRT (min)	334 ± 96	430 ± 42	382 ± 85
$T_{1/2}{}^{\lambda}$ (min)	217 ± 64	252 ± 30	234 ± 49
CL/F (mL/min/kg)	15.0 ± 5.5	9.2 ± 2.4	12.1 ± 5.0
V_z/F (L/kg)	4.4 ± 0.7	3.4 ± 1.1	3.9 ± 1.0
F (%)	32 ± 6	43 ± 9	38 ± 9

Table 3.5. Pharmacokinetic Parameters after a PO dose of S-4 at 10 mg/kg.

No gender-related differences in pharmacokinetics were seen. Plasma concentration profiles of females were generally higher than those of males, but these differences were not statistically significant.

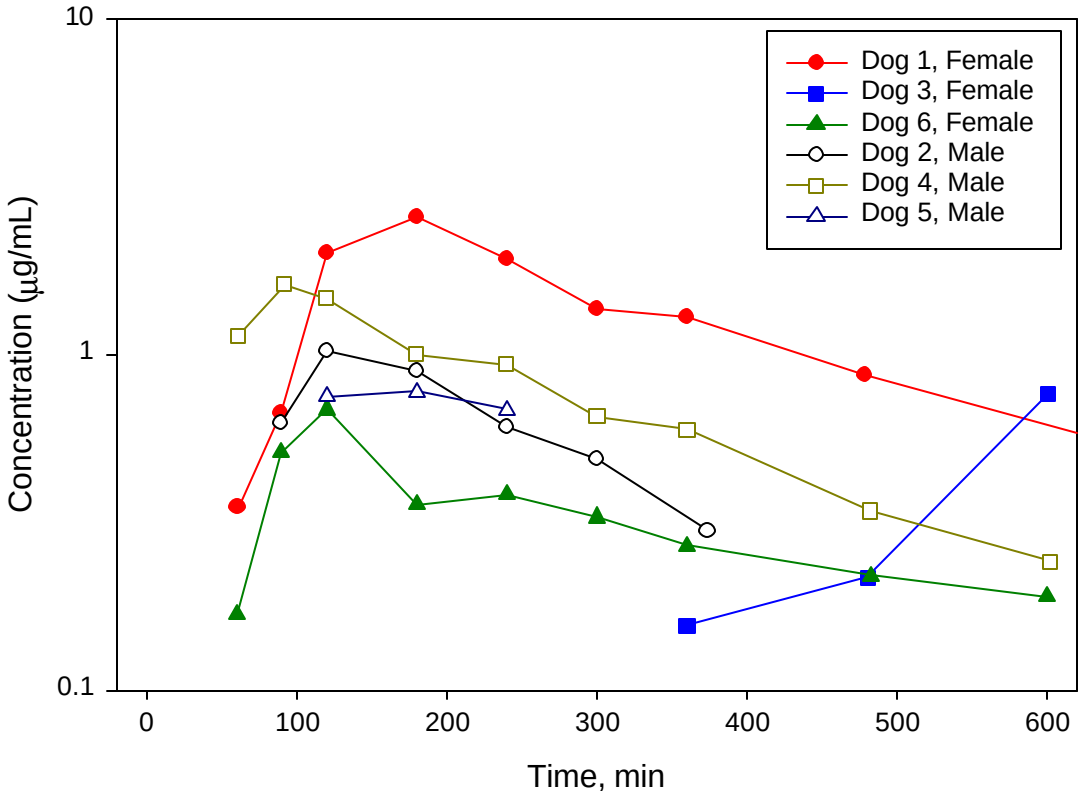

Figure 3.5. Plasma Concentration-Time Profiles for individual Animals After PO Administration of S-4 with capsule.

The concentration-time profiles after capsule administration showed erratic absorption. Only 2 profiles of each gender were complete, therefore no statistical analysis could be preformed.

	Capsule		
	Male (n=2)	Female (n=2)	All (n=4)
T_{max} (min)	106	150	128 ± 37
C_{max} (μg/mL)	1.3	1.6	1.5 ± 0.8
$AUC_{0-\infty}$ (μg•min/mL)	382	596	489 ± 304
MRT (min)	289	487	388 ± 133
$T_{1/2}{}^{\lambda}$ (min)	157	288	227 ± 100
CL/F (mL/min/kg)	28.0	24.5	26.2 ± 13.1 *
V_z/F (L/kg)	6.0	11.6	8.8 ± 7.5
F (%)	15	23	19 ± 10 *

* Significantly different from oral solution

Table 3.6. Relevant Pharmacokinetic Parameters after administration of a PO capsule.

Overall oral CL and bioavailability were significantly different from those of the oral solution at 10 mg/kg, suggesting of a solubility problem with the capsule formulation within the gastrointestinal tract.

animals of each gender had a complete plasma concentration-time profile no statistical analysis was done between genders. Significant differences in pharmacokinetic parameters were seen between the capsule formulation and the oral solution. Bioavailability was much lower for the capsule (19% for capsule versus 38% for oral solution), and oral CL was 2 times that seen with oral solution. Erratic absorption of the capsule formulation of S-4 was suggestive of a dissolution problem with the compound at the intestinal site.

3.3.3 Results of Pharmacokinetic Study #2

Initial pharmacokinetic studies were conducted with IV doses of 3 and 10 mg/kg. These were equivalent to or exceeded the highest dose of S-4 used in the pharmacologic activity study (1 mg/day in 250g rats). Pharmacokinetic studies of bicalutamide in beagle dogs showed dose dependent bioavailability. Given that pharmacologic activity was seen in doses as low as 0.3 mg/day of S-4, we were interested in the bioavailability of S-4 at these doses. Therefore, a second pharmacokinetic study was conducted and the result combined with those in the first study.

After a single IV bolus dose of 1mg/kg, the concentrations of S-4 declined rapidly in a biexponential manner. Concentrations of S-4 were detectable at 600 minutes post-dose in all animals (Figure 3.6). No statistically significant differences were found between clearance, volume on distribution or $T_{1/2}$ for all doses, with the mean values over dosing range of 0.1 to 10 mg/kg being 4.6 mL/min/kg, 1.4 L/kg and 200 min. respectively. The clearance and $T_{1/2}$ after the 0.1mg/kg dose appear to be difference from the higher doses. However these differences are not statistically significant. This may be

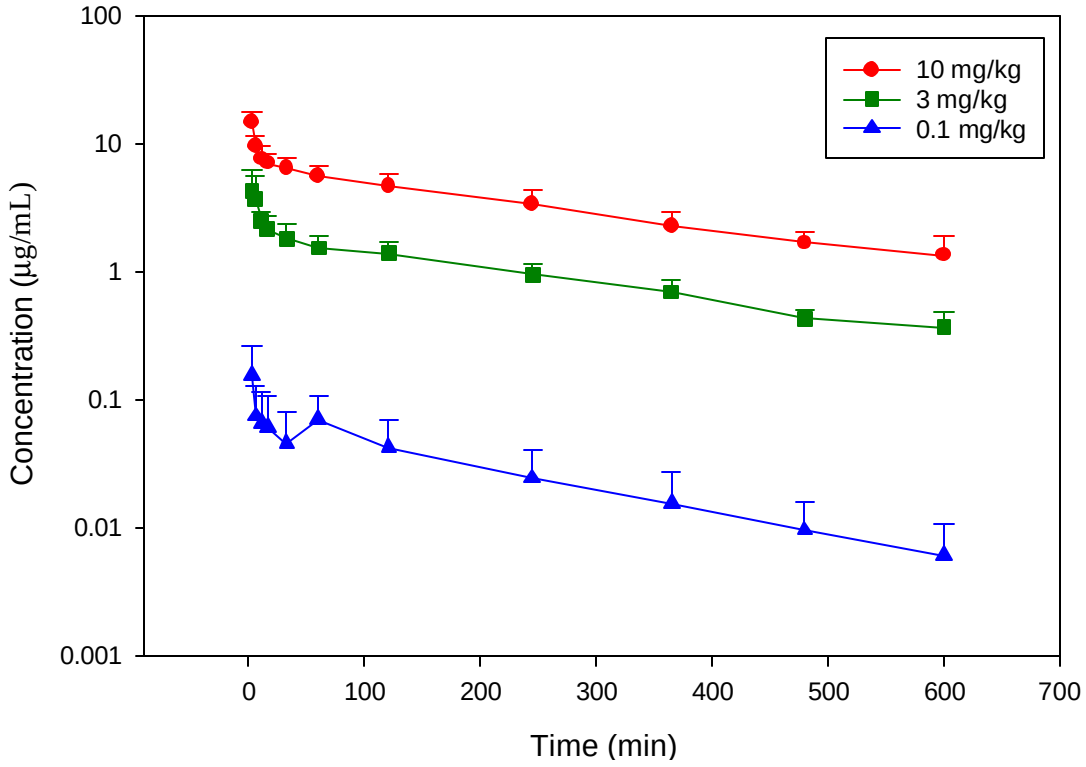

Figure 3.6. Concentration Time Profiles After All IV Doses.

The concentration-time profile after the 0.1 mg/kg dose in study 2 was compared to the 10 and 3 mg/kg dose of study 1. Pharmacokinetic parameters were calculated for each animal individually. The concentration-time profiles show the average concentration and standard deviation at each point.

due to the high variability in these parameters at the lowest dose. $AUC_{0-\infty}$ increased proportionally to dose, demonstrating linear pharmacokinetics over the IV dosing range of 0.1 to 10 mg/kg. The pharmacokinetic parameters of S-4 after IV administration are summarized in Table 3.7.

After oral solution doses of 1 and 0.1 mg/kg, plasma concentrations increased slowly and then decreased monexponentially (Figure 3.7). Interestingly, the T_{max} for the 1 and 0.1 mg/kg PO doses were not significantly different at 60 and 53.5 minutes respectively, while the T_{max} for the 10-mg/kg PO dose was significantly longer at 110 minutes, indicating decreased solubility at the highest oral dose. Oral clearance and oral $T_{1/2}$ were significantly different between all doses. In addition the AUC did not increase proportionately with dose. This would be suggestive of nonlinear pharmacokinetics over the PO dosing range. However, the calculation of oral bioavailability showed a dose dependant pattern. The pharmacokinetic parameters of S-4 after PO administration are summarized in Table 3.8.

3.4. Discussion

S-4 is a structural analog of bicalutamide. However, its pharmacokinetics was quite different than that of bicalutamide. Bicalutamide has a plasma $T_{1/2}$ of 7 days in dogs after IV administration[79]. The $T_{1/2}$ of S-4 is shorter at 3.5 to 4 hours after IV administration. This difference is due to rapid clearance of S-4 from plasma. S-4 showed a plasma clearance and $T_{1/2}$ of 4.7 mL/min/kg and 200 min. respectively and R-

Parameters	Dose (mg/kg)		
	10	3	0.1
AUC (µg*min/mL)	2497 ± 544	664 ± 123	21.1 ± 7.2
$T_{1/2}$? (min)	242 ± 42	213 ± 34	143 ± 97
CL (mL/min/kg)	4.2 ± 0.9	4.6 ± 0.9	5.2 ± 1.9
V_{ss} (L/kg)	1.4 ± 0.3	1.4 ± 0.3	1.3 ± 0.5

Table 3.7. Relevant Pharmacokinetic parameters after All IV Doses.

The pharmacokinetic parameters after the 0.1 mg/kg dose in study 2 were compared to the pharmacokinetic parameter following the 3 and 10 mg/kg doses of study 1. Given that AUC value of each dose was proportionally to dose and no significant difference in CL between doses was seen, the IV doses showed linear pharmacokinetics.

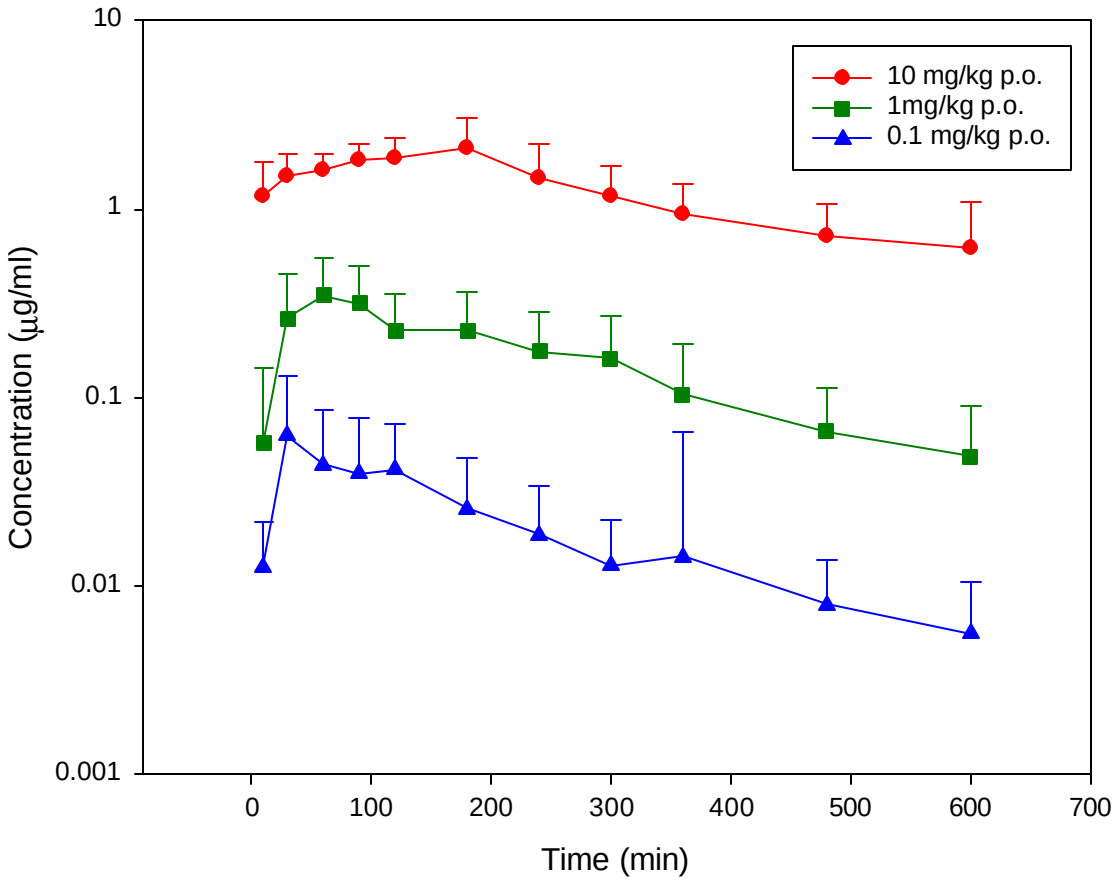

Figure 3.7. Plasma Concentration-Time Profiles After All Oral Doses of S-4.

The concentration-time profile after the 0.1 and 1 mg/kg dose in study 2 was compared to the 10 mg/kg dose of study 1. Pharmacokinetic parameters were calculated for each animal individually. The concentration-time profiles show the average concentration and standard deviation at each point.

Parameters	Dose (mg/kg)		
	10	1	0.1
AUC (μg*min/mL)	940 ± 357[a]	131.5 ± 31.8[a]	19.2 ± 7.5[a]
$T_{1/2}$? (min)	234 ± 49	161 ± 27	335 ± 254
CL/F (mL/min/kg)	12.1 ± 5.0[b]	5.5 ± 3.1[b]	3.6 ± 1.6[b]
V_z/F (L/kg)	3.9 ± 1.0[b]	1.3 ± 0.76[b]	1.7 ± 1.6[b]
C_{max} (μg/mL)	2.5 ± 0.62	0.460 ± 0.03	0.083 ± 0.06
T_{max} (min)	110[c]	53.5	60
F (%)	38	62	91

a. AUC did not change proportionally to dose.
b. Oral CL between doses was significantly different (p=0.05)
c. T_{max} was significantly longer at 10 mg/kg dose.

Table 3.8. Relevant Pharmacokinetic Parameters After All PO Doses of S-4

S-4 bioavailability increased to 91% at the lowest dose administered. The 10 mg/kg PO dose showed a significantly longer $T_{1/2}$, suggesting decrease absorption rate at higher doses.

bicalutamide has a clearance and $T_{1/2}$ of 0.8mL/min/kg and 1 day respectively. This is further evidenced by the relatively small difference in volume of distribution between S-4 and bicalutamide (1.4 L/kg for 3 mg/kg dose of S-4 and 0.8 L/kg for a 2.5 mg/kg dose of bicalutamide).

The low oral bioavailability seen at the 10 mg/kg dose of S-4 in dogs was unexpected considering the mean clearance of S-4 after an IV dose was 4.7 mL/hr/kg. Assuming all clearance of drug is hepatic, the hepatic extraction ratio of S-4 would be less than 0.15 (the hepatic blood flow in the dog is 30.9 mL/min/kg[80]). This would suggest that the oral bioavailability of S-4 should be approximately 85%. The decreased bioavailability seen after oral doses of S-4 may be attributed to several reasons: 1) low aqueous solubility of the compound in the gastrointestinal tract, 2) active transporter mediated efflux in the GI membrane, and 3) pre-systemic degradation of the compound. High oral bioavailability is a key issue in the development of this compound as a novel nonsteroidal SARM, given that oral bioavailability is a disadvantage of testosterone therapy. Studies by Cockshott *et al.*[77] showed dose dependent oral bioavailability of bicalutamide in both rats and dogs. This led to the investigation of oral bioavailability of S-4 at lower oral doses. The increase in oral bioavailability of S-4 as the dose of S-4 decreases suggests that aqueous solubility in the GI tract is responsible for the low oral bioavailability seen at higher doses. These finding are supported by the low bioavailability seen after the capsule dosing as well as the increase in T_{max} at the higher PO doses of S-4. Giving S-4 in a capsule causes larger particle size within the gastrointestinal tract and therefore lower solubility. The pharmacologic activity study

showed that S-4 showed anabolic activity at doses below 1 mg/day. At these lower doses, S-4 would show high bioavailablity.

In addition to the pharmacokinetic studies, plasma protein binding was determined in three species. Plasma protein binding assays showed that S-4 was highly bound in the plasma of rats, dogs and humans. Extensive plasma protein binding can decrease the systemic clearance of drugs that have a low intrinsic hepatic clearance, decrease the rate of glomerular filtration, and influence the volume of distribution of the drug. S-4 showed a large volume of distribution (mean value 1.4 L/kg) given that the total body water of a dog is 0.6 L/kg[80]. Since S-4 has a low extraction ratio, its clearance is determined by the intrinsic clearance of the drug and the fraction of drug unbound in plasma. Therefore factors that affect the protein binding of this compound could change the rate of clearance.

From these studies we ascertained that the pharmacokinetics of S-4 were favorably influenced by the substitution of the oxygen atom for the sulfur atom in the R_3 position (i.e. increase in half-life and decrease in clearance). The following chapter will explore the final disposition and metabolism of S-4 in rats and dogs. These studies will determine if the oxygen substitution protected the labile R_3 position for enzymatic degradation, thereby preventing the conversion of the AR agonist to an antagoinst.

CHAPTER 4

THE METABOLISM AND DISPOSITION OF A STRUCTURALLY OPTIMIZED SELECTIVE ANDROGEN RECEPTOR MODULATOR, S-4.

4.1. Introduction

In vitro studies with acetothiolutamide (compound R-1 in Table 2.1) showed that it was a potent androgen agonist that bound tightly to the AR[78]. However, *in vivo* pharmacological studies showed that this compound was inactive. Pharmacokinetic and metabolic studies demonstrated that the inconsistency between *in vivo* and *in vitro* pharmacologic activity was caused by the rapid clearance and conversion of R-1 to an androgen antagonist. We hypothesized that the substitution of the labile sulfur atom with an oxygen atom would create an androgen agonist whose pharmacokinetics and metabolism would not alter its *in vivo* activity. A structurally optimized AR ligand, S-4, was designed and synthesized in an attempt to mimic the favorable structure-activity relationships identified for R-1, protect labile sites from *in vivo* metabolism, and determine whether AR ligands with *in vivo* pharmacologic activity could be achieved. The studies described in this chapter were designed to qualitatively and quantitatively identify the metabolites of S-4 in rats and dogs, as a first step toward testing this hypothesis.

The lead compound S-4 and compound R-1 were designed as an analog of bicalutamide, an antiandrogen used in the clinical management of prostate cancer. Therefore, evaluation of the metabolism of bicalutamide should be considered when investigating the metabolic profile of S-4 to determine if any of its metabolites contain possible AR antagonist activity. The metabolic profile of bicalutamide showed differences between species. Figure 4.2 shows the proposed metabolic profile of bicalutamide in several species[81]. We noted numerous similarities and differences in the metabolism and disposition of S-4 as compared to bicalutamide. Studies by Boyle et al. showed that 20 to 30% of the dose given to rats and mice was cleaved by hydrolysis to yield metabolites 1 and 2, while little of these metabolites was seen in dogs or rabbits. Bicalutamide is also highly glucuronidated in all species. While rats and mice excrete these phase II metabolites into the feces, humans and dogs excrete the glucuronidated bicalutamide metabolites into the urine[81]. This may be due to the species differences in the minimum molecular weight threshold requirements for excretion of metabolites into the bile[82].

In addition to determining the metabolic profile of S-4, it is also important to determine the disposition of these metabolites. Although some of the metabolites formed from S-4 may have antagonist activity, their concentration at the site of action may be negligible. Therefore, evaluation of the final metabolic path and quantitation of the metabolites within each pathway will allow a more complete understanding of pharmacologic relevance of the metabolites of S-4.

A clinically viable SARM must have therapeutic efficacy, a favorable pharmacokinetic profile, and be orally bioavailable, while devoid of many of the sid

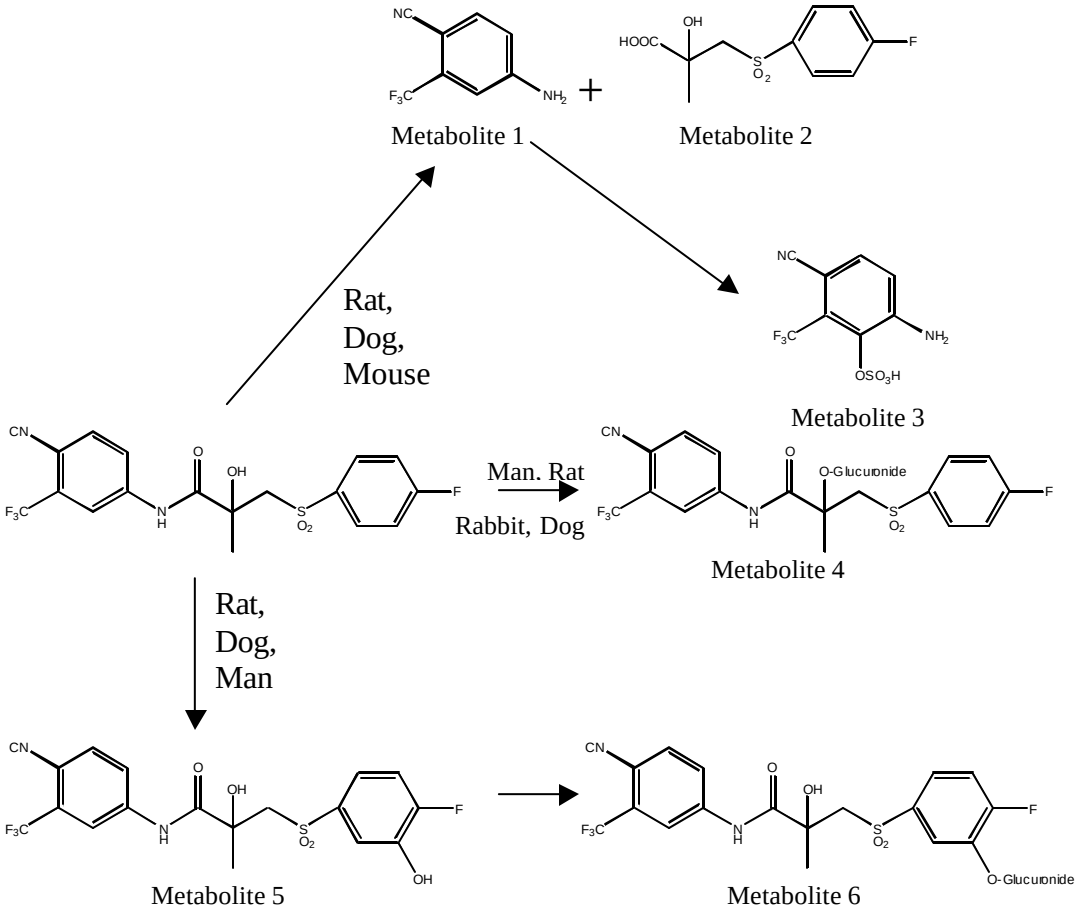

Figure 4.1. Metabolism of Bicalutamide in Laboratory Animals.

Bicalutamide is extensively metabolized by both Phase I and Phase II metabolism. Species differences can be seen in the metabolic pathways. Modified from reference 81.

effects associated with testosterone therapy. The therapeutic efficacy of a SARM can be compromised by enzymatic degradation. This chapter discusses studies that determined the molecular sites of metabolism and the disposition of the metabolites of S-4.

4.2. Materials and Methods

4.2.1 Animals

Beagle dogs were procured from approved vendors at The Ohio State University (OSU). The animals were between 2 and 6 years old and weighed 11.4 to 14.7 kg. Dogs were individually housed in the Animal Care Facility, and acclimated for at least one week prior to the study. The animal facility is accredited by the American Association for Laboratory Animal Care, and directed by full-time veterinarians. Male Sprague Dawley rats weighing approximately 250 g were purchased from Harlan (Indianapolis IN). The animals were maintained on a 12-hour cycle of light and dark, and had free access to food and water unless otherwise stated. The animal protocols were reviewed and approved by the Institutional Laboratory Animal Care and Use Committee of Ohio State University.

4.2.2 Metabolism Study

The purpose of these studies was to qualitatively identify the major urinary and fecal metabolites of S-4 in rats and dogs using non-radiolabeled drug. A catheter was implanted in the right jugular vein of adult rats. Animals were housed individually in Nalgene® metabolism cages, and given a 100 mg/kg IV dose of S-4 dissolved in PEG

300. Urine and feces samples were collected prior to dosing and at 8 and 24 hours after dosing. All samples were stored at -20°C until analysis.

For the dog study, a catheter was implanted in the right saphenous vein of the animals. The dogs were housed individually in metabolism cages, and given a 300 mg/kg dose of S-4 by oral gavage. Urine and feces samples were collected prior to dosing and 8 and 24 hours after dosing. Samples were stored at -20°C until analysis.

Urine samples were thawed and centrifuged at 1000g for 5 minutes. The supernatant was filtered through a 0.22 μm filter and diluted 1:1 with HPLC grade water. An aliquot (20μL) was injected in the LC/MS system for analysis.

Fecal samples were homogenized in 10 mL of HPLC grade water with a mechanical homogenizer (Pro Scientific, Monroe, CT). A 5 mL aliquot of the homogenate was mixed with 5 mL of a mixture of methanol/ethyl acetate [2:1 (v/v)], shaken for 40 minutes at room temperature and then centrifuged at 3000g for 10 min. The supernatants was removed and placed in a clean glass tube. The extraction procedure was repeated two additional times using an identical volume of methanol/ethyl acetate, and the supernatant fractions were combined. The samples were evaporated under a stream of nitrogen. The resulting residue was reconstituted in 500 μL of mobile phase. The reconstituted sample was then filtered through a 0.22 μm filter and a 20 μL aliquot was injected for analyzed by LC/MS.

4.2.3 LC/MS and LC/MS^2 Analysis

Metabolites were qualititatively identified using liquid chromatography (LC) mass spectrometry (MS). LC/MS, LC/MS^2, and LC/MS^3 analyses were performed

on a ThermoFinnigan (San Jose, CA) LCQ Deca Ion Trap System, which consisted of a Surveyor Pump, Surveyor Autosampler, and Surveyor PDA coupled to a LCQ Deca Ion Trap mass detector using an atmospheric pressure chemical ionization (APCI) interface. Data acquisition was controlled by Xcaliber software. The urine and fecal samples were separated using a reverse-phase column (Xterra C8 column, 2.1 mm X 50mm length, 3.5 µm particle size, Waters Corp., Milford, MA) and eluted with a gradient mobile phase consisting of methanol and water at a flow rate of 0.300 mL/min (Table 4.1). The effluent was introduced into the APCI interface of the mass spectrometer that was set at the following conditions: vaporization temperature 450 °C, sheath gas (nitrogen) flow 660 mL/min, auxiliary gas (nitrogen) flow 60 mL/min, discharge current 10µA, capillary temperature 150 °C, capillary voltage –19.00V, tube lens offset 35.00V, multipole 1 offset 2.25V, lens voltage 88 V, multipole 2 offset 16.5 V, multipole RF amplitude 510.0 V p-p, entrance lens voltage 30 V, and electron multiplier voltage –900.0 V. All analyses were conducted in negative ion mode. The scan range for full-scan spectrometry analysis was 100-2000 m/z. For MS^2, and MS^3 analysis, precursor ions were isolated with a width of 4 m/z and fragmented with a fragmentation voltage of 26 V and 53 V respectively. Mass spectra data was then analyzed by Metabolite ID software, version 1.0 (ThermoFinnigan Corp. San Jose, CA). The background of the blank urine samples was subtracted from the treated urine samples to identify drug-related peaks. The LC/MS^2 spectra of these peaks and LC/MS^3 of the base peaks were then compared to the parent compound to determine the metabolite structure.

Elution Time (min)	Mobile Phase Composition	
	% Methanol	% Water
0	10	90
40	100	0
45	100	0
45.1	10	90
60	10	90

Table 4.1. Elution Gradient for LC/MS Analysis.

The initial mobile phase contained 10% (v/v) methanol in water. The percentage of methanol in the mobile phase increased from 10% to 100% over the first 40 minutes of the gradient in a linear fashion. The mobile phase consisted of 100% methanol from 40 to 45 minutes and was immediately returned to starting conditions.

4.2.4 Radioactive Disposition Study

The purpose of these studies was to quantitatively examine the disposition and identify the major urinary and fecal metabolites of S-4. The quantitative disposition of S-4 and its metabolites was determined using radiolabeled S-4 (specific activity of 5.4 mCi/mmol). Uniformly labeled ^{14}C-S-4 was synthesized and purified in the Radiochemistry Laboratory at The Ohio State University Comprehensive Cancer Center (Dr. Michael Darby). Catheters were surgically implanted in the right external jugular vein of male Sprague-Dawley rats and animals were allowed to recover for 24 hours. Animals were then placed in Nalgene® metabolism cages. One hundred millicurie of [^{14}C] S-4 was dissolved in 1 mL of ethanol and diluted in PEG 300. The final concentration of ethanol was less than 5% of the dosing solution. An IV bolus dose of 100 μCi [^{14}C] S-4 in 100 μL was administered through the jugular catheter over a 5 minute period, corresponding to a total dose of 3.3 mg/kg of S-4. The catheter was then flushed with 0.2 mL of saline. Feces and urine samples were collected prior to dosing and at 8, 24 and 48 hours after the dose was administered. The animals were sacrificed 24 and 48 hours after dosing and the following organs harvested: liver, spleen, heart, kidneys, intestines (small and large), levator ani muscle, pancreas, stomach wall, abdominal fat and prostate. In addition, a terminal blood sample was obtained via the inferior vena cava and the intestinal and stomach contents were collected. Blood samples were centrifuged at 1000g and the plasma collected and stored at -20° C until analysis. All organs were cleaned of extraneous tissue, weighed and stored at -20° C until analysis.

4.2.5 Tissue Sample Preparation

Total radioactivity in each organ was determined for the purpose of mass balance. Organs were thawed at room temperature, and then organ samples were weighed and minced with a scalpel. Aliquots of each organ sample were then placed in 1 mL of ScintiGest® tissue solubilizer (Fisher Scientific Company, Fair Lawn, NJ). The tissue samples were then homogenized in a Pro 200 homogenizer (Pro Scientific, Monroe, CT). The samples were incubated at 60°C until the tissue dissolved. An aliquot (200 µL) of 30% hydrogen peroxide was added to decolorize the samples and 70 µL of glacial acetic acid was added to prevent chemiluminescence within the samples. An aliquot (10 mL) of ScintiVerse® scintillation cocktail (Fisher Scientific Company, Fair Lawn, NJ) was added to each sample and the total radioactivity was determined in a Beckman LS6000 IC liquid scintillation counter (Beckman-Coulter, Fullerton, CA).

4.2.6 Radioactive Metabolite Determination

Feces, intestinal contents, and stomach contents samples were homogenized in of distilled water (2 times the volume) and the resultant mixture was stored at -20° C until analysis. Feces samples were thawed and centrifuged at 3000g for 10 minutes. The supernatant was removed and filtered through a 0.22 µm filter. An aliquot (20 µL) of filtrate was then analyzed by HPLC. The fecal pellet was extracted 4 times with ethyl acetate/methanol [2:1 (v/v)]. The supernatants were pooled and evaporated under nitrogen. The resulting residue was reconstituted in 300 µL of mobile phase of methanol/water [1:1 (v/v)]. An aliquot (20µL) was analyzed by HPLC. Urine samples

were thawed and centrifuged at 1000g for 5 minutes. The supernatant was filtered through a 0.22 µm filter and a 20 µL of the filtrate was injected in the HPLC system for analysis.

The original HPLC gradient method showed closely eluting metabolite peaks. Therefore, a new HPLC was specifically adapted to identify highly hydrophilic metabolite that may be located in the solvent front of the chromatogram as well as baseline separation of known metabolite to facilitate quanititation. The purpose of these studies was to quantify the major metabolites, and determine their elution characteristics during reversed-phase chromatography as a prelude to their identification by LC/MS. The fecal and urine samples were separated using a reverse-phase column (5µm, 2mm x 250 mm, Ultrasphere ODS C18 column, Alltech, Deerfield IL). A gradient elution program (Table 4.2) with a mobile phase consisting of methanol and water at a flow rate of 0.200 mL/min was used. The effluent was introduced into a HPLC system consisting of a Hewlett Packard 1050 quaternary pump, Hewlett Packard 1050 autosampler, Hewlett Packard 1050 diode array detector. Eluted fractions were collected at 2 minute intervals over a HPLC run. The fractions were analyzed using a Beckman LS6000 IC liquid scintillation counter (Beckman-Coulter, Fullerton, CA). Data acquisition was controlled by ChemStation software.

4.2.7 Determination of Major Urinary and Fecal Metabolites

Several metabolites were identified by analysis of non-radioactive dog and rat samples. However, to determine the major metabolite in rats the radioactive disposition study was conducted. This study identified a major urinary metabolite that had not, as

Elution Time (min)	Mobile Phase Composition Composition	
	%Methanol	% Water
0	0	100
15	0	100
20	10	90
65	60	40
67	95	5
72	95	5

Table 4.2. Elution Gradient for Radioactive Disposition Study.

The initial mobile phase contained 100% water and was maintained at this composition for 15 minutes. The percentage of methanol in the mobile phase increased to10% over the next 5 minutes of the gradient in a linear fashion. The percentage of methanol in the mobile phase again increased to 60% over the next 45 minutes of the gradient in a linear fashion. Finally the methanol in the mobile phase was increased to 95% in 2 minutes and remained there for 5 minutes. A longer gradient was developed to separate hydrophilic radioactive metabolites from the solvent front.

yet, been elucidated. In addition, three minor fecal metabolites were also seen in the radiographic chromatogram. To determine the structures of these metabolites, urine and feces samples obtained from animals that received non-radiolabeled doses of S-4, were again fractionated and the fractions containing the unknown metabolites were infused into the ThermoFinnigan LCQ Deca Ion Trap System described in section 4.2.3. The fractions were ionized using an electrospray ionization (ESI) set at the following conditions: sheath gas (nitrogen) 1185 mL/min, auxiliary gas (nitrogen) 60mL/min, Spray voltage 3.5 kV, capillary temperature 180°C, capillary voltage –6V, tube lens offset –55V, multipole 1 offset 6.75V, lens voltage 22V, multipole 2 offset 8.50V and entrance lens voltage 58V. All analyses were conducted in negative ion mode. The scan range for full-scan analysis was 100- 2000 m/z. For MS^2 and MS^3 analysis, molecular and daughter ions were isolated with a width of 4 m/z and fragmented with a fragmentation voltage of 26 V or 53 V respectively. Data acquisition was controlled by Xcaliber software.

4.3. Results

The metabolic profiles of S-4 in urine and feces after high dose IV administration in rats and oral administration in dogs were determined by APCI mass spectrometry after separation by reverse phase HPLC. The total ion spectra of postdose urine samples were compared to urine samples taken prior to dosing to identify drug related peaks. The base peak of each metabolite was then subjected to LC/MS^3 analysis for further elucidation of structure.

4.3.1 Urinary Metabolites in Rats

Urine samples collected at 8 and 24 hours after the dose showed similar metabolic profiles. $[M-H]^-$ corresponding to the parent drug at m/z 440 and five metabolite peaks associated with ions at m/z 410, 426, 454 and 506 (Table 4.3) were found. Chromatographs and fragmentation spectra for all metabolites can be found in Appendix C. All drug-related peaks were further characterized by LC/MS^3 analysis when possible. Proposed metabolite structure and fragmentation patterns of S-4 in rats are discussed below and summarized in Table 4.3.

Parent compound (m/z 440)

Upon collision induced dissociation of the parent compound, $[M-H]^-$ ion eluting at 13.7 minutes, yielded daughter ions of m/z 150, 261, and 289. Figure 4.3 shows the proposed fragmentation pattern of the parent compound. The daughter ion at m/z 261 was the base peak in the spectrum. This daughter ion corresponds to a cleavage of the bond between the chiral carbon and methylene carbon, with a loss of the methyl group. The daughter ion at m/z 289 was likely formed from the cleavage of the bond between the oxygen linker and B ring with the loss of a hydrogen atom from the hydroxyl group from the chiral carbon. The overall fragmentation pattern confirms that the ion at m/z 440 is the deprotonated molecular anion of the parent drug.

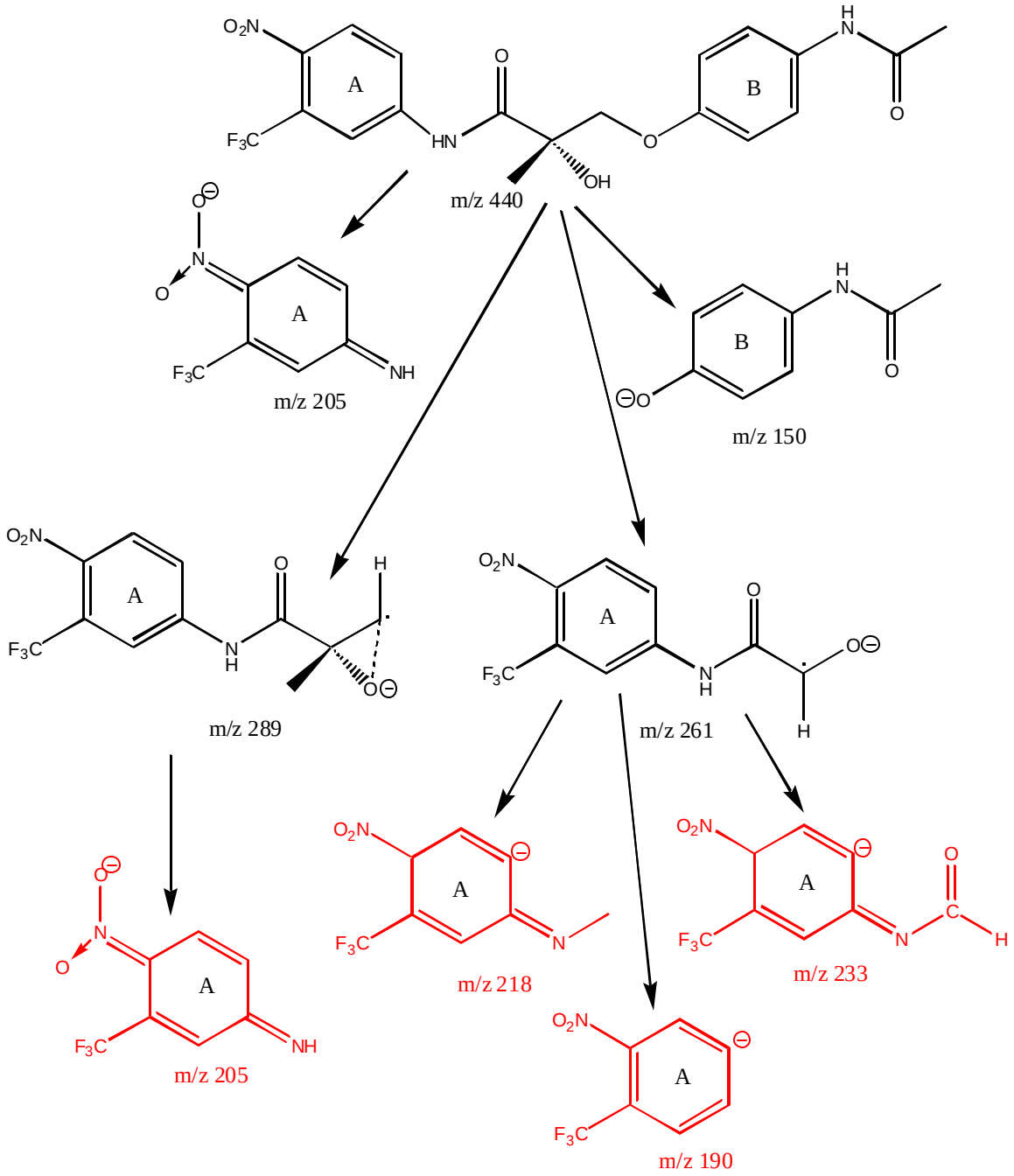

Figure 4.2. Proposed Fragmentation Pattern of S-4

Structural information was determined by LC/MS^2 fragmentation of the parent compound, S-4. Red structures show fragments obtained after LC/MS^3 fragmentation of daughter ions (m/z 205, 218, 190, 233).

Molecular and Daughter ions $[M-H]^-$	Product Ions (m/z values)	Assigned Structures and Proposed Fragmentation Patterns
440 (S-4)	150, 205, 261[a], 289	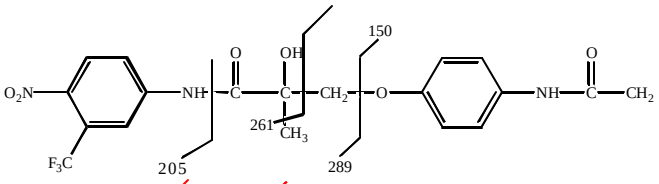
261	190, 218, 233	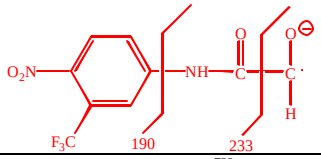
454 (M1)	150, 303[a]	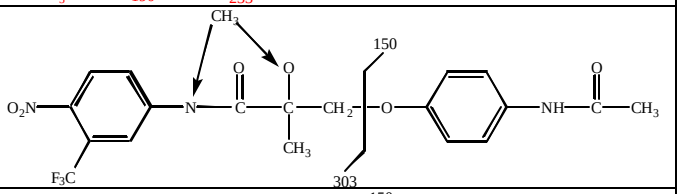
410 (M2)	150[a], 259, 308, 380	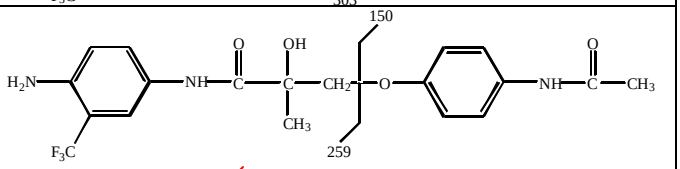
259	175, 201[a], 209	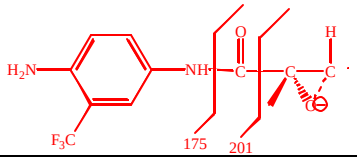
426 (M3)	166[a], 220, 259, 324, 336, 365, 396, 408 [M-H_2O]	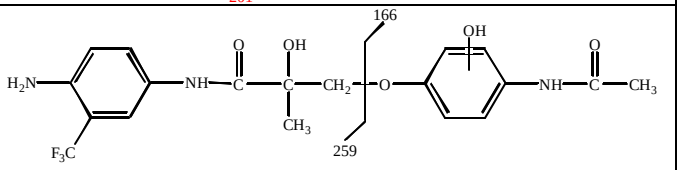
506 (M4)	426[a], 275	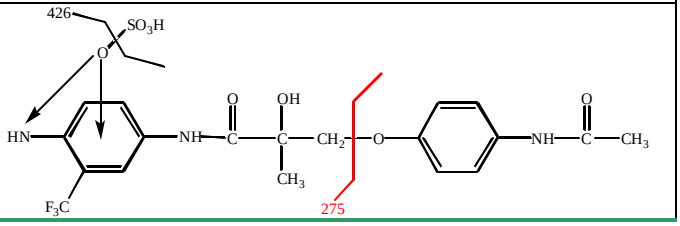
426	255, 275[a], 366, 406	

a. Base peak in LC/MS^2 or LC/MS^3 spectra

Table 4.3. Proposed Structure of Urinary Metabolites in Rats.

Metabolite structure was determined by using LC/MS^2 fragmentation of metabolite peaks. Fragmentation patterns of the metabolites were compared to the parent compound to determine the sites of metabolic modification. Red structures show structural information gathered by LC/MS^3 fragmentation (m/z 261, 259, and 426).

Metabolite M1

This $[M-H]^-$ at m/z 454 corresponds to the addition of a methyl group to the parent compound and eluted at 12.3 minutes. Fragmentation of this molecular ion produced daughter ions at m/z 150 and 303, with the latter being the base peak. The daughter ion at m/z 303 also gained 14 Da. relative to the daughter ion at m/z 289 produced from the fragmentation of the parent drug. Thus, metabolite M1 appears to be the methylated metabolite of S-4. There are two potential methylation sites. One at the hydroxyl group of the chiral carbon, and the other at the para-amino linkage on A ring. Differentiation between these sites was not possible from further fragmentation because of the relatively low abundance of the daughter ions. However, it is likely the methylation occurred at the amino group based on the structural preference in metabolism. Radioactive disposition studies, discussed below indicated that approximately 32 % of unchanged drug was excreted in the feces.

Metabolite M2

The $[M-H]^-$ at m/z 410 appears to correspond to the reduction of the nitro group to an amine group and eluted at 14.3 minutes. MS^2 fragmentation produced daughter ions at m/z 150 and 259 with the former being the base peak in the spectrum. The proposed structure was also supported by the 30 Da. decrease in the daughter ion at m/z 259 relative to the corresponding daughter ion at m/z 289 produced by the parent compound. In addition, the simultaneous detection of the daughter ion at m/z 150, which was present in the MS^2 spectrum of the parent compound, suggests no change in the B ring of the metabolite. Further fragmentation of the base peak at m/z 259 produced granddaughter

ions at m/z 209, 201, and 175 (410 → 259 →275), the last of which was also 30 Da. lower than the equivalent granddaughter ion at m/z 205 (440 → 289 →205) produced from the parent drug. This fragment corresponds to the cleavage of the amide bond. The overall fragmentation pattern confirms that the ion at m/z 410 is the deprotonated molecular anion of the amine metabolite. Radioactive disposition studies showed that 15% of the parent compound was converted to this metabolite and excreted in the urine and feces of rats.

Metabolite M3

The $[M-H]^-$ at m/z 426 is postulated as the sequential oxidation metabolite of the amine metabolite M2 and eluted at 11.8 minutes. There are four possible sites of oxidation: i) oxidation of the amino group, ii) hydroxylation of the aromatic A ring, iii) hydroxylation of the methylene carbon, or iv) hydroxylation of the aromatic B ring. Fragmentation of this molecular ion produced daughter ions at m/z 166, 259, 396, 336, 408, with the daughter ion at m/z 166 being the base peak in the spectrum. The proposed structure was supported by the 16 Da. increase in the daughter ion at m/z 166 relative to the corresponding daughter ion at m/z 150 produced by the parent compound. This suggested an oxidation of the B ring of the amine metabolite M2. Since a fragment at m/z 259 was present in the MS^2 spectrum of this metabolite, it suggested that there was no oxidation occurring at the other three sites mentioned above. Because of the relatively small size of the peak at m/z 166, further fragmentation was not possible.

Metabolite M4

The $[M-H]^-$ at m/z 506 was proposed to be the sulfated product of the amine metabolite M2 (m/z 410) and eluted at 23.0 minutes. Fragmentation of this molecular ion produced daughter ions at m/z 275, and 426 with the latter being the base peak in the spectrum. The ion at m/z 426, being 80 Da. lower $[M-H]^-$ at 506, is consistent with the loss of a SO_3 moiety, suggesting that this is a sulfate conjugate of the amine metabolite. The daughter ion at m/z 426 is the resultant oxidated amine metabolite. Further fragmentation of the daughter ion at m/z 426 produced granddaughter ions at m/z 275, 254, 406, and 366. There are at least two possibilities to account for the ion at m/z 426: i) the oxidation of the amine group on the A ring, and ii) the hydroxylation of the A ring itself. Both these structures could produce the fragmentation pattern seen for the daughter ion at m/z 426. It should be noted that the site of oxidation of the molecular ion at m/z 506 differs from the oxidized amine metabolite at m/z 426. Radioactive disposition studies, discussed below, indicated that less than 1% of the parent compound was converted to this metabolite and excreted in the feces.

4.3.2 Fecal Metabolites in Rats.

Fecal samples collected at 8 and 24 hours after dosing showed similar metabolic profiles. Fecal samples showed molecular ions similar to those found in urine samples; $[M-H]^-$ deprotonated anion corresponding to the parent drug (m/z 440) and metabolite peaks associated with the m/z 410 and 426, while the metabolites at m/z 454 and 506 were not found in the feces. All drug related peaks produced fragmentation patterns that

were similar to those found in rat urine. These similarities indicated that these molecular ions are structurally the same as those found in the urine samples.

4.3.3 Urinary Metabolites in Beagle Dogs

Urine samples collected at 8 and 24 hours after dosing showed similar metabolic profiles. Urine samples showed the molecular ion corresponding to the parent drug (m/z 440). Both the molecular ions for the parent compound and the amine metabolite at m/z 440 and 410 respectively, were also seen and they were identical to those seen in rat urine as evidenced by MS^2 and MS^3 analysis. This observation was also supported by the matching HPLC retention times of the molecular ions in both samples, which were 35.2 and 13.9 for ion at m/z 440 and 410 respectively. Additional drug related molecular ions were detected at m/z 424, 368, and two peaks at m/z 426 that were not seen in rats. Table 4.4 shows the proposed metabolite structure and fragmentation patterns of S-4 in dogs.

Metabolite M5 (m/z 424)

The $[M-H]^-$ at m/z 424 is proposed to correspond to the loss of an oxygen molecule from the parent compound resulting for the reduction of the nitro group to a nitroso group and eluted and 11.4 minutes. This molecular ion produced daughter ions at m/z 150, 245, and 273, with the daughter ion at m/z 245 being the base peak in the spectrum. The proposed structure was also supported by the 16 Da. decrease in the daughter ion at m/z 245 relative to the corresponding daughter ion at m/z 261 produced by the parent compound. This suggests a loss of oxygen from the nitro-group on the para-position of the A-ring.

Molecular and Daughter Ions $[M-H]^-$	Product Ions (m/z values)	Assigned Structures and Proposed Fragmentation Patterns
440	150, 205, 261[a], 289	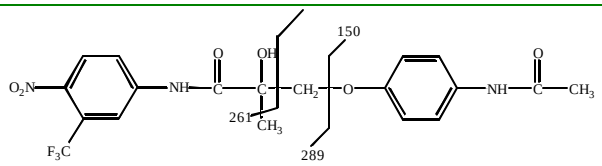
424 (M5)	150, 245[a], 273	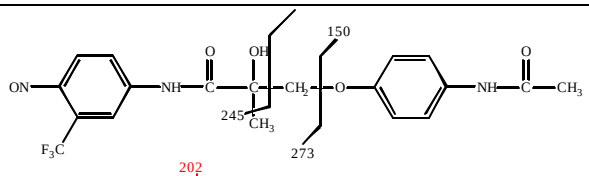
245	183, 202[a]	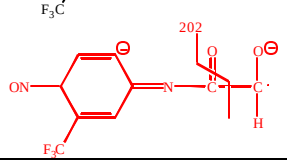
368 (M6)	108, 175, 201, 231, 259[a]	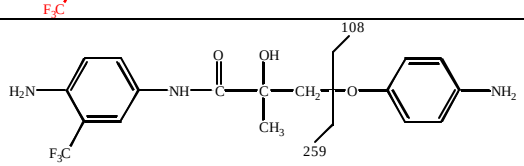
259	175, 201[a], 239	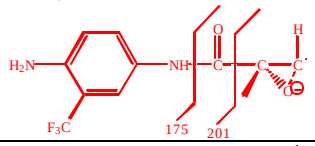
426 (M7)	150, 245[a], 275, 405	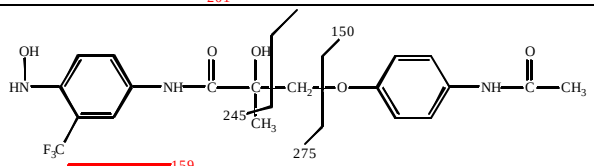
245	159	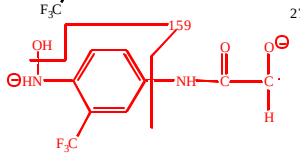
426 (M8)	161, 216[a], 275	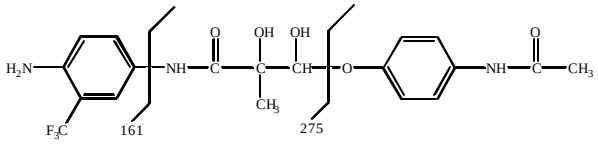
216	160[a], 186	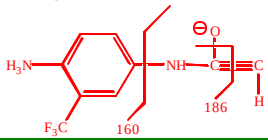

a. Base peak in LC/MS^2 or LC/MS^3 spectra

Table 4.4. Proposed Structures for the Metabolite in Beagle Dog Urine.

Metabolite structure was determined by using LC/MS^2 fragmentation of metabolite peaks. Fragmentation patterns of the metabolites were compared to the parent compound to determine the sites of metabolic modification. Red structures show structural information gathered by LC/MS^3 fragmentation (m/z 245, 259, and 216).

The presence of the daughter ion at m/z 273 further supports this structural identification, showing a loss of 16 Da relative to the corresponding daughter ion at m/z 289 produced by the parent compound. Further fragmentation of the daughter ion at m/z 245 produced granddaughter ions at m/z 183 and 202 (424 → 245 →202), the last of which was also 16 Da. lower than the equivalent granddaughter ion at m/z 218 (440 → 261 →218) produced from the parent drug. The overall fragmentation pattern confirms that the ion at m/z 424 is the deprotonated molecular anion of the reduced parent compound.

Metabolite M6 (m/z 368)

The $[M-H]^-$ at m/z 368 is thought to correspond to the loss of acetyl group from the amine metabolite, M2. Fragmentation of the molecular ion at m/z 368 produced daughter ions at m/z 108, 175, 201, 231, and 259. The proposed structure was also supported by the 42 Da. decrease in the daughter ion at m/z 108 relative to the corresponding daughter ion at m/z 150 produced by the parent compound. This suggests the deacetylation in the B ring, forming an amine group. The daughter ions at m/z 231 and 259 were present in the fragmentation spectra on the amine metabolite (m/z 410). Further fragmentation of the base peak at m/z 259 produced a fragmentation spectrum similar to that seen in the molecular ion at m/z 410. These finding suggest that this metabolite was likely produced from the amine metabolite M2.

Metabolite M7 and M8

Two ions were detected at m/z 426 (Figure 4.4). Both these $[M-H]^-$ ions were found to correspond to the addition of an oxygen molecule to the amine metabolite.

Though both these molecular ions showed the same m/z ratio, they showed different fragmentation patterns and retention times. As stated previously, there are four possible sites for oxidation on the amine metabolite, i) oxidation of the amine , ii) hydroxylation of the A ring iii) hydroxylation of the methylene carbon, or iv) hydroxylation of the B ring. The fragmentation pattern for peak at 5.4 minutes produced daughter ions at m/z 161, 216, 275, with the daughter ion at m/z 216 being the base peak in the spectrum. The presence of a daughter ion at m/z 275 corresponds to the addition of an oxygen molecule at either the aromatic A ring, the amine group at the para-position of the A ring, or the methylene carbon. Further fragmentation of the daughter ion at m/z 216 produced granddaughter ions at m/z 160 and 186. The presence of these ions and the absence of their corresponding oxidated ions suggests that there was no oxidation to the amine or the A ring. Therefore, these findings suggest the oxidation occurred at the methylene carbon. The fragmentation of the peak at 8 minutes produced daughter ions at m/z 150, 245, and 275, with the daughter ion at m/z 245 being the base peak in the spectrum. Further fragmentation of the daughter ion at m/z 245 produced the granddaughter ion at 159. This ion was produced by the fragmentation of the hydroxyl group from the amine on the para position of the A ring. These findings suggest that oxidation occurred on the amine group of the A ring.

4.3.4 Fecal Metabolites in Dogs.

Fecal samples collected at 8 and 24 hours after dosing showed similar metabolic profiles. Fecal samples showed molecular ions similar to those found in urine samples;

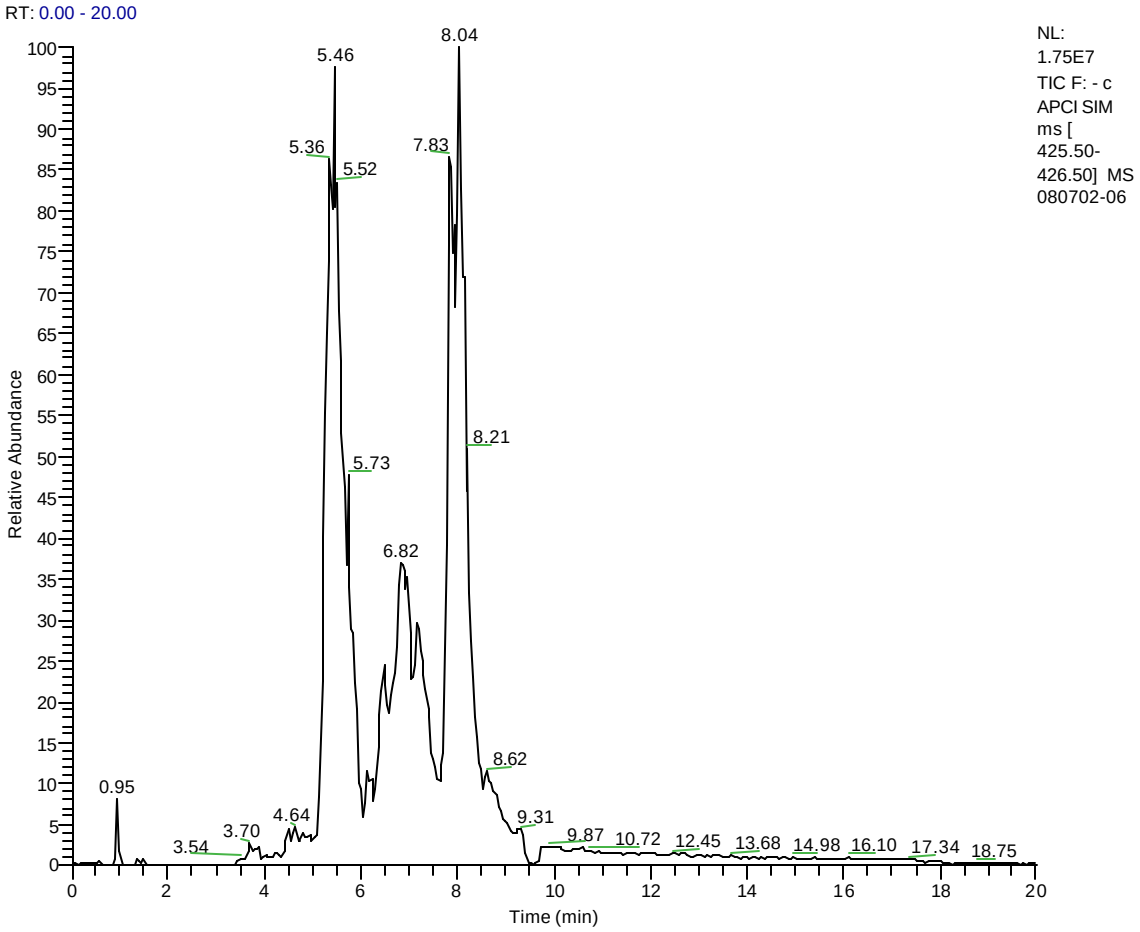

Figure 4.3. Chromatograph of Metabolites M7 and M8.

Two distinct peaks having at m/z 426 were detected in dog urine. Each peak showed a different fragmentation pattern.

$[M-H]^-$ deprotonated anion corresponding to the parent drug (m/z 440) and metabolite peaks associated with the m/z 410. All drug related peaks produced fragmentation patterns that were similar to those found in rat and dog urine. These similarities indicated that these molecular ions are structurally the same as those found in the urine samples.

4.3.5 Radioactive Disposition of S-4 in Rats

A 100μCi dose of $[C^{14}]$ S-4 (3.3 mg/kg) was administered via a jugular catheter to two rats. The rats were sacrificed at 24 and 48 hours and radioactivity was measured in selected tissues, urine and feces. Table 4.5 shows the percentage of the injected dose at 24 and 48 hours. Ninety-seven percent and 83% of the injected dose was recovered from the tissues and excreta at 24 and 48 hours respectively. Of the tissues analyzed, the liver and the intestines showed the greatest amount of radioactivity after 24 and 48 hours. The final disposition of radioactive material was fairly evenly divided between the feces and urine at 48 hours (35.7% and 37.0% in urine and feces respectively). However, at 8 hours after the dose, a slightly higher percentage of the injected dose was found in the urine as compared to the feces.

The 24-hour urine and feces samples were fractionated to quantitate the amount of metabolite because these samples contained the highest amount of radioactivity. The disintegrations per minute (DPM) of each point on the peak were added to determine the amount of radioactivity in each metabolite peak relative to the injected dose. Analysis of the effluent fractions showed two major peaks in the urine. Figure 4.4 shows the chromatograph after column separation. The peak eluting at approximately 5 minutes represents 25% of the injected dose with a secondary peak

Organs/Sample	24 Hours		48 Hours	
	Radioactivity in Organ/Sample (DPM)	% Injected Dose	Radioactivity in Organ/Sample (DPM)	% Injected Dose
Heart	33112	0.025	11782	0.009
Muscle	60	0	1020	0.001
Spleen	1101	0.001	15678	0.011
Pancreas	60540	0.05	8184	0.006
Intestines	11690121	8.88	966112	0.70
Liver	4285486	3.25	2258339	1.63
Kidney	18197	0.014	66182	0.048
Prostate			2195	0.002
Stomach Wall			48691	0.035
Fat			10073	0.007
Feces 0-8 hr.	525367	0.40	118204	0.085
Feces 8-24 hr.	46358623	35.2	42798292	30.9
Feces 24-48 hr.			8458155	6.10
Urine 0-8 hr.	16887732	12.8	7189691	5.18
Urine 8-24 hr.	36995976	28.1	29056378	21.0
Urine 24-48 hr.			13312800	9.60
Stomach Contents			2307571	1.66
Intestinal Contents	7977803	5.09	8212016	5.92

Table 4.5. Disposition of Radiolabeled S-4 in Organs, Urine and Feces of Rats.

Distribution of total radioactivity after a dose of 100μCi of [C^{14}] S-4 was equal between the feces and urine, 37% and 35% inject dose, respectively, after 48 hours. Tissues showed minimal radioactivity at 24 or 48 hours. Total recovery of radioactivity in all tissues and excreta was 97% and 83% at 24 and 48 hours, respectively.

accounting for 11% of the injected dose, which was later identified as the amine metabolite. Separate experiments showed that [^{14}C] S-4 eluted at about 52 minutes using the same column and mobile phase gradient. Therefore, neither of the peaks found in the urine were the parent compound. The aqueous and organic layers of the fecal samples were also analyzed.

The organic extract showed two major peaks (Figure 4.5) with one correlating to that of the parent compound, with a retention time of approximately 53 minutes and another correlating to the amine metabolite M2, at approximately 41 minutes. The parent compound peak accounted for 21% of the injected dose, and the amine metabolite accounted for 1.4% of the injected dose. The chromatograph of the aqueous layer of the fecal extract (Figure 4.6) contained two major peaks, which were seen in organic layer, and three minor peaks at approximately 7, 15, and 27 minutes. The parent compound accounted for 6.7% of the injected dose and the amine metabolite M2 accounted for 2% of the injected dose. The minor peaks accounted for 1.2% of the injected dose. Overall % of the injected dose in the feces would be parent compound, while 4% of the injected dose would be the anime metabolite M2.

The fractions containing the major urinary metabolites and the three fecal metabolites were analyzed by LC/MS using an ESI interface. The urinary fractions showed molecular ions at m/z 252 and 410. The fecal fractions, containing the minor metabolite peaks, showed molecular ions at m/z 602, and 506. The fragmentation patterns of the molecular ions at m/z 506 and 410 were the same as those seen for32

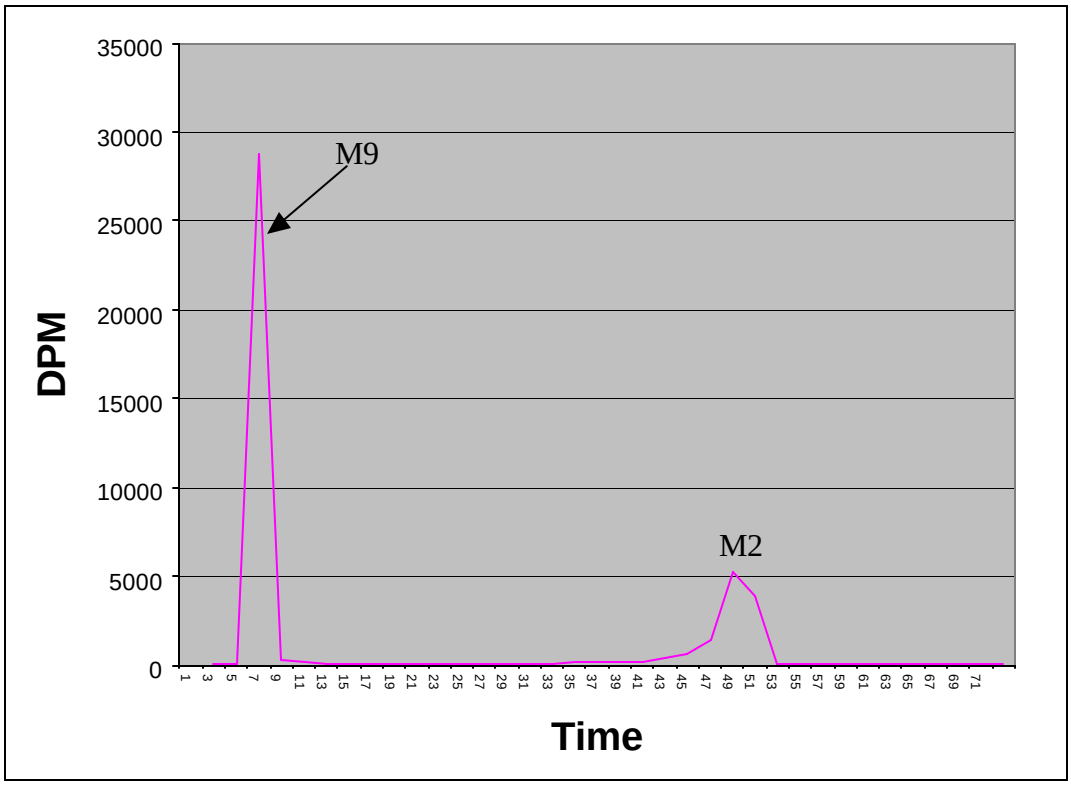

Figure 4.4. Chromatograph of 24-hour urine sample after HPLC separation.

Two major peaks were identified at 5 and 47 minutes. The peak at 5 minutes corresponds to 25% of the injected dose, while the 47 minute peak corresponded to 11% of the injected dose.

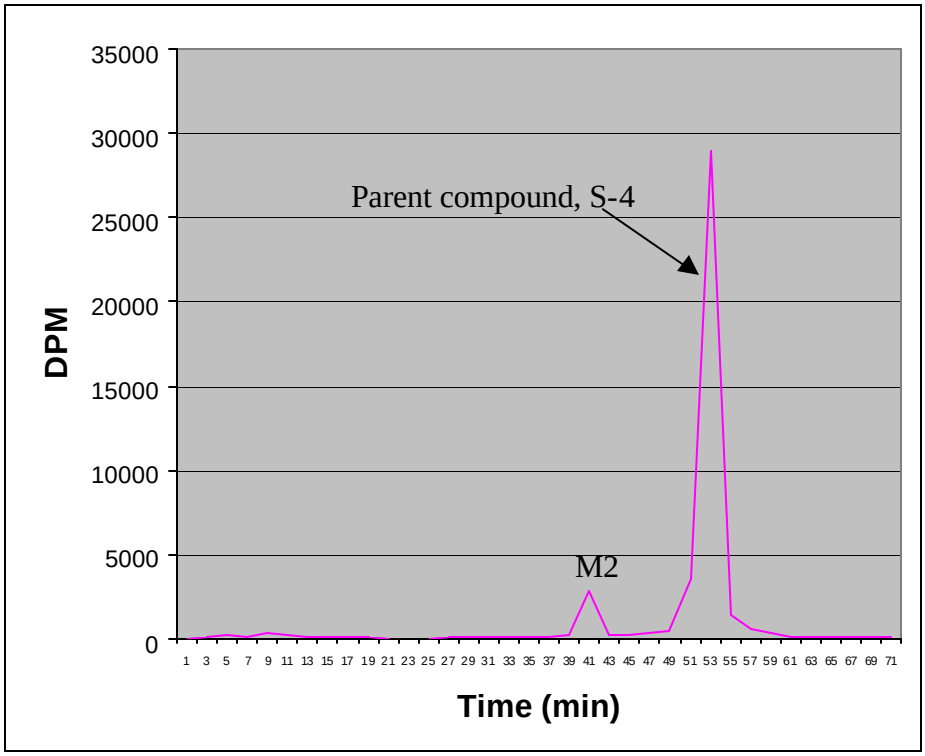

Figure 4.5. Chromatograph of the Organic Phase of the 24-hour Fecal Sample after HPLC Separation.

Two major peaks were seen at 41 and 53 minutes. The peak at 53 minute corresponds to 21% injected dose, while the 41 minute peak corresponded to 1.4% of the injected dose.

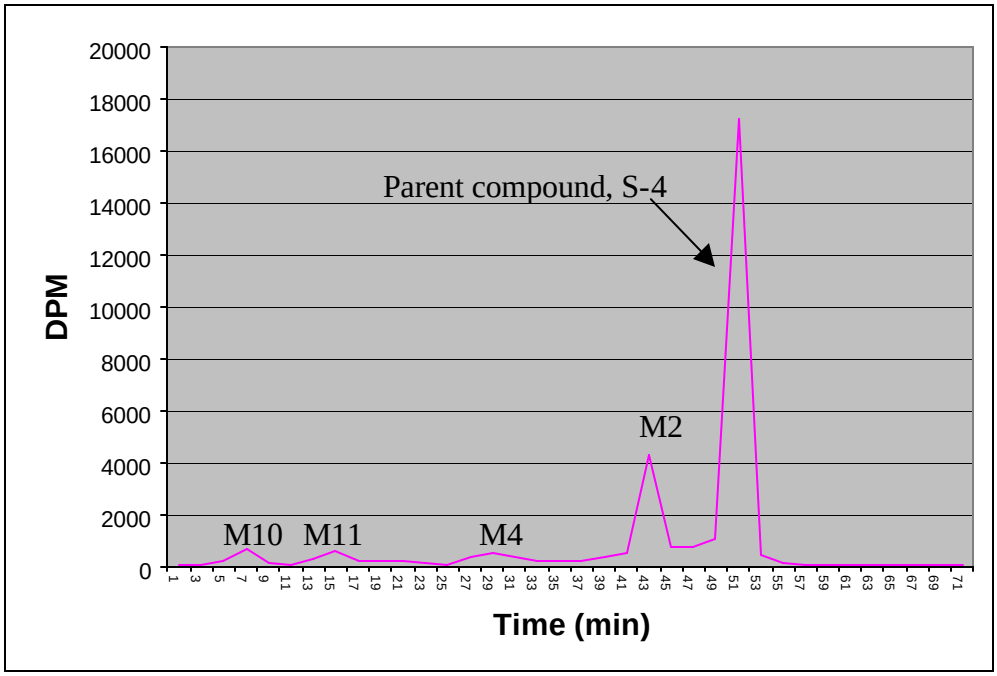

Figure 4.6. Chromatograph of the Aqueous Phase of the 24-hour Fecal Sample after HPLC Separation.

Two major peaks were seen at 43 and 51 minutes, with three minor peaks at 7, 15 and 27 minutes. The peak at 51 minutes corresponds to 6.7% of the injected dose, while the 43 minute peak corresponded to 2% of the injected dose. The minor peaks accounted for 1.2% of the dose.

metabolites M4 and M2, respectively. Therefore we concluded that these ions were the amine metabolite at m/z 410 and the sulfated conjugate of the amine metabolite at m/z 506. Table 4.6 shows the structure and proposed fragmentation patterns for the metabolites at m/z 252, and 602.

Metabolite M9

The $[M-H]^-$ at m/z 252 was found to correspond to the hydrolysis product of the parent compound, S-4, presumably at the amide bond. Fragmentation of this molecular ion produced daughter ions at m/z 155, 193, and 208, with the daughter ion at m/z 193 being the base peak in the spectrum. The daughter ion at m/z 208 was likely formed from the cleavage of the acetyl group on the B ring to an amine, while the daughter ion at m/z 193 corresponds to the loss of the N-acetyl group from the B ring (loss of 59 Da.). The origin of the metabolite could not be determined given that the A-ring portion of the metabolite could not be detected.

Metabolite M10 and M11 (m/z 602)

Two peaks at $[M-H]^-$ at m/z 602 were found to correspond to the glucuronidated, hydroxylated amine metabolite. Fragmentation of both these peaks produced daughter ions at m/z 426, which were produced by the loss of the glucuronide conjugate (176 Da). Further fragmentation of the daughter ion at m/z 426 of the peak eluting at 7 minutes produced granddaughter ions at 166, 337, and 396. These daughter ions were similar to those produced by metabolite M3 in rats. The presence of the fragment at m/z 166 suggests that the metabolite was hydroxylated and then glucuronidated on the B ring.

Molecular and Daughter Ions [M-H]$^-$	Product Ions (m/z values)	Assigned Structures and Proposed Fragmentation Patterns
252 (M9)	155,193,208,	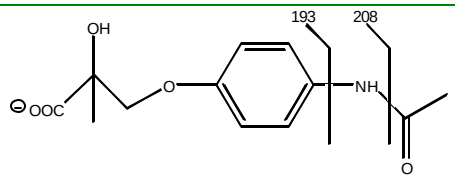
602 (M10) 426 602 (M11) 426	426 255, 275, 366, 386, 406 426 166, 337, 396	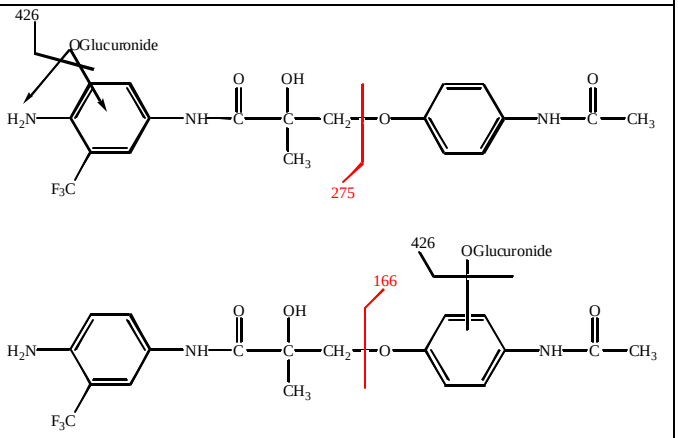

Table 4.6. Urinary and Fecal Metabolites Found in Rats.

Metabolites were extracted from feces and urine samples obtained at 24 hours after an IV dose of S-4 (10 mg/kg). Samples were analyzed using an ESI ionization source, to ease the identification of polar phase II metabolites.

Fragmentation of the peak eluting at 15 minutes produced granddaughter produced ions at m/z 255, 275, and 406. These daughter ions were the similar to those produced by metabolite M7 in dogs. The presence of the fragment ion at m/z 275 suggests that the metabolite was hydroxylated and then glucuronidated on either the A ring, or the amine on the A ring.

4.4. Discussion

Prior studies determined that R-1 was rapidly cleared and metabolically converted from an agonist to an antagonist[78]. These findings prompted the design, synthesis and evaluation of the metabolism of S-4, a structurally optimized AR ligand. Figure 4.1 shows the proposed metabolic profile of R-1. R-1 was metabolized extensively with many of these metabolites containing the sulfone moiety at the linker position of the molecule (R_3). The primary metabolite (Metabolite 4) was synthesized and tested using the *in vitro* assays described in Chapter 2. Metabolite 4 bound the AR with high affinity and demonstrated potent *in vitro* antagonist activity for the AR in cotransfection assays.

High doses of S-4 were administered to rats and dogs and the structures of these metabolites were determined by LC/MS^2 and LC/MS^3 analyses. The fragmentation patterns of the metabolite were compared to those of the parent compound to determine the site of metabolism.

Initial analysis by LC/MS of urine and feces from both dogs and rats showed that the major metabolite in urine was the A-ring reduced amine metabolite M2. In addition, several minor metabolites were identified in the urine. Independent *in vitro* enzyme studies, conducted by other members within the laboratory, showed that only P450

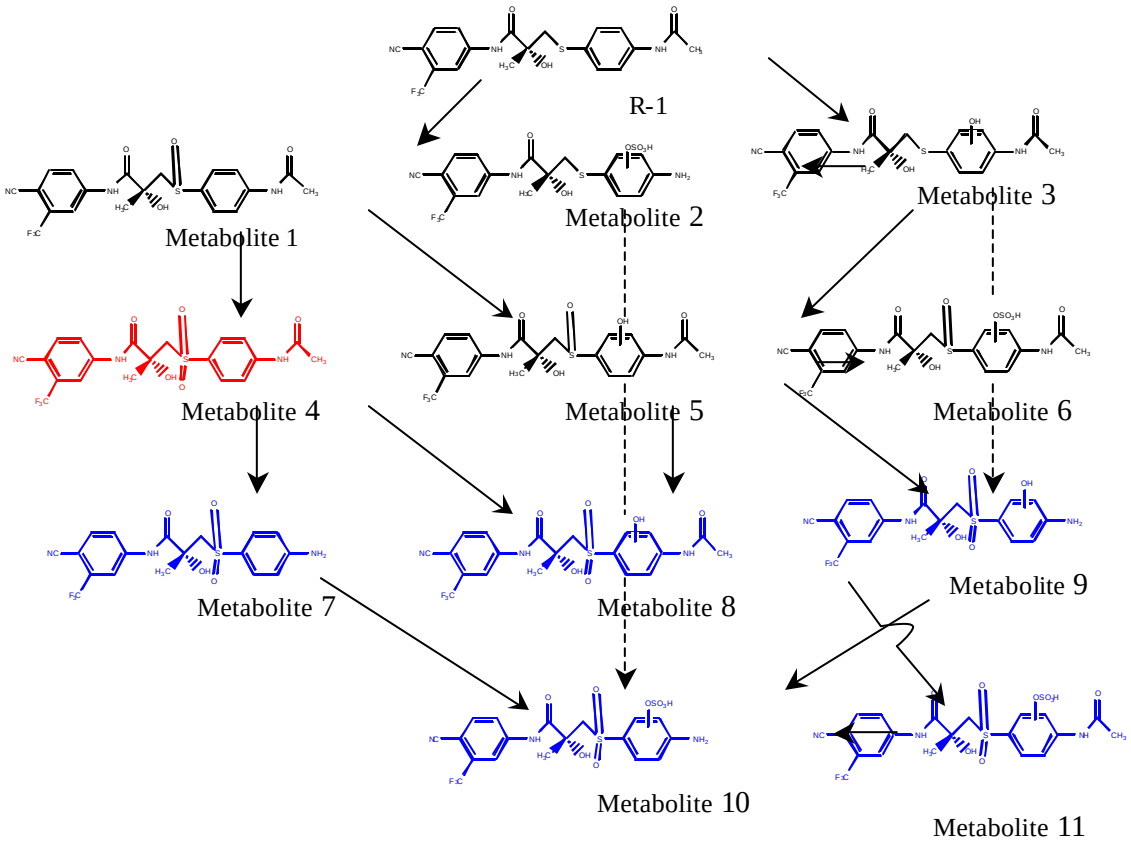

Figure 4.7. Proposed Metabolism of R-1.

The blue structures show metabolites that are possible AR antagonists (Metabolites 7, 8, 9, 10, and 11). The red chemical structure, Metabolite 4, was shown to be an antagonist in *in vitro* transcriptional activation studies. Adapted from reference 63.

CYP3A4 was involved in the metabolism of S-4. The findings in this study support the reduction of the nitro group to amine via CYP3A4. The presence of metabolite M5 (Table 4.4) suggests a step-wise reduction of the nitro group on the para position of the A ring. This step-wise reduction is common in P450 reduction reactions[83]. However, nitro-reduction can also be catalyzed by enzyme systems other than the P450s, such as DT-diaphorase or NADPH-cytochrome P450 reductase[84].

Species differences were seen in the metabolism of S-4. Oxidation of the B-ring was seen in rats and is absent in dogs, while oxidation at the methylene carbon was only seen in dogs. Oxidation of the A ring amine was seen in both species. These differences can be attributed to substrate specificities of the CYP P450 system[85]. Metabolite M6 was only found in beagle dog urine because dogs lack N-acetyltransferase (NAT)[86]. Interestingly, this metabolite showed antagonist activity in *in vitro* assays. Since both rats and humans possess this enzyme, metabolite M6 can be acetylated to form the parent compound in these species. In humans, polymorphism in NAT exists and can cause a slow acetylator phenotype[86]. Given the possible antagonist activity of metabolite M6, the polymorphism of NAT may play an important role in the pharmacologic affect of S-4 in humans.

During the first set of LC/MS studies, APCI ionization was chosen because of its advantages in ionizing relatively nonpolar compounds such as S-4, and because it is less affected by the salt content found in biological samples. However, APCI ionization can cleave phase II conjugated metabolites[88,89]. Initial analysis identified only two Phase II conjugates of S-4, metabolite M1 (methylated S-4) and metabolite M6 (sulfated amine metabolite). Analyzes of metabolites after the radioactive mass balance study were

conducted using electrospray ionization (ESI), which sacrificed some sensitivity, but allowed the identification of other phase II metabolites.

The metabolism studies of S-4 identified metabolite M6 as a possible AR antagonist.

To determine its possible affect, quantify of the metabolite is necessary. While LC/MS analysis can identify metabolites, it cannot quantitate the amount of each metabolite, because of differences in ionization between molecules and co-elution of endogenous substituents that blunt the ionization of drug or metabolite molecules. Therefore, disposition studies using radiolabel drug were conducted to determine the amount of each metabolite present and their metabolic pathway. These studies showed that a relatively hydrophilic metabolite, metabolite M9, constituted 25% of the injected dose, with the amine metabolite M2 constituting 11%. Within the feces the parent compound was the predominant radioactive constituent, accounting for approximately 32% of injected dose. The feces also contained the amine metabolite constituting approximately 4% of the injected dose. Three other minor metabolites, which were later identified by LC/MS analysis to be the sulfated amine conjugate (metabolite M4) and two glucuronidated conjugated of the amine metabolite. These phase II metabolites constituted 1.2% of the injected dose. The remaining radioactivity was found in the stomach contents, intestinal contents and organs (1.7%, 6% and 2.4% respectively).

The major metabolite of S-4 is the hydrolysis produce formed from the cleavage of the amide bond of S-4. This metabolite is primarily excreted in the urine. These findings are similar to the metabolic path seen with bicalutamide. Rats and mice cleave approximately 20 to 30 % of the bicalutamide dose to the carboxylic acid metabolite[81]. The amine portion of S-4 was not identified in either urine or feces. However it is

important to note that humans do not produce the carboxylic acid metabolite of bicalutamide. Thus, this phenomenon may be limited to animal species and contribute little, if any, to the human metabolism of S-4.

Radiographic analysis showed the presence of the parent compound in the feces, which is interesting given that the dose of radioactive S-4 was given intravenously. This may suggest biliary excretion of S-4. One of the most important factors in biliary excretion is the molecular weight of the compound[82,90]. A minimum molecular weight of between 200 and 325 is necessary for biliary excretion in rats, while the human molecular weight threshold is around 400 to 500[82]. Therefore, S-4 and many of its metabolites would meet this requirement. Bile is an aqueous solution, hence drugs that are commonly excreted in the bile are relatively hydrophilic or have been conjugated by phase I or phase II processes[90]. In addition, gut flora, such as β-glucuronidase, can hydrolyze the drug conjugates to liberate the parent compound within the intestines, which can then be reabsorbed into the plasma[91,92]. Boyle et al. which showed that 30% of the dose of bicalutamide given to rats was recovered in the bile as glucuronidated metabolites that were then cleaved within the intestines[81] . S-4 may also show some enterohepatic recirculation as is seen in the pharmacokinetic data. The concentration time profile of S-4 after IV administration showed an increase in the plasma concentration at around 30 to 60 minutes after the dose was given (Figure 3.6). Additional bile studies are needed to determine if S-4 is eliminated unchanged in the feces, or if it is cleaved within the intestines to the parent compound.

Examination of the feces using the longer mobile phase gradient, modified extraction procedure, and ESI ionization identified two glucuronidated amine

metabolites. These findings are expected, given that bicalutamide is extensively glucuronidated. However, the site of glucuronidation differs between S-4 and bicalutamide. Bicalutamide is glucuronidated on both the hydroxyl group on the chiral carbon and the oxidated B ring[81].

Figure 4.8 shows the proposed metabolic pathways of S-4 in dogs and Figure 4.9 shows the metabolic pathway in rats. From the extent of hydrolysis observed by the 32 % of injected dose converted to this metabolite, we can conclude that this process may be faster than oxidation or nitro reduction. However, the equivalent reaction of bicalutamide does not occur in humans. Since the amount of metabolite M6 is only present in dogs and since no other metabolite fits into know SARs for AR antagonism, we can conclude that the metabolism of S-4 does not appear to adversely affect the AR agonist activity of the compound.

The substitution of the oxygen atom for the sulfur atom in compound R-1 to produce optimized AR ligand S-4 provided an advantageous pharmacokinetics as well as slowed the rapid metabolism of the compound to an AR antagonist. This can be seen in the decrease in CL from 45 mL/min/kg for R-1 versus 4.7 mL/min/kg for S-4, as well as the increase in $T_{1/2}$ from 30 minutes for R-1 to 3.5 hours for S-4. In addition, the metabolites produced from S-4 do not appear to possess antagonist activity as seen in the pharmacologic studies conducted on S-4[78]. Therefore, the optimization of this compound has led to the development of a novel SARM that is orally bioavailable, selectively anabolic, while retaining its *in vivo* activity.

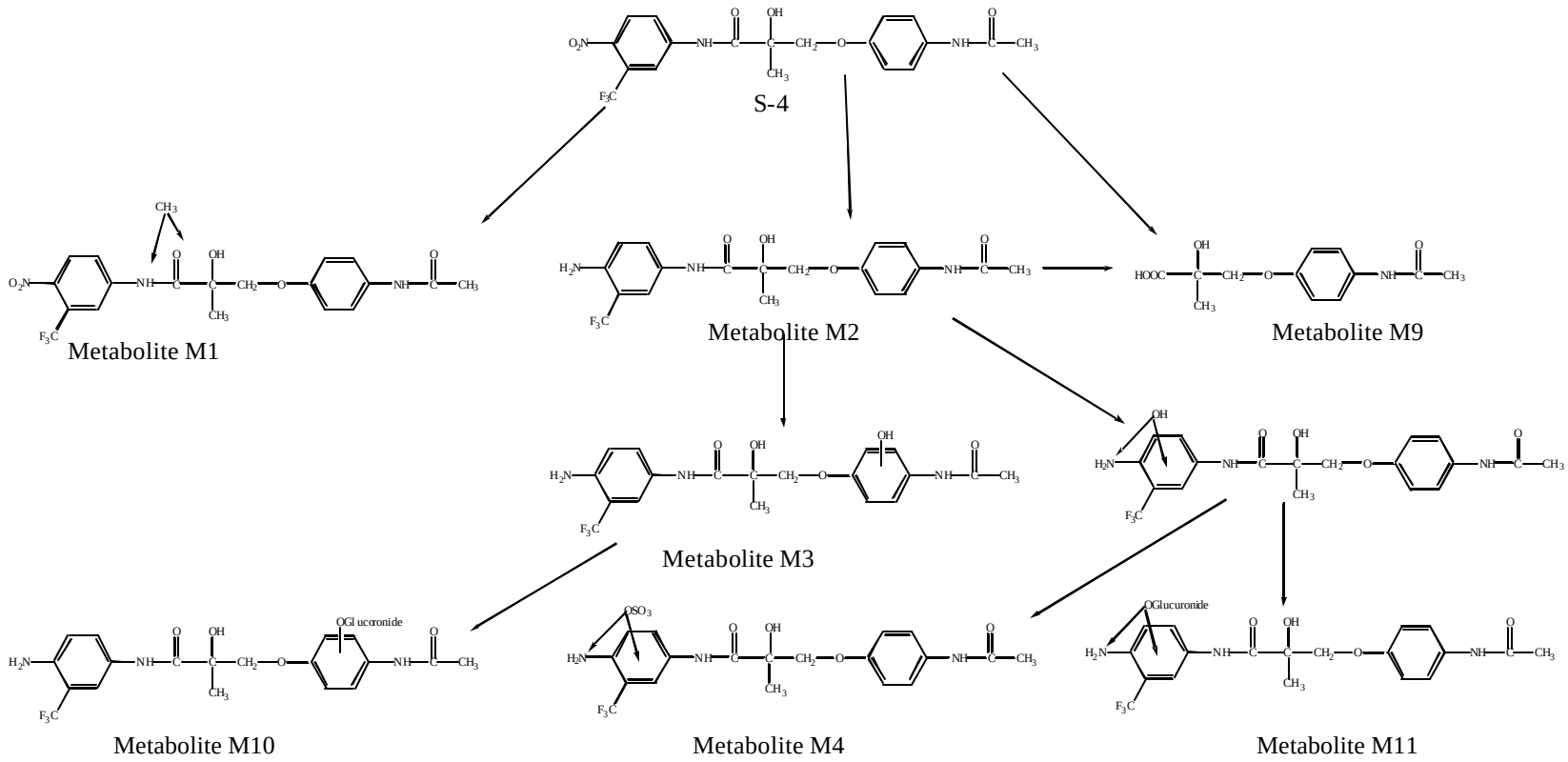

Figure 4.8. Proposed Metabolic Profile of S-4 in Rats.

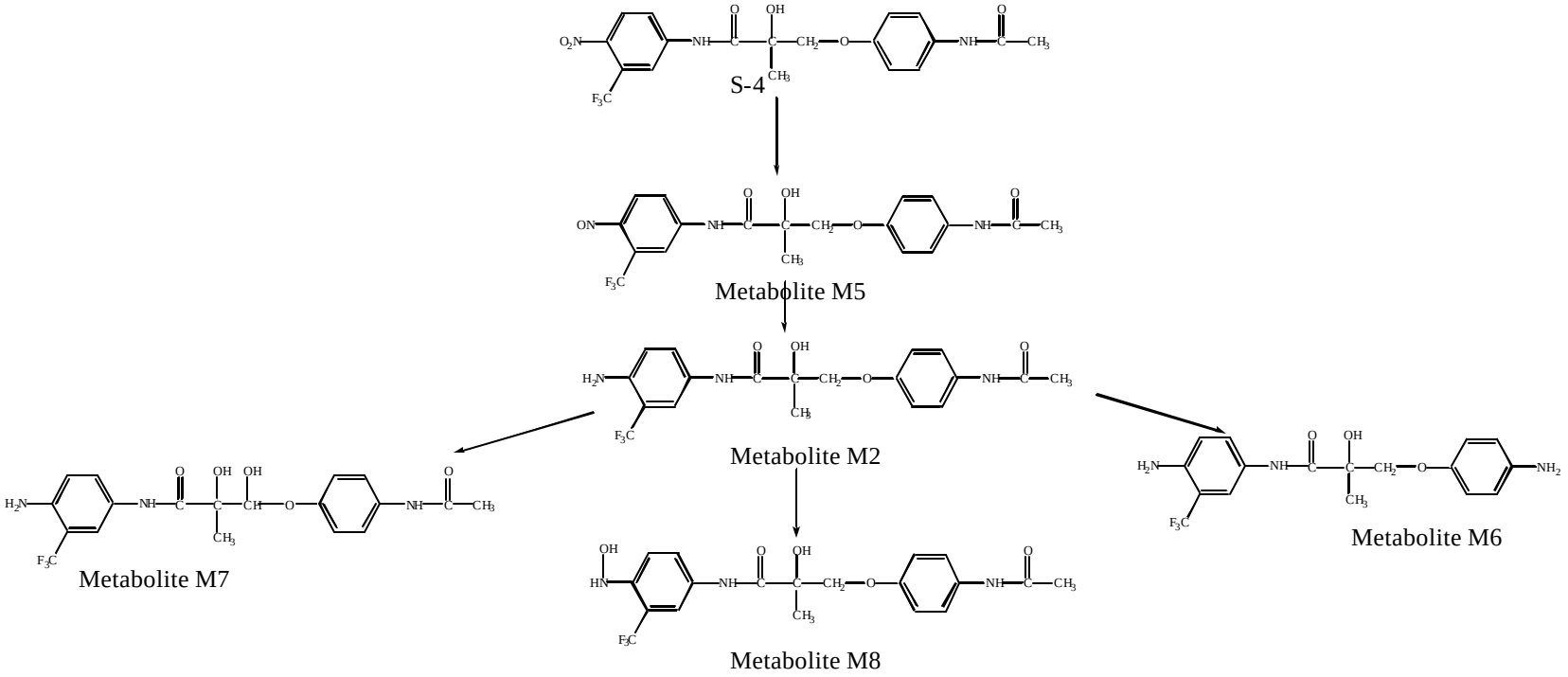

Figure 4.9. Proposed Metabolic Profile of S-4 in Dogs.

CHAPTER 5

DISCUSSION AND FUTURE STUDIES

5.1. Discussion

Testosterone, the endogenous male hormone, is responsible for a vast number of biological effects and can also be used therapeutically to treat many disorders such as those described in Chapter 1. However, there are disadvantages, which have limited the usefulness of testosterone, and these limitations prompted the development of SARMs. In an effort to develop a therapeutic SARM, we investigated a series of bicalutamide analogs for AR agonist activity. In this dissertation, we reported on a novel set of nonsteroidal AR agonists that were studied by both *in vitro* and *in vivo* assays to determine their pharmacologic action. A lead compound, S-4, was identified and further studies to qualitatively and quantitatively examine its absorption, distribution, metabolism, and elimination were completed.

The *in vitro* and *in vivo* assay described in Chapter 2 helped to establish the SARs used to develop potent AR agonists. Previous studies showed that the electron-withdrawing capacity of the substituents on the B ring plays an important role in AR binding, along with chirality and fixed conformational structure[10,43]. These findings were corroborated by studies showing that a TFAc functional group was the most potent B ring substituent. However, since TFAc is a better leaving group than Ac, the Ac substituent was used in the development of later compounds.

These studies also contributed new information to the known SARs, with the finding that higher AR binding and transcriptional activation could be seen with compounds bearing the trifluoromethyl group on the chiral carbon. However, difficulty in synthesis of these compounds precluded further studies of their pharmacologic properties. In addition, we discovered that the presences of a hydrogen bond acceptor at the para-position of the A ring, may be important to AR binding. Elucidation of the amino acids involved in AR binding of these SARMs may aid in the development of future compounds. This may be accomplished by crystallizing the AR bound to a SARM.

The highest potency and efficacy, at 10nM and 646% of testosterone respectively, was seen with R-2, which has a trifluoromethyl group at the chiral carbon. It was postulated that this may be due to the electron-withdrawing properties of this group, increasing the hydrogen donor capacity of the hydroxyl group on the chiral carbon. Determining the pharmacologic activity of this compound would be beneficial and would increase knowledge regarding the SAR for AR binding, in this portion of the nonsteroidal pharmacophore.

During *in vivo* pharmacologic studies, we discovered the first nonsteroidal anabolic SARM (R-7). This compound showed little affect on prostate and seminal vesicles, although a significant increase in levator ani muscle weight was seen. With the identification of a compound with selective activity, other compounds in this series were also tested in the *in vivo* pharmacologic activity assay.

To date, the SARM that have been developed have selective anabolic activity. Further pharmacologic evaluation and knowledge of SAR for AR binding and activation

is needed to develop SARMs that demonstrate selective androgenic activity. In addition, while selective activity was seen in two potential SARMs, the mechanism for this selectively has not been elucidated. Differences in coactivator/corepressor interactions, potency, tissue distribution, and tissue-selective amplification of the pharmacologic effect (e.g., testosterone conversion to dihydrotestosterone by 5α-reductase) may play a role, and are the focus of ongoing investigations in the laboratory. .

Studies conducted on a promising SARM, R-1, showed high binding affinity (K_i = 2.1nM), and full *in vivo* agonist activity. However, R-1 showed little pharmacologic effect in the animal model[63]. These inconsistencies were caused by the pharmacokinetics and metabolism of R-1, in which R-1 was converted by oxidation of the sulfur atom to an AR antagonist. We hypothesized that the substitution of an oxygen atom for the sulfur atom on the para position of the B-ring would decrease this conversion, and result in a compound with enhanced pharmacologic effect.

Rational structural modification of compound R-1 led to the development of S-4, an optimized ligand for the AR. The pharmacokinetic studies described in Chapter 3 found that replacement of the thioether linkage with an ether linkage resulted in lower clearance of S-4 as compared to R-1, which had a mean CL of 45 ml/min/kg and a mean half –life of around 30 minutes. However, the half-life ($T_{1/2}$ = 4 hr.) was still substantially shorter than bicalutamide ($T_{1/2}$ = 7 days after IV administration) [78]. In addition, we found that S-4 exhibited dose-dependent oral bioavailability. Higher oral bioavailability was seen at doses of 0.1 mg/kg. These findings are similar to the dose-dependent oral bioavailability of bicalutamide observed by Cockshott et al during preclinical studies[78]. The pharmacokinetics of S-4 allow it to overcome the

disadvantages of both testosterone (oral bioavailability) and compound R-1 (rapid clearance). The substitution of the oxygen atom in S-4 also hindered the metabolic conversion of the compound to the AR antagonist seen during R-1 metabolism (Figure 4.2). Overall, the structural modifications that led to the development of S-4 were advantageous to its role as a potential SARM.

Future studies are still need to full evaluate the pharmacokinetics of S-4. There are many possibilities for the dose-dependent oral bioavailability seen with S-4. While a likely cause is its low aqueous solubility, other mechanisms should be explored. Transporter and enzymatic studies that may contribute to pre-systemic degradation may be helpful.

The metabolism of S-4 was then investigated to determine what metabolites were formed and if they could affect the pharmacologic response of S-4. Metabolites were identified using LC/MS analysis. Radioactive disposition studies were conducted to determine the excretion pathways and the amount of each metabolite in each pathway. These studies showed that S-4 was excreted approximately equally in the urine and feces of rats after 48 hours. These studies also showed that the hydrolysis product of S-4 was the major metabolite, comprising 25 % of injected dose, with the amine metabolite comprised about 15% of the injected dose. S-4 comprised the majority of radioactivity seen in the feces, at about 32% of injected dose with minor amounts of glucuronidated amine metabolites and a sulfated amine metabolite. One urinary metabolite was identified as a potential AR antagonist. However, since both human and rats possess the enzyme N-acetyltransferase (NAT), these species can convert this possible antagonist back to the parent compound.

The studies in this dissertation examined the pharmacology, pharmacokinetics and metabolism of S-4 and related SARMs. The selective anabolic nature of S-4 would be conducive to the treatment of andropause as discussed in Chapter 1. Since S-4 showed minimal effect on the prostate, this would allow older men to maintain muscle mass while eliminating the concern over prostatic hypertrophy. Separate experiments on plasma LH and FSH level in rats showed that S-4 did not affect the endogenous feedback loop involved in testosterone release. Therefore, aging men would maintain their nature testosterone production while supplementing the androgens needed to preserve muscle mass.

5.2. Conclusions

In Chapter 1 we hypothesized that by using known SARs for the AR we could synthesize a novel nonsteroidal SARM containing high binding affinity and full agonist activity. We reported that specific structural modification (i.e. TFAc and Ac group on the R_4 position of the molecule and sulfur atom of the R_3 position of the molecule) increased the binding and AR mediated transcriptional activation that could be achieved. These discoveries led to the development of the lead compound, S-4. In Chapter 2 we hypothesized that the substitution of an oxygen atom for the sulfur atom at position R_3 would improve the rapid elimination seen with compound R-1. We reported that the half-life of the compound increased to 4 hours and that the clearance decreased to 4.7 mL/min/kg (R-1 showed a clearance of 45 mL/min/kg). We could then conclude that substitution of the oxygen atom provided a favorable pharmacokinetic result. In Chapter 4, we hypothesized that the substitution of the oxygen atom prevented the conversion of

this AR agonist to an antagonist. We reported that the major metabolites of S-4 were not known antagonists. Therefore, the metabolism of S-4 would not adversely affect the pharmacologic activity of the compound. The finding in these studies will be useful in the development of further structurally optimized nonsteroidal SARMs with anabolic and androgenic activity. Studies to examine the efficacy and pharmacokinetics of such compounds are now underway and may someday lead to the development of a new class of drugs for the treatment of osteoporosis, male hormone replacement, muscle wasting, or male contraception.

BIBLIOGRAPHY

1. Hiort O. Androgens and puberty. *Best Pract Res Clin Endocrinol Metab* **16**(1):31-41, 2002.

2. Sharpe RM. hCG-induced decrease in availability of the rat testis receptors. *Nature* **264**: (5587):644-646, 1976.

3. Matsumoto AM, Bremner WJ. Modulation of pulsatile gonadotropin secretion by testosterone in man. *J Clin Endocrinol Metab* **58**(4):609-614, 1984.

4. Steers WD. 5α Reductase Activity in the Prostate. *Urology* **58**(Suppl. 6A):17-24, 2001.

5. Deslylypree JP, Young M, Wilson JD, McPhaul MJ. Testosterone and 5 alpha-dihydrotestosterone interact differently with the androgen receptor to enhance transcription of the MMTV-CAT reporter gene. *Mol Cell Endocrinol* **88**:15-22, 1992.

6. Bruchovsky N, Wilson JD. The conversion of testosterone to 5α-androstan-17β-ol-3-one by rat prostate *in vivo* and *in vitro*. *J Biol Chem* **243**:2012-2021, 1964.

7. Roy AK, Tyagi RK, Song CS, Lavrovsky Y, Ahn SC, Oh TS, and Chatterjee B. Androgen Receptor: Structure Domains and Functional Dynamics after Ligand Receptor Interactions *Ann NY Acad Sci* **949**:44-57, 2001.

8. Heinlein CA, Chang C. Androgen Receptor (AR) Coregulators: An Overview. *Endocrine Reviews* **23**(2):175-200, 2002.

9. Haendler B. Androgen-selective gene regulation in the prostate. *Biomed Pharmacother* **56**(2):78-83, 2002.

10. Singh SM, Gauthier S, Labrie F. Androgen Receptor Antagonist (Antiandrogens): Structure-Activity Relationships. *Curr Med Chem* **7**(2): 211-247, 2000.

11. DeFranco DB. Regulation of steroid receptor subcellular trafficking. *Cell Biochem Biophys*;30(1):1-24, 1999.

12. Sack JS, Kish KF, Wang C, Attar RM, Kiefer SE, An Y, Wu GY, Scheffler JE, Salvati ME, Krystek SR Jr., Weinmann R, Einspahr HM. *Proc Natl Acad Sci* **98**(9):4904-4909, 2001.

13. Matias PM, Donner P, Coelho R, Thmaz M, Peixoto C, Macedo S, Otto N, Joschko S, Scholz P, Wegg A, Basler S, Schafer M, Egner U, Carrondo MA. Structural evidence for the ligand specificity in the binding domain of the human androgen receptor. Implications for the pathogenic gene mutations. *J Biol Chem* **275**(34): 26164-26171, 2000

14. Marhefka CA, Moore BM, Bishop TC, Kirkovsky L, Mukherjee A, Dalton JT, and Miller DD. Homology Modeling Using Multiple Molecular Dynamics Simulations and Docking Studies of the Human Androgen Receptor Ligand Binding Domain Bound to Testosterone and Nonsteroidal Ligands *J Med Chem* **44**(11): 1729-1740, 2001.

15. Weinbauer GF, Nieschlag E. The role of testosterone in spermatogenesis. In: E. Nieschlag, H.M. Behre S. Nieschlag (eds.). Testosterone: action, deficiency, substitution. Berlin; New York: Springer, 187-207, 1998.

16. Gonzales GF. Function of seminal vesicles and their role on male fertility. *Asian J Androl* **3**(4): 251-258, 2001

17. McLachlan RI, O'Donnell L, Meachem SJ, Stanton PG, de Kretser DM, Pratis K, Robertson DM. Identification of specific sites of hormonal regulation in spermatogenesis in rats, monkeys, and man. *Recent Prog Horm Res* **57**:149-179, 2002.

18. Randall VA. Role of 5 alpha-reductase in health and disease. *Baillieres Clin Endocrinol Metab* **8**(2):405-431, 1994.

19. Imperato-McGinley J, Sanchez RS, Spencer JR, Yee B, Vaughan ED. Comparison of the effects of the 5α-reductase inhibitor finasteride and the antiandrogen flutaminde on prostate and genital differentiation: Dose-response studies. *Endocrinolo* **131**:1149-1159, 1992.

20. Niu YJ, Ma TX, Zhang J, Xu Y, Han RF, Sun G. Androgen and prostatic stroma. *Asian J Androl* **5**(1):19-26, 2003.

21. Antonio J, Wilson JD, George FW. Effects of castration and androgen treatment on androgen-receptor levels in rat skeletal muscles. *Appl Physiol* **87**(6):2016-2019, 1999.

22. Mooradian AD, Morley JE, Korenman SG. Biological actions of Androgens *Endocrinol Rev* **8**:1-27, 1987.

23. Sartok T, Dahlberg E, Gustafsonn JA. Relative binding affinity of anabolic-androgenic steroids: Comparison of the binding to the androgen receptor in skeletal muscle and in prostate, as well as to sex hormone-binding globulin. *Endocrinolo* **114**:2100-2106, 1984.

24. Snyder PJ, Peachey H, Berlin JA, Hannoush P, Haddad G, Dlewati A, Santanna J, Loh L, Lenrow DA, Holmes JH, Kapoor SC, Atkinson LE, Strom BL. Effects of testosterone replacement in hypogonadal men. *J Clin Endocrinol Metab* **85**(8):2670-2677, 2000.

25. Manolagas SC and Kousteni S. Prespectives: Nonreproductive Sites of Action of Reproductive Hormones *Endocrinol* **142**(6): 2200-2204, 2001.

26. Mongolas SC, Kousteni S, Jilka RL. Sex steroids and bone. *Recent Prog Horm Res* **57**:385-409, 2002.

27. Finkelestein JS. Androgens and Bone Metabolism. In: E. Nieschlag, H.M. Behre S. Nieschlag (eds.). Testosterone: action, deficiency, substitution. Berlin; New York: Springer, 187-207, 1998.

28. Gunness M, Orwoll E. Early induction of alterations in cancellous and cortical bone histology after orchiectomy in mature rats. *J Bone Miner Res* **10**(11): 1735-1744, 1995.

29. Krabbe S, Christensen T, Worm J, Christiansen C, Transbol I. Relationship between hemoglobin and serum testosterone in normal children and adolescents and in boys with delayed puberty. *Acta Paediatr Scand* 67(5):655-658, 1978.

30. Fried W, Gurney CW. The erythropoietic response to testosterone in male and female mice. *J Lab Clin Med* **67**(3):420-426, 1966.

31. Zhi L and Martinborough E. Selective Androgen Receptor Modulators (SARMs)

32. Anderson RA, Van Der Spuy ZM, Dada OA, Tregoning SK, Zinn PM, Adeniji OA, Fakoya TA, Smith KB, Baird DT. Investigation of hormonal male contraception in African men: suppression of spermatogenesis by oral desogestrel with depot testosterone. *Hum Reprod* **17**(11): 2869-2877, 2002.

33. Liu PY, Handelsman DJ. Androgen therapy in non-gonadal disease. In: E. Nieschlag, H.M. Behre S. Nieschlag (eds.). Testosterone: action, deficiency, substitution. Berlin; New York: Springer, 187-207, 1998.

34. Badatell CJ, Bremner WJ. Drug Therapy: Androgen in Men – Uses and Abuses. *New Engl J Med* **334**(1): 707-714, 1996.

35. Reid P, Kantoff P, Oh W. Antiandrogens in prostate cancer. *Invest New Drugs* **17**: 271-284, 1999.

36. Neri RO, Monahan M. Effects of a novel nonsteroidal antiandrogen on canine prostatic hyperplasia. *Invest Urol* **10**(2): 123-130, 1972.

37. Mahler C, Verhelst J, Denis L. Clinical Pharmacokinetics of Antiandrogens and Their Efficacy in Prostate Cancer. *Clin Pharmacokinet* **35**(5): 405-417, 1998.

38. Staiman VR, Lowe FC. Tamoxifen for flutamide/finasteride-induced gynecomastia. *Urology* **50**(6): 929-933, 1997.

39. Harnois C, Malenfant M, Dupont A, Labrie F. Ocular toxicity of Anandron in patients treated for prostatic cancer. *Br J Ophthalmol* **70**(6):471-483, 1986.

40. Tucker H, Crook JW, Chesterson GJ. Nonsteroidal antiandrogens. Synthesis and structure-activity relationships of 3-substituted derivatives of 2-hydroxypropionanilides. *J Med Chem* **31**(5): 954-959, 1988.

41. Kovenbag GJ, Furr BJ, Blackledge GR. Receptor affinity and potency of non-steriodal antiandrogens: translation of preclinical findings into clinical activity. *Prostate Cancer Prostatic Dis* **1**(6): 307-314, 1998.

42. Mukherjee A, Kirkovsky L, Yao XT, Yates RC, Miller DD, Dalton JT. Enantioselective binding of Casodex to the androgen receptor. *Xenobiotica* **26**(2): 117-122, 1996.

43. Morris JJ, Hughes LR, Glen AT, Taylor PJ. Non-steroidal antiandrogens. Design of novel compounds based on an infrared study of the dominant conformation and hydrogen-bonding properties of a series of anilide antiandrogens. *J Med Chem* **34**(1): 447-55, 1991.

44. Poujol N, Wurtz JM, Tahiri B, Lumbroso S, Nicolas JC, Moras D, Sultan C. Specific Recognition of Androgens by Their Nuclear Receptor. *J Biol. Chem* **275**(31): 24022-24031, 2000.

45. Swerdloff RS, Wang C. Androgens and the aging male. In: Lunenfeld B, Gooren L (eds.) Textbook of Men's Health. Boca Raton: Parthenon Pub. Group 148-166, 2002.

46. Gupta SK, Lindemulder EA, Sathyan G. Modeling of Circadian Testosterone in Healthy Men and Hypogonadal Men *J Clin Pharmacol* **40**:731-738, 2000.

47. Negro-Vilar A. Selective Androgen Receptor Modulators (SARMs): A Novel Approach to Androgen Therapy for the Millennium. *J Clin Endocrinol Metab* **84**(10): 3459-3462, 1999.

48. Lambert SWJ, van der Beld AW, van der Lely AJ. The Endocrinology of Aging. *Science* **278**(5337): 419-424, 1997.

49. Gruenewald DA, Matsumoto AM. Testosterone Supplimentation Therapy for Older men: Potential Benefits and Risks. *J Am Geriatr Soc* **51**(1): 101-115, 2003.

50. Bremmer WJ, Vitiello WV, Prinz PN. Loss of Circadian Rhythmicity in Blood Testosterone Levels with Aging. *J Clin Endocrinol Metab* **56**(6): 1278-1281, 1983.

51. Nilsson p, Moller L, Solstad K. Adverse effects of psychosocial stress on gonadal function and insulin levels in middle aged males. *J Intern Med* **237**(5):479-86, 1995.

52. Penson DF, Ng C, Cai L, Rajfer J, Gonzalez-Cadavid NF. Androgen and pituitary control of penile nitric oxide synthase and erectile function in the rat. *Biol Reprod* **55**(3):567-74, 1996.

53. Aversa A, Isidori AM, Spera G, Lenzi A, Fabbri A. Androgens improve cavernous vasodilatation and response to sildenafil in patients with erectile dysfunction. *Clin Endocrinol* **58**(5):632-638, 2003.

54. Sinha-Hikim I, Artaza J, Woodhouse L, Gonzalez-Cadavid N, Singh AB, Lee MI, Storer TW, Casaburi R, Shen R, Bhasin S. Testosterone-induced increase in muscle size in healthy young men is associated with muscle fiber hypertrophy. *Am J Physiol Endocrinol Metab* **283**(1):E154-E164, 2002.

55. Jensen MD. Androgen effect on body composition and fat metabolism. *Mayo Clin Proc* **75** (Suppl):S65-S69, 2000.

56. van der Beld AW, de Jong FH, Grobbee DE, Pols HAP, Lamberts SWJ. Measures of Bioavailable Serum Testosterone and Estradiol and Their Relationship with Muscle Strength, Bone Density, and Body Composition in Elderly Men. *J Clin Endocrinol Metab* **85**(9): 3276-3282, 2000.

57. Khosla S, Melton LJ 3rd, Atkinson EJ, O'Fallon WM. Relationship of serum sex steroid levels to longitudinal changes in bone density in young versus elderly men. *J Clin Endocrinol Metab* **86**(8): 3555-3561, 2001.

58. Kenny AM, Prestwood KM, Gruman CA, Marcello KM, Raisz LG. Effects of transdermal testosterone on bone and muscle in older men with low bioavailable testosterone levels. *J Gerontol A Biol Sci Med Sci* **56**(5): M266-M272, 2001.

59. Cherrier MM, Anawalt BD, Herbst KL, Amory JK, Craft S, Matsumoto AM, Bremner WJ. Cognitive effects of short-term manipulation of serum sex steroids in healthy young men. *J Clin Endocrinol Metab* **87**(7): 3090-6, 2002.

60. Cherrier MM, Asthana S, Plymate S, Baker L, Matsumoto AM, Peskind E, Raskind MA, Brodkin K, Bremner W, Petrova A, LaTendresse S, Craft S. Testosterone supplementation improves spatial and verbal memory in healthy older men. *Neurology* **57**(1): 80-88, 2001.

61. Ferrando AA, Sheffield-Moore M, Yeckel CW, Gilkison C, Jiang J, Achacosa A, Lieberman SA, Tipton K, Wolfe RR, Urban RJ. Testosterone administration to older men improves muscle function: molecular and physiological mechanisms. *Am J Physiol Endocrinol Metab* **282**(3): E601-E60, 2002.

62. Sih R, Morley JE, Kaiser FE, Perry HM 3rd, Patrick P, Ross C. Testosterone replacement in older hypogonadal men: a 12-month randomized controlled trial. *J Clin Endocrinol Metab* **82**(6): 1661-1667, 1997.

63. Yin D, Xu H, He Y, Kirkovsky LI, Miller DD, Dalton JT. Pharmacology, pharmacokinetics, and metabolism of acetothiolutamide, a novel nonsteroidal agonist for the androgen receptor. *J Pharmacol Exp Ther* **304**(3): 1323-1333, 2003.

64. Dalton JT, Mukherjee A, Zhu Z, Kirkovsky L, Miller DD. Discovery of nonsteroidal androgens. *Biochem Biophys Res Commun* **244**(1): 1-4, 1998.

65. Wurtz JM, Bourguet W, Renaud JP, Vivat V, Chambon P, Moras D, Gronemeyer H. A canonical structure for the ligand-binding domain of nuclear receptors. *Nat Struct Biol* **3**(2): 206, 1996.

66. Yin D, He Y, Perera MA, Hong SS, Marhefka C, Stourman N, Kirkovsky L, Miller DD, Dalton JT. Key structural features of nonsteroidal ligands for binding and activation of the androgen receptor. *Mol Pharmacol* **63**(1): 211-223, 2003.

67. Hershberger LG, Shipley EG, and Meyer RK. Myotrophic activity of 19-nortestosterone and other steroids determined by modified levator ani muscle method *Proc Soc Exp Biol Med* **83**:175-180, 1953.

68. Yamada T, Kunimatsu T, Sako H, Yabushita S, Sukata T, Okuno Y, Matsuo M. Comparative Evaluation of a 5-Day Hershberger Assay utilizing Mature Males

Rats and a Pubertal Male Assay for Detection of Flutaminde's Antiandrogenic Activity. *Toxicologi Sci* **53**:289-296, 2000.

69. Kim HS, Han SY, Kim TS, Kwack SJ, Lee RD, Kim IY, Lee BM, Yoo SD, Park KL. No androgenic/anti-androgenic effects of bisphenol-A in Hersberger assay using immature castrated rats. *Toxicol Lett* **135**:111-123, 2002

70. Niu YJ, Ma TX, Zhang J, Xu Y, Han RF, Sun G. Androgen and prostatic stroma. *Asian J Androl* **5**(1): 19-26, 2003

71. Kirkovsky L, Mukherjee A, Yin D, Dalton JT, Miller DD. Chiral nonsteroidal affinity ligands for the androgen receptor. 1. Bicalutamide analogues bearing electrophilic groups in the B aromatic ring. *J Med Chem* **43**(4): 581-590, 2000.

72. Williams DA, Lemke TL. Drug Design and Relationship of Functional Groups to Pharmacologic Activity. In: Foye's Principles of Medicinal Chemistry 5th Ed. Philidelphia: Lippincott Williams & Wilkins, 2001

73. Dressman JB. Comparison of Canine and Human Gastrointestinal Physiology. *Pharm Res* **3**(3): 123-131, 1986.

74. Lui CY, Amidon GL, Berardi RR, Fleisher D, Youngberg C, Dressman JB. Comparison of Gastointestinal pH in Dogs and Humans: Implications on the Use of the Beagle Dog as a Model for Oral Absorption in Humans. *J Pharm Sci* **75**(3): 271-274, 1986.

75. Jiunn LH. Species Similarities and Differences in Pharmacokinetics. *Drug Met & Disp* **23**(10): 1008-1021, 1995.

76. Tibbitts J. Issues related to the Use of Canines in Toxicology Pathology-Issues with Pharmacokinetics and Metabolism. *Tox Pathol* **31**(Suppl.): 17-24, 2003.

77. Ohmori S, Taniguchi T, Rikihisa T, Kanakubo Y, Kitada M. Species differences of testosterone 16-hydroxylases in liver microsomes of guinea pig, rat and dog. *Xenobiotica* **23**(4): 419-426, 1993.

78. Yin D, Gao W, Kearbey JD, Xu H, Chung K, He Y, Marhefka CA, Veverka KA, Miller DD, Dalton JT. Pharmacodynamics of selective androgen receptor modulators. *J Pharmacol Exp Ther* **304**(3): 1334-1340, 2003

79. Cockshott ID, Plummer GF, Cooper KJ, and Warwick MJ. The pharmacokinetics of Casodex in laboratory animals. *Xenobiotica* **21**(10): 1347-1355, 1991.

80. Davies B, and Morris T. Physiological parameters in laboratory animals and humans. *Pharm Res* **10**(7): 1093-1095, 1993.

81. Boyle GW, McKillop D, Phillips PJ, Harding JR, Pickford R, McCormick AD. Metabolism of Casodex in Laboratory Animals. *Xenabiotica* **23**(7): 781-798, 1993.

82. Gibaldi M. Biopharmaceutics and Clinical Pharmacokinetics 4th Edition. Philadelphia: Lea & Febiger, 1991.

83. Seree EJ, Pisano PJ, Placidi M, Rahmani R, Barra YA. Identification of the human and animal hepatic cytocrome P450 involved in clonazepam metabolism. *Fundam Clin Pharmacol* **7**(2): 69-75, 1993.

84. Gibson GG, Skett P. Introduction to Drug Metabolism 2nd Edition. Blackie Academic & Professional, 1996. *Environ Health Perspect.* **106**(10): 633-641, 1998.

85. Lewis DF, Ioannides C, Parke DV. Cytochromes P450 and species differences in xenobiotic metabolism and activation of carcinogen.

86. King CM, Glowinski IB. Acetylation, Deacetylation and Actyltransfer. *Enviorn. Health Perspec.***49**:43-50, 1983.

87. Hein DW. Molecular genetics and function of NAT1 and NAT2: role in aromatic amine metabolism and carcinogenesis. *Mutat Res* **506-507**:65-77, 2002.

88. Ganguly AK, Pramanik BN, Chen G, Shipkova PA. Characterization of Pharmaceutical and Natural Products by Electrospray Ionization Mass Spectrometry. In: Pramanik BN, Ganguly AK, Gross ML. (eds.) Applied Electrospray Mass Spectrometry. New York: Marcel Dekker, Inc., 149-186, 2002.

89. Thurman EM, Ferrer I, Barcelo D. Choosing between Atmospheric Pressure Chemical Ionization and Electrospray Ionization Interfaces for the HPLC/MS Analysis of Pesticides. *Anal. Chem.* **73**: 5441-5449, 2001.

90. Roberts MS, Magnusson BM, Burczynski FJ, Weiss M. Entrohepatic Circulation Physiological, Pharmacokinetic, and Clinical Implications. *Clin Pharmcokinet* **41**(10): 751-790, 2002.

91. Hazenberg MP, de Herder WW, Visser TJ. Hydrolysis of iodothyronine conjugates by intestinal bacteria. *FEMS Microbiol Rev.* **4**(1): 9-16, 1988.

92. Kuhn JG. Pharmacology of irinotecan. *Oncology (Huntingt).* **12**(8 Suppl 6): 39-42, 1998.

Appendix A

Data Related to Chapter 2

Concentration (μM)	Reading 1	Reading 2	Reading 3	% specific Binding			
10	65	76.4	97	1.3938384	3.1859156	6.424230582	
5	79.6	67.2	67.4	3.6889548	1.7396778	1.771117783	
1	106.2	112	111	7.8704683	8.7822269	8.625027176	
0.5	129.4	150.4	133.4	11.517503	14.818698	12.14630173	
0.1	320.4	316.8	337.2	41.542656	40.976737	44.18361215	
0.05	618	613	640.4	88.325304	87.539305	91.84657838	
0.01	740.2	692	784.6	107.53511	99.958086	114.5147833	
0.001	644	770.6	742.4	92.412498	112.31399	107.8809536	
0.0001	595.6	742.4	674	84.804029	107.88095	97.12849021	
0.00001	721.8	716.8	714.8	104.64264	103.85664	103.5422403	Average
			EC 50	0.078954	0.056226	0.07223	
			Ki	12.606101	8.9772605	11.53252101	
			Corrected Ki	2.407678	1.7145945	2.202631579	2.108301

Relative Binding Affinity (RBA) % 2.108301

Table A.1. Competitive binding of Compound R-1 to the AR.

The specific binding of ^{3}H-MIB with increasing concentration of test compound was expressed as a percentage of ^{3}H-MIB binding in the absence of test compound. Nonspecific binding was subtracted form total binding to obtain specific binding. Experiment was preformed in triplicate.

Concentration (μM)	Reading 1	Reading 2	Reading 3	% specific Binding			
10	53.6	68.6	61.1	0.354143	1.871901	1.113022	
5	48	45	46	0	0	0	
1	93.2	66.8	80	4.361024	168977	3.025397	
0.5	100.8	78.6	89.7	5.130021	2.88374	4.006881	
0.1	86.4	85.4	85.8	3.672974	3.57179	3.622382	
0.05	218	199	205.5	16.98877	15.06628	16.02752	
0.01	859.6	830.6	844.5	81.90833	78.974	80.44116	
0.001	1243.4	1311.8	1277.6	120.7427	127.6637	124.2032	
0.0001	1278	1301.2	1289.6	124.2437	126.5911	125.4174	
0.00001	1241.4	1300	1300	120.5403	126.4697	123.505	Average
			EC 50	0.015543	0.013647	0.14595	
			Ki	2.481655	2.178933	2.330294	
			Corrected Ki	1.552288	1.362933	1.457611	1.46093

Relative Binding Affinity (RBA) % 18.52347

Table A.2. Competitive binding of Compound R-2 to the AR.
The specific binding of ^{3}H-MIB with increasing concentration of test compound was expressed as a percentage of ^{3}H-MIB binding in the absence of test compound. Nonspecific binding was subtracted form total binding to obtain specific binding. Experiment was preformed in triplicate.

Concentration (μM)	Reading 1	Reading 2	Reading 3	% specific Binding			
10	91	99	78	3.325843	3.865169	2.449439	
5	134	89	70	6.22472	3.191012	1.910113	
1	179	158	138	9.258429	7.842698	6.494383	
0.5	290	272	258	16.74158	15.52809	14.58427	
0.1	577	506	597	36.0899	31.30338	37.43821	
0.05	1436	1516	1383	94.00002	99.39328	90.42699	
0.01	1504	1304	1649	98.58429	85.10114	108.3596	
0.001	1566	1673	1431	102.7641	109.9776	93.66294	
0.0001	1560	1453	1413	102.3596	95.14609	92.44946	
0.00001	1326	988	531	86.58429			Average
			EC 50	0.090501	0.092816	0.089112	
			Ki	14.44974	14.81936	14.22797	
			Corrected Ki	9.257143	9.514286	9.128571	9.3

Relative Binding Affinity (RBA) % 2.912686

Table A.3. Competitive binding of Compound R-3 to the AR.
The specific binding of ^{3}H-MIB with increasing concentration of test compound was expressed as a percentage of ^{3}H-MIB binding in the absence of test compound. Nonspecific binding was subtracted form total binding to obtain specific binding. Experiment was preformed in triplicate.

Concentration (μM)	Reading 1	Reading 2	Reading 3	% specific Binding			
10	246.6	245.6	222	12.18794	12.12574	10.65771	
5	458.8	383.4	415.2	25.38774	20.69752	22.67562	
1	905.6	893	816.2	53.18072	52.39695	47.61964	
0.5	1074.4	1164.4	1111.2	63.68085	69.27926	65.96998	
0.1	1422.6	1455.2	1415.8	85.34047	87.36833	84.91748	
0.05	1196.6	1571	1513.4		94.57162	90.98864	
0.01	1613	1594	1614	97.18421	96.00232	97.24641	
0.001	1630.8	1556.4	1447	98.29145	93.66343	86.85826	
0.0001	1512.6	1491.8	1532.6	90.93887	89.64502	92.18296	
0.00001	1487.4	1585.6	1455	89.37132	95.4798	87.35589	Average
			EC 50	1.321042	1.337422	1.268063	
			Ki	210.9227	213.538	202.4638	
			Corrected Ki	47.06033	47.6405	45.16364	46.62149

Relative Binding Affinity (RBA) % 0.577864

Table A.4. Competitive binding of Compound R-4 to the AR.
The specific binding of ^{3}H-MIB with increasing concentration of test compound was expressed as a percentage of ^{3}H-MIB binding in the absence of test compound. Nonspecific binding was subtracted form total binding to obtain specific binding. Experiment was prefo rmed in triplicate.

Concentration (μM)	Reading 1	Reading 2	Reading 3	% specific Binding			
10	40.8	38	39.4	0	0	0	
5	43	47.8	45.4	0	0.445411	0.19681	
1	61.6	65.4	63.5	1.874871	2.26849	2.07168	
0.5	90.6	78.2	84.4	4.878807	3.594365	4.236586	
0.1	184.6	195	189.8	14.6157	15.69298	15.15434	
0.05	737.2	679	708.1	71.85623	65.82764	68.84193	
0.01	1205	1221.2	1231.1	120.3128	121.9909	121.1519	
0.001	1257.8	1234.6	1246.2	125.7821	123.3789	124.5805	
0.0001	1212.6	1196	1204.3	121.1001	119.3806	120.2403	
0.00001	1122.2	929.8	1026	111.7361	91.80651	101.7713	Average
			EC 50	0.056283	0.055357	0.05582	
			Ki	8.986361	8.838513	8.912437	
			Corrected Ki	3.035336	2.985397	3.010367	3.007125

Relative Binding Affinity (RBA) % 8.969008

Table A.5. Competitive binding of Compound R-5 to the AR.

The specific binding of ^{3}H-MIB with increasing concentration of test compound was expressed as a percentage of ^{3}H-MIB binding in the absence of test compound. Nonspecific binding was subtracted form total binding to obtain specific binding. Experiment was preformed in triplicate.

Concentration (μM)	Reading 1	Reading 2	Reading 3	% specific Binding			
10	60.8	57.6	59.2	1.746102	3.30344	-0.80227	
5	70	66.4	68.2	2.737136	-0.37754	8.966489	
1	82.2	86.4	84.3	11.51486	12.78905	10.38225	
0.5	121	114.8	117.9	24.11515	19.30155	25.95564	
0.1	235.6	276	255.8	59.36762	51.29778	56.5361	
0.05	354.2	332.8	343.5	66.44644	69.27796	74.94101	
0.01	709.4	709.4	709.4	105.2383	126.05	110.9014	
0.001	838.8	865.2	852	122.9353	101.8405	103.9641	
0.0001	843.6	821.6	832.6	107.6451	110.6182	112.6003	Average
			EC 50	0.090996	0.091902	0.114511	
			Ki	9.08	10.24	8.67	
			Corrected Ki	4.086	4.608	3.9015	4.1985

Relative Binding Affinity (RBA) % 2.912686

Table A.6. Competitive binding of Compound R-6 to the AR.
The specific binding of ^{3}H-MIB with increasing concentration of test compound was expressed as a percentage of ^{3}H-MIB binding in the absence of test compound.

Nonspecific binding was subtracted form total binding to obtain specific binding.

Experiment was preformed in triplicate.

.

Concentration (μM)	Reading 1	Reading 2	Reading 3	% specific Binding			
10	123.8	102.8	116.6	0.5648081	0	0	
5	139.4	128.8	132	2.2592324	1.1078928	1.4554671	
1	169.2	146.6	135.6	5.4960174	3.0412744	18464881	
0.5	171.6	180.01	118.4	5.756698	6.6701665	0	
0.1	240.8	253.21	244.41	13.274077	14.620927	13.665098	
0.05	319.6	316.81	340.81	21.833092	21.528965	24.135771	
0.01	596.4	675.02	672.42	51.899348	60.43664	60.154236	
0.001	886.03	836.03	896.63	83.355902	77.925054	84.507241	
0.0001	1014.8	991.04	958.84	97.34685	94.761767	91.264301	
0.00001	883.8	943.64	943.64	83.116944	89.613324	89.613324	Average
			EC 50				
			Ki	2.17	2.65	2.95	
			Corrected Ki	0.9765	1.1925	1.3275	1.2

Relative Binding Affinity (RBA) % 0.577864

Table A.7. Competitive binding of Compound R-7 to the AR.
The specific binding of ^{3}H-MIB with increasing concentration of test compound was expressed as a percentage of ^{3}H-MIB binding in the absence of test compound. Nonspecific binding was subtracted form total binding to obtain specific binding. Experiment was preformed in triplicate

Concentration (μM)	Reading 1	Reading 2	Reading 3	% specific Binding			
10	87.5	80	101	-10.5572	-13.4897	-2.78592	
5	91	102	115	-6.45161	-9.97067	-14.2229	
1	276.5	267	250	5.42522	2.785924	-1.6129	
0.5	360	370	343	10.26393	8.944282	17.44868	
0.1	581.5	582.5	621.5	38.8563	24.19355	19.35484	
0.05	902	861	853	47.50733	46.33431	36.51026	
0.01	917.5	877	748	60.26393	60.55718	55.27859	
0.001	886.5	877.5	839	66.42229	62.02346	62.17009	
0.0001	860.5	832	840	83.28446	63.34311	65.68915	
0.00001	832	892.5	860.5	69.35484	73.90029	48.68035	Average
			EC 50	0.042123	0.03436	0.031126	
			Ki	7.1	4.98	6.72	
			Corrected Ki	3.195	2.241	3.042	2.82

Relative Binding Affinity (RBA) %	9.6

Table A.8. Competitive binding of Compound R-8 to the AR.

The specific binding of ^{3}H-MIB with increasing concentration of test compound was expressed as a percentage of ^{3}H-MIB binding in the absence of test compound. Nonspecific binding was subtracted form total binding to obtain specific binding. Experiment was preformed in triplicate.

Concentration (μM)	Reading 1	Reading2	% specific Binding		
10	42.6	26.4	1.621622	-0.36855	
5	37	35.4	0.933661	0.737101	
1	44.8	40.8	1.891892	1.400491	
0.5	67.6	74.2	4.692875	5.503686	
0.1	186	214.4	19.23833	22.72727	
0.05	672.8	396.2	79.04177	45.06143	
0.01	901.8	882.8	107.1744	104.8403	
0.001	922.8	756.6	109.7543	89.33661	
0.0001	810.6	801.6	95.97052	94.86486	
0.00001	707.6	404	83.31695	46.01966	Average
		EC 50	0.070307	0.073222	0.071765
		Ki	11.22549	11.69091	11.4582
		Corrected Ki	4.252916	4.429246	4.341081
relative binding affinity		6.219649			

Table A.9. Competitive binding of Compound R-10 to the AR.
The specific binding of ^{3}H-MIB with increasing concentration of test compound was expressed as a percentage of ^{3}H-MIB binding in the absence of test compound. Nonspecific binding was subtracted form total binding to obtain specific binding. Experiment was preformed in duplicate.

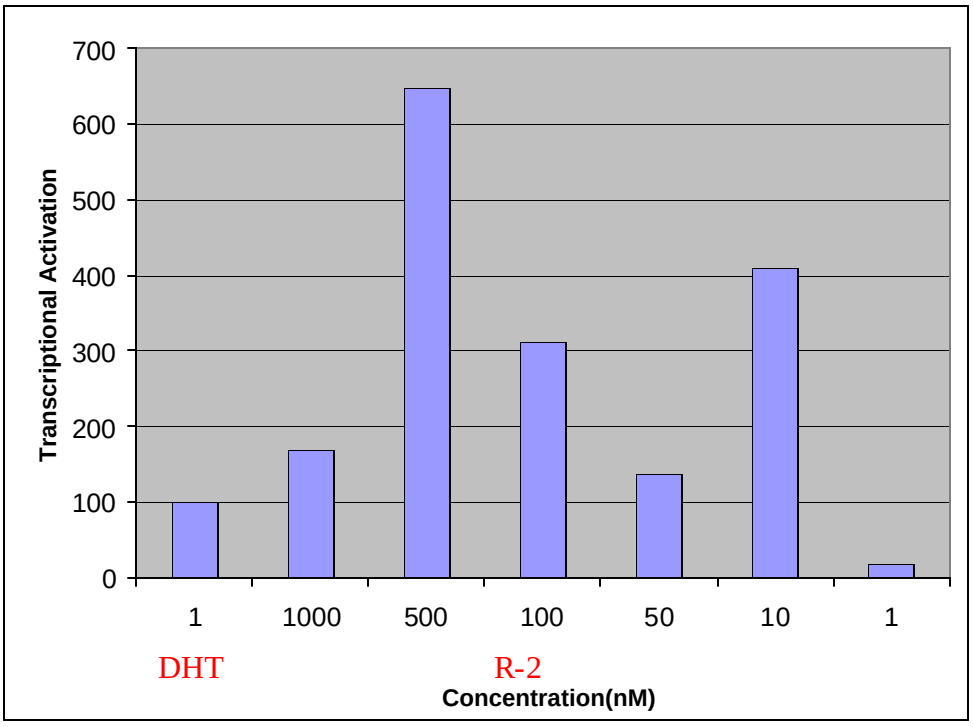

A.10. AR-mediated transcriptional activation of R-2.

CV-1 monkey kidney cell culture were transfected with human AR receptor plasmid, an androgen-sensitive luciferase reporter plasmid, and a plasmid for constitutive expression of beta galactosidease. Potency was defined as the lowest concentration that resulted in transcriptional activation equal to or greater than that observed with 1 nM DHT. Efficacy was defined as the maximal percentage of transcriptional activation seen for each ligand, at any concentration. None of the compounds showed potencies equal to DHT (1 nM).

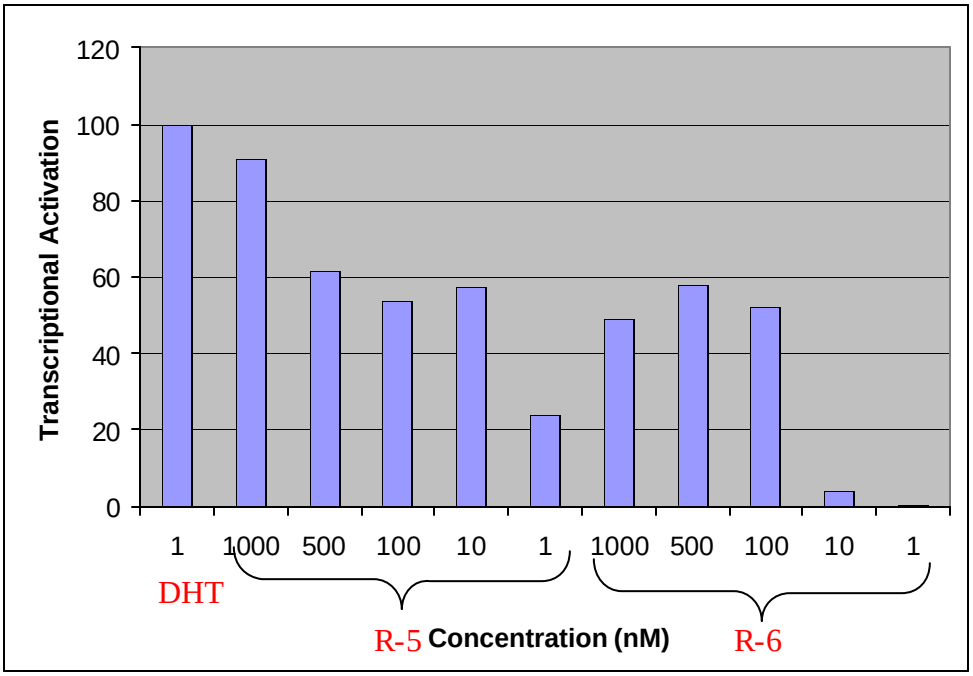

A.11. AR-mediated transcriptional activation of R-5 and R-6.
CV-1 monkey kidney cell culture were transfected with human AR receptor plasmid, an androgen-sensitive luciferase reporter plasmid, and a plasmid for constitutive expression of beta galactosidease. Potency was defined as the lowest concentration that resulted in transcriptional activation equal to or greater than that observed with 1 nM DHT. Efficacy was defined as the maximal percentage of transcriptional activation seen for each ligand, at any concentration. None of the compounds showed potencies equal to DHT (1 nM).

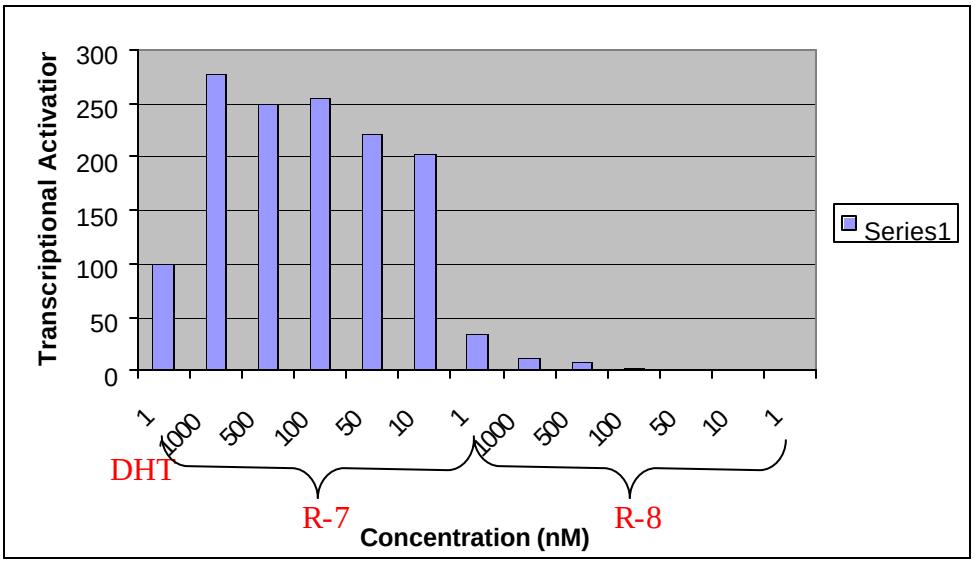

A.12. AR-mediated transcriptional activation of R-7 and R-8
CV-1 monkey kidney cell culture were transfected with human AR receptor plasmid, an androgen-sensitive luciferase reporter plasmid, and a plasmid for constitutive expression of beta galactosidease. Potency was defined as the lowest concentration that resulted in transcriptional activation equal to or greater than that observed with 1 nM DHT. Efficacy was defined as the maximal percentage of transcriptional activation seen for each ligand, at any concentration. None of the compounds showed potencies equal to DHT (1 nM).

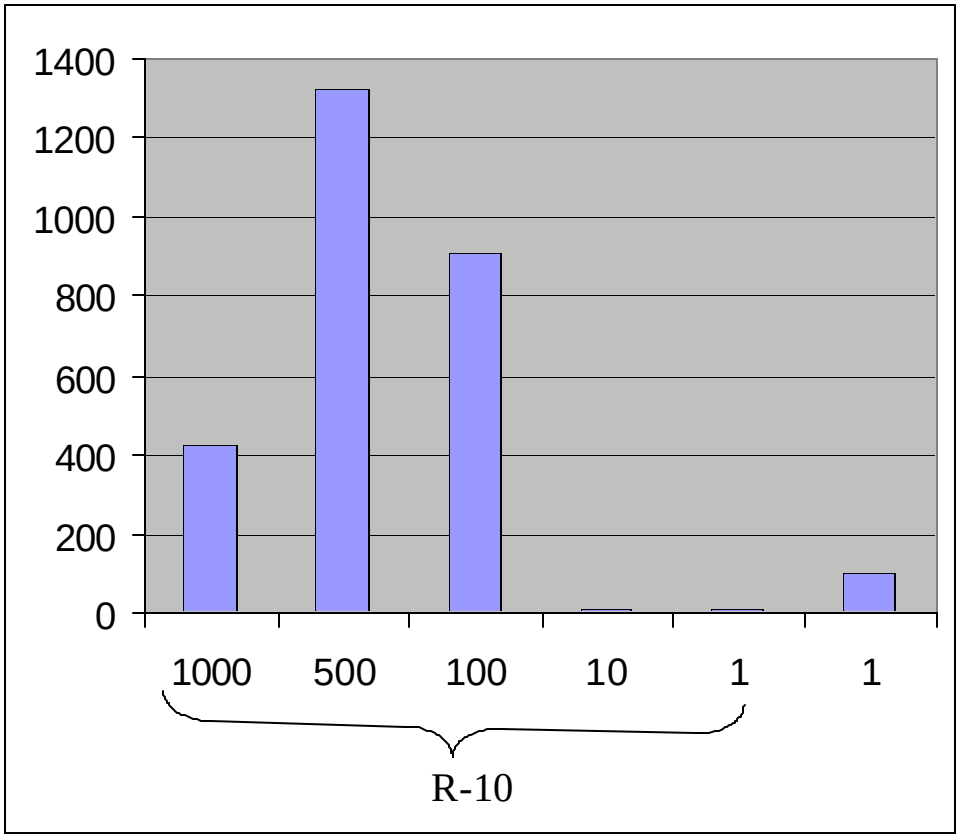

A.13. AR-mediated transcriptional activation of R-10.
CV-1 monkey kidney cell culture were transfected with human AR receptor plasmid, an androgen-sensitive luciferase reporter plasmid, and a plasmid for constitutive expression of beta galactosidease. Potency was defined as the lowest concentration that resulted in transcriptional activation equal to or greater than that observed with 1 nM DHT. Efficacy was defined as the maximal percentage of transcriptional activation seen for each ligand, at any concentration. None of the compounds showed potencies equal to DHT (1 nM).

Appendix B

Data Related to Chapter 3

Female						Male					
Dog 1		Dog 3		Dog 6		Dog 2		Dog 4		Dog 5	
Time Post dose (min)	Conc. (ug/mL)	Time Post dose (min)	Conc. (ug/mL)	Time Post dose (min)	Conc. (ug/mL)	Time Post dose (min)	Conc. (ug/mL)	Time Post dose (min)	Conc. (ug/mL)	Time Post dose (min)	Conc. (ug/mL)
2	4.661958	2	3.734181	2	7.49099	2	4.742153	2	2.576992	2	2.523488
5	3.45244	5	3.020486	6	3.042082	5	2.836714	8	7.520596	5	1.886145
10	2.815378	10	1.717398	11	2.741847	10	2.775778	11	2.551388	10	2.267385
15	2.81462	15	1.942844	17	2.746477	15	2.41753	15	1.510454	15	1.435616
30	2.538587	30	1.665066	31	1.658102	31	2.218024	30	1.035289	30	1.696072
64	2.053926	60	1.333705	60	1.871049	64	1.589367	67	0.989744	60	1.318636
121	1.550547	120	1.88287	124	1.352805	120	1.448343	120	1.036009	120	0.969379
240	1.18819	240	1.13954	244	0.939036	240	0.716173	240	0.642714	242	1.019056
398	0.869765	360	0.704528	360	0.617291	324	0.744594	360	0.425871	360	0.799604
480	0.531631	482	0.423389	480	0.446375	480		479	0.421909	480	0.325793
600	0.485281	600	0.288445	600	0.476913	600		600	0.227516	600	0.353446
1445		1440		1468		1440		1442		1506	
2891		2922		2881		2880		2894		2885	
4320		4322		4323		4321		4327		4332	

Table B.1. Plasma concentrations of S-4 after an intravenous (IV) dose of 3 mg/kg in beagle dogs (n=6).

The IV dose of S-4 was administer in the right saphenous vein and blood samples were drawn through the left saphenous vein catheter. The concentration of S-4 was quantified by a specified HPLC method.

Female						Male					
Dog 1		Dog 3		Dog 6		Dog 2		Dog 4		Dog 5	
Time Post dose (min)	Conc. (ug/mL)	Time Post dose (min)	Conc. (ug/mL)	Time Post dose (min)	Conc. (ug/mL)	Time Post dose (min)	Conc. (ug/mL)	Time Post dose (min)	Conc. (ug/mL)	Time Post dose (min)	Conc. (ug/mL)
2	14.11431	4	15.013	3	9.368037	2	19.02463	4	16.58465	3	12.7446
5	8.425559	6	11.28996	5	9.156945	5	10.02195	5	11.46815	6	6.800583
10	5.38961	14	10.08471	13	6.599463	10	7.748743	11	9.3075	11	5.880734
15	6.603433	19	8.482472	15	5.164504	15	6.558709	25	8.380908	16	6.75388
30	6.230704	28	8.432183	31	5.066829	30	5.97152	30	7.68352	33	5.253025
60	5.498104	59	6.938841	62	5.410399	60	5.864921	60	5.897914	60	3.813641
120	5.347713	120	5.620117	122	3.156676	120	4.145316	122	5.884336	121	3.461619
240	4.084375	240	4.469071	241	2.837105	240	2.354668	240	4.047185	245	2.461725
360	3.101064	360	2.64588	360	1.797469	360	1.441595	361	2.716458	365	1.871258
482	1.950715	480	1.99054	480	1.596158	480	1.058785	480	2.036973	480	1.375948
602	1.260453	600	1.698069	600	2.156768	600	0.615371	600	1.456747	600	0.836098
1445		1444		1441		1440		1442		1442	0.162983
2887		2880		2880		2880		2880		2888	
4320		4322		4320		4320		4320		4325	

Table B.2. Plasma concentrations of S-4 after an intravenous (IV) dose of 10 mg/kg in beagle dogs (n=6).
The IV dose of S-4 was administer in the right saphenous vein and blood samples were drawn through the left saphenous vein catheter. The concentration of S-4 was quantified by a specified HPLC method.

.

Females						Males					
Dog 1		Dog 3		Dog 6		Dog 2		Dog 4		Dog 5	
Time Post dose (min)	Conc. (ug/mL)	Time Post dose (min)	Conc. (ug/mL)	Time Post dose (min)	Conc. (ug/mL)	Time Post dose (min)	Conc. (ug/mL)	Time Post dose (min)	Conc. (ug/mL)	Time Post dose (min)	Conc. (ug/mL)
11	0.845392	10		10	1.891496	10	0.804759	12		10	
31	1.36723	31	1.074362	30	2.108685	30	2.049638	30	0.955371	30	1.388703
62	1.509622	60	1.246606	60	2.220831	60	1.691997	62	1.331339	60	1.70513
90	2.382689	90	1.980256	92	2.083468	93	1.473644	92	1.390631	90	1.567885
121	1.945808	120	2.834207	120	1.6302	120	1.35457	122	1.573301	120	1.847191
182	1.806778	180	2.932843	180	1.636102	181	1.029349	180	3.51837	180	1.759193
244	1.599924	240	2.880767	240	1.113893	240	0.641467	240	1.354966	240	1.16883
305	1.27501	300	2.042843	300	1.019209	300	0.466399	304	1.185747	300	1.032304
360	0.829455	360	1.630113	360	0.927166	360	0.437096	359	1.166809	360	0.713981
491	0.69071	480	1.347121	480	0.718469	480	0.291836	482	0.755315	480	0.513301
600	0.556193	600	1.40957	600	0.559406	600	0.205277	606		600	0.348481
1440		1445		1440		1440		1440		1440	
2879		2884		2881		2880		2880		2880	
4323		4331		4320		4321		4321		4320	

Table B.3. Plasma concentrations of S-4 after an oral (PO) dose of 10 mg/kg solution in beagle dogs (n=6).
Dosing solution was prepared aseptically by dissolving an appropriate amount of S-4 in ethanol and diluting to 3 mL in PEG 300. The PO dose of S-4 was administered by oral gavage followed by a 10 mL water flush. Blood samples were drawn through the left saphenous vein catheter. The concentration of S-4 was quantified by a specified HPLC method

Females						Males					
Dog 1		Dog 3		Dog 6		Dog 2		Dog 4		Dog 5	
Time Post dose (min)	Conc. (ug/mL)	Time Post dose (min)	Conc. (ug/mL)	Time Post dose (min)	Conc. (ug/mL)	Time Post dose (min)	Conc. (ug/mL)	Time Post dose (min)	Conc. (ug/mL)	Time Post dose (min)	Conc. (ug/mL)
10		11		10		10		11		10	
30		30		30		30		30		30	
61	0.349344	60		60	0.16811	60		61	1.136365	60	
90	0.67054	90		90	0.509297	90	0.625447	92	1.611284	90	
120	1.99894	120		120	0.684436	120	1.021321	120	1.462841	120	0.750224
180	2.555327	180		180	0.355631	180	0.89552	180	0.999987	180	0.772932
240	1.908835	240		240	0.380548	240	0.604349	240	0.93118	240	0.683337
300	1.363009	300		300	0.326013	300	0.484473	300	0.65403	300	
360	1.284405	360	0.155087	360	0.268824	374	0.296774	360	0.596519	360	
479	0.871117	480	0.216692	483	0.21867	480		482	0.341103	486	
634	0.558417	600	0.761452	600	0.190204	634		602	0.241804	600	
1448		1440		1442		1448		1443		1441	
2887		2882		2886		2887		2883		2884	
4404		4325		4340		4407		4320		4338	

Table B.4. Plasma concentrations of S-4 after an oral dose (PO) of a 10 mg/kg capsule to beagle dogs (n=6).
Gelatin capsules were prepared by packing an appropriate amount of S-4 into a size 0 gelatin capsule. The capsule of S-4 was administered placed in the back of the dog's throat and the dog was made to swallow. Blood samples were drawn through the left saphenous vein catheter. The concentration of S-4 was quantified by a specified HPLC method.

Dog Number	1	3	6	2	4	5	Average
Sex	F	F	F	M	M	M	
Dose (ug)	39600	34500	36000	39600	34500	44100	38050
Tmax	0	0	0	0	8	0	
Cmax	5.6955	4.3014	11.755	6.6796	7.5206	3.064	
AUClast	717.2282	610.4908	603.3997	425.9899	423.4886	506.0657	
Lambda_z	0.003	0.0039	0.0034	0.0041	0.0029	0.0027	
t1/2_Lambda_z	228.2908	175.6661	205.8493	170.9304	240.5862	254.5091	212.6387
AUC_%Extrap(obs.)	18.2233	10.6937	19.0103	30.1206	15.7165	20.4104	
AUCINF(predicted)	858.5821	680.7208	730.7147	581.1714	507.9925	625.2163	664.0663
AUCINF(predicted)/D	0.0217	0.0197	0.0203	0.0147	0.0147	0.0142	0.01755
Vz(predicted)	15190.652	12844.37	14631.16	16802.92	23572.58	25899.19	
Cl(predicted)	46.1226	50.6816	49.2668	68.1383	67.9144	70.5356	58.77655
AUMC_%Extrap(obs.)	49.8735	33.5215	51.7062	67.7952	46.9549	53.0674	
AUMCINF(predicted)	280659.3	183660.6	232856.1	138316.5	164524.4	226248	204377.5
AUMC_%Extrap(pred.)	46.8069	32.6344	49.0426	64.0174	48.645	50.9352	
MRTINF(observed)	339.578	272.2548	329.7826	253.5108	317.0067	371.9885	
Vss(observed)	15332.281	13740.34	15935.11	16468.03	21766.47	25799.88	
MRTINF(predicted)	326.887	269.8032	318.669	237.9961	323.8718	361.8715	306.5164
Vss(predicted)	15076.864	13674.05	15699.81	16216.64	21995.56	25524.82	18031.29
BW (kg)	13.2	11.5	12	13.2	11.4	14.7	12.66667
Cl(predicted) ml/min/kg	3.4941364	4.407096	4.105567	5.161992	5.957404	4.79834	4.654089
Vss(predicted) L/kg	1.1421867	1.189048	1.308318	1.228533	1.929435	1.736382	1.422317

Table B.5. Plasma concentrations of S-4 after an oral (PO) dose of 3 mg/kg solution in beagle dogs (n=6).
Concentration time profiles were analyzed using a non-compartmental model in WinNonlin (Version 3.1, Pharsight Corporation, Mountain View, CA). The area under the plasma concentration-time curve (AUC) was calculated by the trapezoidal rule with extrapolation to time infinity.

Dog ID	1	3	6	2	4	5	Average
Sex	F	F	F	M	M	M	
Dose (ug)	132000	114700	120000	132000	114700	147000	126733.3
Tmax	0	0	0	0	0	0	
Cmax	19.9083	26.5472	9.6938	29.167	72.5369	23.884	
AUClast	2227.796	2470.505	1684.348	1612.034	2475.16	1961.181	
Lambda_z	0.0027	0.003	0.0027	0.0041	0.0028	0.0023	
t1/2_Lambda_z	257.8108	231.2939	252.2435	169.6373	243.8868	299.2314	242.3506
AUC_%Extrap(obs.)	17.3854	18.6565	31.7862	8.5442	17.1556	3.4634	
AUCINF(predicted)	2752.721	2963.009	2209.587	1847.189	3181.867	2025.991	2496.727
AUCINF(predicted)/D	0.0209	0.0258	0.0184	0.014	0.0277	0.0138	0.0201
AUC_%Extrap(pred.)	19.0693	16.6217	23.7709	12.7304	22.2104	3.1989	
Vz(predicted)	17835.59	12917.22	19763.54	17488.73	12683.65	31322.87	
Cl(predicted)	47.9526	38.7107	54.3088	71.4599	36.048	72.5571	53.50618
AUMC_%Extrap(obs.)	48.2197	51.1159	66.383	31.2769	49.8237	17.3938	
AUMCINF(predicted)	1001561	965794.2	889405.6	478176.5	1164019	747530.5	874414.5
AUMC_%Extrap(pred.)	51.045	47.6131	56.9238	41.5419	57.7896	16.2448	
MRTINF(predicted)	363.8441	325.9505	402.5212	258.8671	365.8289	368.9703	347.6637
Vss(predicted)	17447.25	12617.76	21860.44	18498.62	13187.41	26771.41	18397.15
BW (kg)	13.2	11.5	12	13.2	11.4	14.7	12.66667
Cl(predicted) ml/min/kg	3.632773	3.366148	4.525733	5.413629	3.162105	4.935857	4.172708
Vss(predicted) L/kg	1.321762	1.097196	1.821703	1.401411	1.15679	1.821184	1.436674

Table B.6. Pharmacokinetic parameters of S-4 in beagle dogs (n=6) after an intravenous dose of 10 mg/kg.
Concentration time profiles were analyzed using a non-compartmental model in WinNonlin (Version 3.1, Pharsight Corporation, Mountain View, CA). The area under the plasma concentration-time curve (AUC) was calculated by the trapezoidal rule with extrapolation to time infinity.

Dog ID	1	3	6	2	4	5	Average
Sex	F	F	F	M	M	M	
Dose (ug)	132000	115000	120000	132000	115000	132000	124333.3
Tmax	90	180	60	30	180	120	110
Cmax	2.3827	2.9328	2.2208	2.0496	3.5184	1.8472	2.491917
AUClast	726.0981	1120.279	713.5459	435.0083	694.2736	607.358	
Lambda_z	0.0029	0.003	0.0024	0.004	0.0024	0.0037	
t1/2_Lambda_z	242.2508	228.1859	286.0665	174.129	290.3154	186.3291	234.5461
AUC_%Extrap(obs.)	21.1178	29.2893	24.4458	10.5983	31.3027	13.3627	
AUCINF(predicted)	907.2159	1534.478	999.2834	479.8454	1024.679	695.9172	940.2363
AUCINF(predicted)/D	0.0069	0.0133	0.0083	0.0036	0.0089	0.0053	0.007717
AUC_%Extrap(pred.)	19.9641	26.9928	28.5942	9.3441	32.2447	12.7255	
Vz(predicted)/F	50851.42	24671.79	49560.32	69106.38	47006.16	50988.42	48697.41
Cl(predicted)/F	145.5001	74.9441	120.0861	275.0886	112.2303	189.6777	152.9212
AUMC_%Extrap(obs.)	51.3901	57.7897	58.7778	34.5336	64.8633	37.0669	
AUMCINF(predicted)	346553.7	699814.9	453340.4	121381.1	452017	215125.2	381372.1
AUMC_%Extrap(pred.)	49.623	54.9966	63.8302	31.4431	65.8473	35.766	
MRTINF(predicted)	381.9969	456.0607	453.6655	252.9588	441.1306	309.1247	382.4895
IV AUCINF(predicted)/D	0.0209	0.0258	0.0184	0.014	0.0277	0.0138	0.0201
Fpo (%)	33.01435	51.55039	45.1087	25.71429	32.12996	38.4058	37.65391
BW (kg)	13.2	11.5	12	13.2	11.4	13.2	12.41667
Cl/F(predicted) ml/min/kg	11.02273	6.516878	10.00718	20.84005	9.844763	14.36952	12.10019
Vz(predicted)/F, L/kg	3.852381	2.145373	4.130027	5.235332	4.123347	3.862759	3.891536

Table B.7. Pharmacokinetic parameters of S-4 in beagle dogs (n=6) after an oral of 10 mg/kg solution.

Concentration time profiles were analyzed using a non-compartmental model in WinNonlin (Version 3.1, Pharsight Corporation, Mountain View, CA). The area under the plasma concentration-time curve (AUC) was calculated by the trapezoidal rule with extrapolation to time infinity.

Dog ID	1	3	6	2	4	5	Average
Sex	F	F	F	M	M	M	
Dose (ug)	131688	116138	125194	129372	112200	145626	126703
Tmax	180		120	120	92		128
Cmax	2.5553		0.6844	1.0213	1.6113		1.468075
AUClast	752.6585		179.3397	216.9187	429.3474		
Lambda_z	0.0032		0.0019	0.0055	0.0037		
t1/2_Lambda_z	215.3186		361.174	125.5484	188.6461		222.6718
AUC_%Extrap(obs.)	18.7303		35.5932	19.8595	13.2906		
AUCINF(predicted)	918.5981		273.9168	271.8449	492.5631		489.2307
AUCINF(predicted)/D	0.007		0.0022	0.0021	0.0044		0.003925
AUC_%Extrap(pred.)	18.0644		34.5277	20.205	12.834		
Vz(predicted)/F	44532.47		238152.8	86199.51	61994.54		
Cl(predicted)/F	143.3576		457.0511	475.9038	227.7881		326.0252
AUMC_%Extrap(obs.)	42.7838		69.4305	42.0573	36.6501		
AUMCINF(predicted)	375892.1		154946.2	71602.51	154697.2		189284.5
AUMC_%Extrap(pred.)	41.7016		68.4283	42.5838	35.7218		
MRTINF(predicted)	409.2019		565.6689	263.3947	314.0657		388.0828
iv AUCINF(predicted)/D	0.0209		0.0184	0.014	0.0277		0.0201
Fpo (%)	33.49282		11.95652	15	15.88448		19.08346
BW (kg)	13.2		12	13.2	11.4		12.45
Cl/F(predicted) ml/min/kg	10.86042		38.08759	36.05332	19.98141		26.24569
Vz(predicted)/F, L/kg	3.373672		19.84607	6.530266	5.438118		8.797032

Table B.8. Pharmacokinetic parameters of S-4 in beagle dogs (n=6) after an oral of 10 mg/kg capsule.
Concentration time profiles were analyzed using a non-compartmental model in WinNonlin (Version 3.1, Pharsight Corporation, Mountain View, CA). The area under the plasma concentration-time curve (AUC) was calculated by the trapezoidal rule with extrapolation to time infinity.

Dog 1		Dog 2		Dog 3		Dog 4	
Time Post dose (min)	Conc. (ng/mL)	Time Post dose (min)	Conc. (ng/mL)	Time Post dose (min)	Conc. (ng/mL)	Time Post dose (min)	Conc. (ng/mL)
2	199.8213	2	274.5777	2	213.2359	2	75.10149
5	124.6334	5	83.26171	5	121.1521	5	40.80763
10	97.75107	10	50.55452	10	130.8823	10	47.33861
15	56.5464	15	72.61716	15	131.6831	15	39.57398
30	60.34535	30	46.52043	30	89.3355	30	33.0169
60	72.43134	60	50.00961	60	86.73638	60	
120	68.02889	120	37.51209	120	62.73103	120	43.75867
240	39.52434	240	20.41867	240	40.64709	240	21.26856
360	23.54014	360	14.06998	360	30.11022	360	8.750307
480	14.72656	480	11.12237	480	15.21757	480	6.557261
600	10.84434	600	4.982503	600	10.55488	600	4.115568
1445		1440		1468	13.75187	1440	

Table B.9. Plasma concentrations of S-4 after an intravenous dose of 0.1 mg/kg in beagle dogs (n=4).

The IV dose of S-4 was administer in the right saphenous vein and blood samples were drawn through the left saphenous vein catheter. The concentration of S-4 was quantified by a specified LC/MS method.

Dog 1		Dog 2		Dog 3		Dog 4	
Time Post dose (min)	Conc. (ng/mL)	Time Post dose (min)	Conc. (ng/mL)	Time Post dose (min)	Conc. (ng/mL)	Time Post dose (min)	Conc. (ng/mL)
10	74.32557	10	4.533721	10	3.576227	10	201.5498
30	370.6443	32	101.2873	30	433.4553	30	402.816
60	481.3055	60	412.6285	60	419.7564	60	437.8721
90	387.7872	90	486.9483	90	357.4882	90	345.4667
122	286.403	121	316.9517	122	301.1577	120	231.4028
180	335.9843	180	308.3147	180	287.1515	180	210.8483
240	247.7124	240	202.7258	240	268.9987	240	164.938
300	227.5092	303	180.9025	300	291.1529	300	107.2713
360	207.8264	360	135.3574	360		360	71.12488
480	118.0431	480	68.65512	480	99.70058	480	44.63978
600	75.64613	600	48.48525	600	100.1933	600	19.28836
1443	6.502237	1437	7.198394	1442	9.254492	1440	

Table B.10. Plasma concentrations of S-4 after an oral (PO) dose of 1 mg/kg solution in beagle dogs (n=4).
Dosing solution was prepared aseptically by dissolving an appropriate amount of S-4 in ethanol and diluting to 3 mL in PEG 300. The PO dose of S-4 was administered by oral gavage followed by a 10 mL water flush. Blood samples were drawn through the left saphenous vein catheter. The concentration of S-4 was quantified by a specified LC/MS method.

Dog 1		Dog 2		Dog 3		Dog 4	
Time Post dose (min)	Conc. (ng/mL)	Time Post dose (min)	Conc. (ng/mL)	Time Post dose (min)	Conc. (ng/mL)	Time Post dose (min)	Conc. (ng/mL)
10	74.32557	10	4.533721	10	3.576227	10	201.5498
30	370.6443	32	101.2873	30	433.4553	30	402.816
60	481.3055	60	412.6285	60	419.7564	60	437.8721
90	387.7872	90	486.9483	90	357.4882	90	345.4667
122	286.403	121	316.9517	122	301.1577	120	231.4028
180	335.9843	180	308.3147	180	287.1515	180	210.8483
240	247.7124	240	202.7258	240	268.9987	240	164.938
300	227.5092	303	180.9025	300	291.1529	300	107.2713
360	207.8264	360	135.3574	360		360	71.12488
480	118.0431	480	68.65512	480	99.70058	480	44.63978
600	75.64613	600	48.48525	600	100.1933	600	19.28836
1443	6.502237	1437	7.198394	1442	9.254492	1440	

Table B.11. Plasma concentrations of S-4 after an oral (PO) dose of 0.1 mg/kg solution in beagle dogs (n=4).
Dosing solution was prepared aseptically by dissolving an appropriate amount of S-4 in ethanol and diluting to 3 mL in PEG 300. The PO dose of S-4 was administered by oral gavage followed by a 10 mL water flush. Blood samples were drawn through the left saphenous vein catheter. The concentration of S-4 was quantified by a specified LC/MS method.

Dog ID	1	2	3	4	Average
Dose	13.6mg	13.6mg	10.8mg	14.55mg	
Tmax	60	90	30	60	60
Cmax	481.3055	486.9483	433.4553	437.8721	459.8953
AUClast	135474.39	108479.08	137103.84	88905.706	
Lambda_z	0.0038	0.0045	0.0037	0.0055	
t1/2_Lambda_z	180.0468	152.8415	185.0794	126.1561	161.031
AUC_%Extrap(obs.)	12.6668	8.9713	16.327	3.7987	
AUCINF(predicted)	155201.76	118426.68	159665.77	92627.439	131480.4
AUC_%Extrap(pred.)	12.7108	8.3998	14.1307	4.018	
Vz(predicted)/F	22761.566	25322.423	18061.113	2858.9472	17251.01
Cl(predicted)/F	87.6279	114.839	67.6413	15.7081	71.45408
AUMC_%Extrap(obs.)	35.0562	27.2174	42.0834	15.0829	
MRTINF(predicted)	310.9302	266.9993	322.4452	198.2835	
BW	13.6	13.6	11.36	13.4	
Cl (predicted) ml/min/kg	6.4432279	8.4440441	5.9543398	1.1722463	5.503465
vss (predicted) L/kg	1.6736446	1.8619429	1.5898867	0.2133543	1.334707
F(%)	59.732178	71.495348	56.142908	69.078352	64.1122

Table B.12. Pharmacokinetic parameters of S-4 in beagle dogs (n=4) after an intravenous dose of 1 mg/kg.
Concentration time profiles were analyzed using a non-compartmental model in WinNonlin (Version 3.1, Pharsight Corporation, Mountain View, CA). The area under the plasma concentration-time curve (AUC) was calculated by the trapezoidal rule with extrapolation to time infinity.

Dog ID	1	2	3	4	Average
Dose	1.36mg	1.36mg	1.136mg	1.34mg	
Tmax	0	0	0	0	
Cmax	340.0917	707.492	310.847	112.7855	
No._points_Lambda_z	4	4	4	3	
Tlast	600	600	600	600	
Clast	10.4636	4.5177	10.5549	4.1156	
AUClast	23354.98	15220.21	25809.04	12060.32	
Lambda_z_upper	600	600	600	600	
t1/2_Lambda_z	0.1	175.5546	175.9469	220.5391	143.0352
AUC_%Extrap(obs.)	10.6507	6.992	9.4047	9.7941	
AUCINF(predicted)	25982.94	16564.25	28439.17	13409.04	21098.85
AUC_%Extrap(pred.)	10.1142	8.1141	9.2483	10.0583	
Cl(predicted)	52.342	82.1045	39.9449	99.9326	68.581
AUMCINF(predicted)	6651982	3705622	6975380	3367617	
MRTINF(predicted)	256.0135	223.712	245.2737	251.1453	
Vss(predicted)	13400.27	18367.77	9797.432	25097.6	16665.77
BW	13.6	13.6	11.36	13.4	
Cl (predicted) ml/min/kg	3.848676	6.037096	3.516276	7.457657	5.214926
vss (predicted) L/kg	0.985314	1.350572	0.86245	1.872955	1.267823

Table B.13. Pharmacokinetic parameters of S-4 in beagle dogs (n=4) after an intravenous dose of 0.1 mg/kg.

Concentration time profiles were analyzed using a non-compartmental model in WinNonlin (Version 3.1, Pharsight Corporation, Mountain View, CA). The area under the plasma concentration-time curve (AUC) was calculated by the trapezoidal rule with extrapolation to time infinity.

Dog ID	1	2	3	4	Average
Dose	1.4 mg	1.4mg	1.02mg	1.455mg	
Tmax	30	122	30	32	53.5
Cmax	74.2563	40.341	43.651	173.2013	82.8624
AUClast	16976.47	6860.097	11862.179	23577.29	
Lambda_z_upper	600	600	600	600	
t1/2_Lambda_z	272.835	261.6623	699.3692	107.3576	335.306
AUC_%Extrap(obs.)	20.1353	13.6182	48.2332	2.0007	
AUCINF(predicted)	21135.16	8169.613	23432.269	24041.07	19194.53
AUCINF(predicted)/D	0.0151	0.0584	0.023	0.0165	
Cl(predicted)/F	66.2403	17.1367	43.5297	60.5214	46.85703
AUMCINF(predicted)	7747762	2681032	21423334	3867405	
AUMC_%Extrap(pred.)	53.3335	47.7447	86.8959	9.0527	
MRTINF(predicted)	366.5817	328.1712	914.2663	160.8666	
BW	13.6	13.6	11.36	13.4	
Cl (predicted) ml/min/kg	4.87061	1.260051	3.8318398	4.516522	3.619756
Vss (predicted) L/kg	1.91716	0.475667	3.8662374	0.699538	1.739651
F(%)	81.34245	49.32075	82.39435	179.29	98.0869

Table B.14. Pharmacokinetic parameters of S-4 in beagle dogs (n=4) after an oral (PO) dose of 0.1 mg/kg.
Concentration time profiles were analyzed using a non-compartmental model in WinNonlin (Version 3.1, Pharsight Corporation, Mountain View, CA). The area under the plasma concentration-time curve (AUC) was calculated by the trapezoidal rule with extrapolation to time infinity.

APPENDIX C

Data Related to Chapter 4

A.

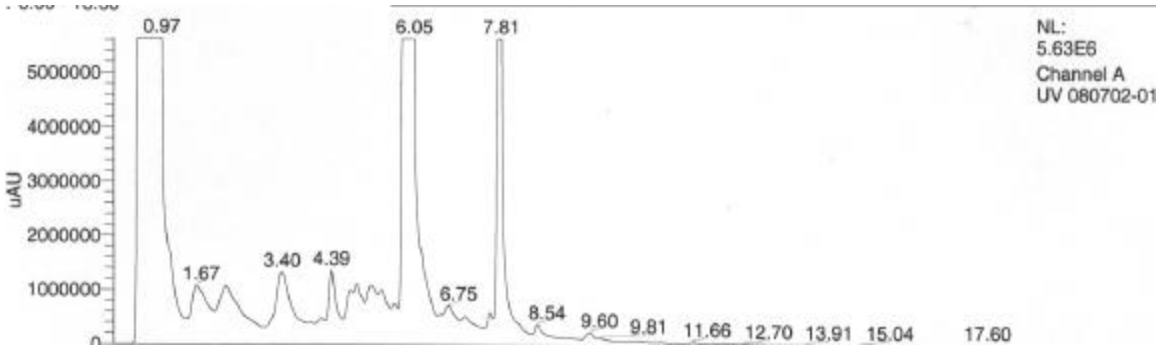

B.

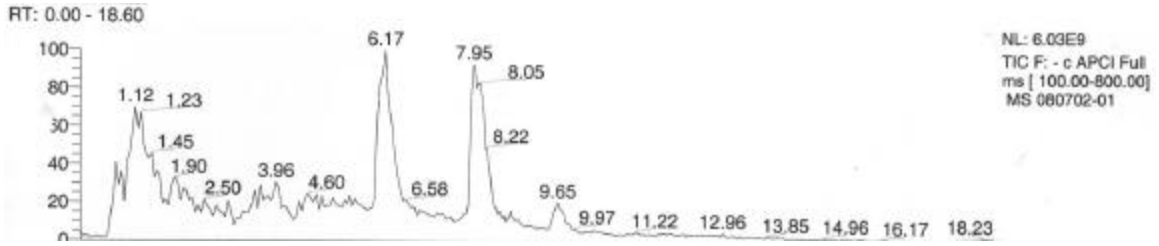

C.1. UV chromatograph and Total Ion Current chromatograph of Dog Urine

A. UV spectra were collected during the LC/MS chromatographs. Treated urine samples from beagle dogs showed two peaks not found in blank urine samples: one associated with the parent drug at 7.81 min. and another at 6.05 min. associated with the amine metabolite.

B. Total Ion Current (TIC) chromatograph shows two peaks that correspond to the peaks seen in the UV chromatograph.

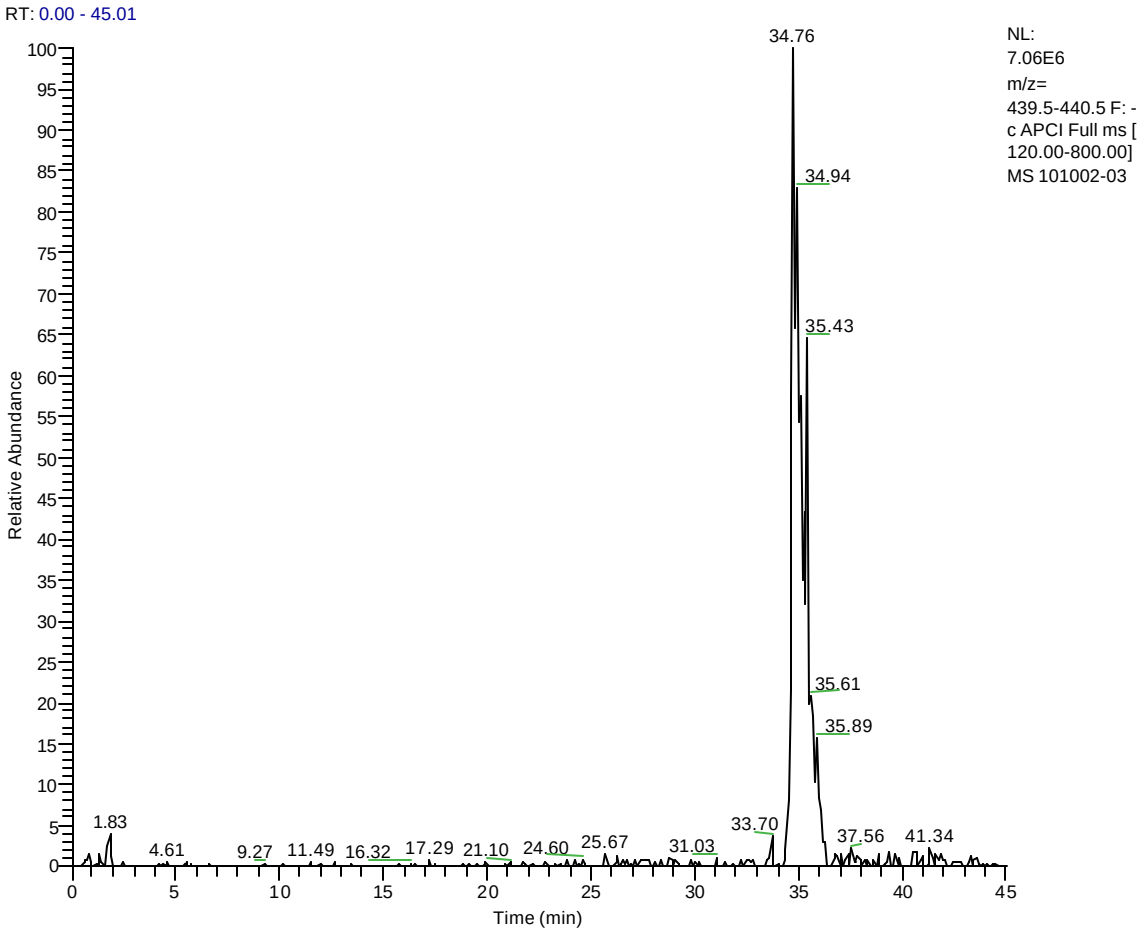

C.2. Chromatograph of S-4 (m/z 440)

Dog and rat urine were separated on a reverse phase column and the resulting chromatograph showed the parent drug peak eluting at 34.7 minutes.

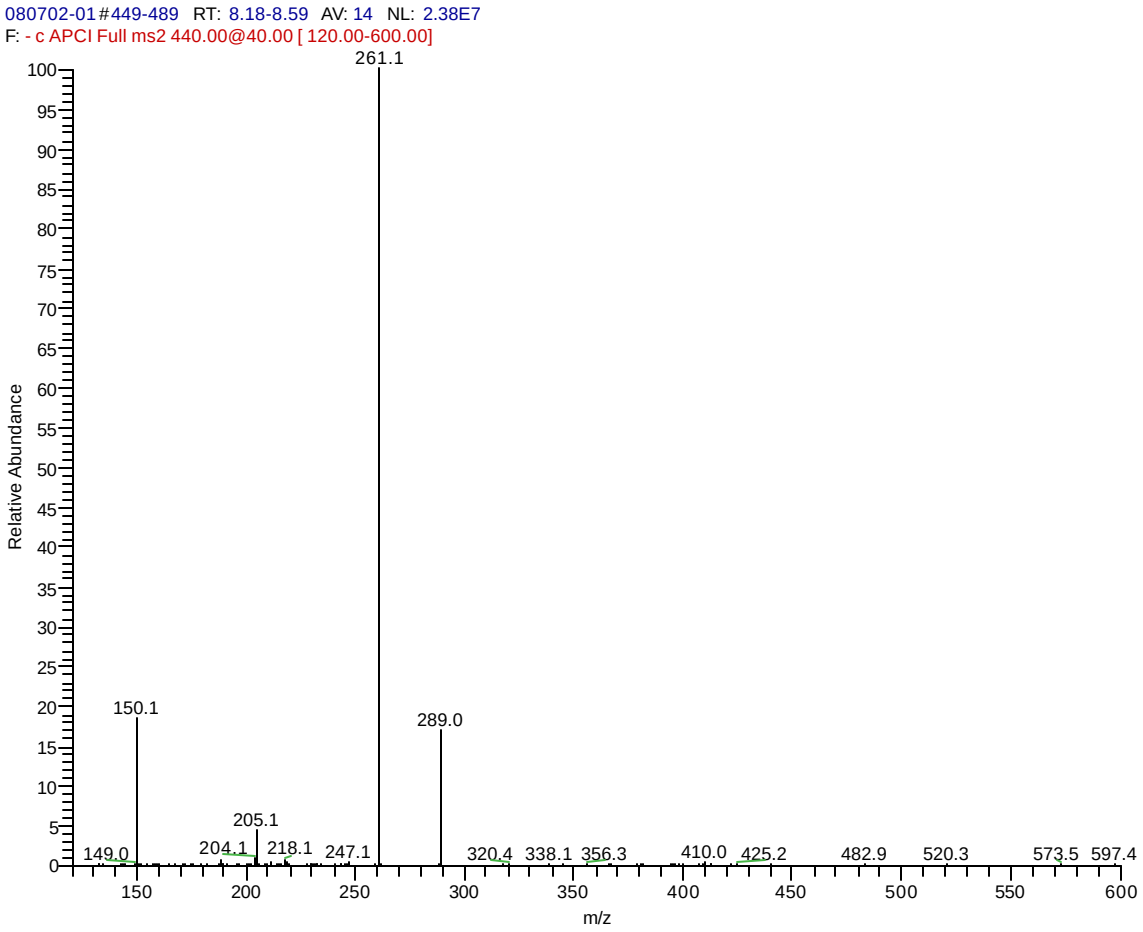

C.3. LC/MS^2 Spectra of S-4 (m/z 440).

A fragmentation voltage of 26V was used to produce the following daughter ions of S-4 at m/z 150, 261, and 289. The daughter ion at m/z 261 corresponds to a cleavage of the bond between the chiral carbon and methylene carbon, with a loss of the methyl group from the chiral carbon. The daughter ion at m/z 289 corresponds to the cleavage of the bond between the oxygen linker and B ring with the loss of a hydrogen atom from the hydroxyl group off the chiral carbon. The overall fragmentation pattern confirms that the ion at m/z 440 is the deprotonated molecular anion of the parent drug.

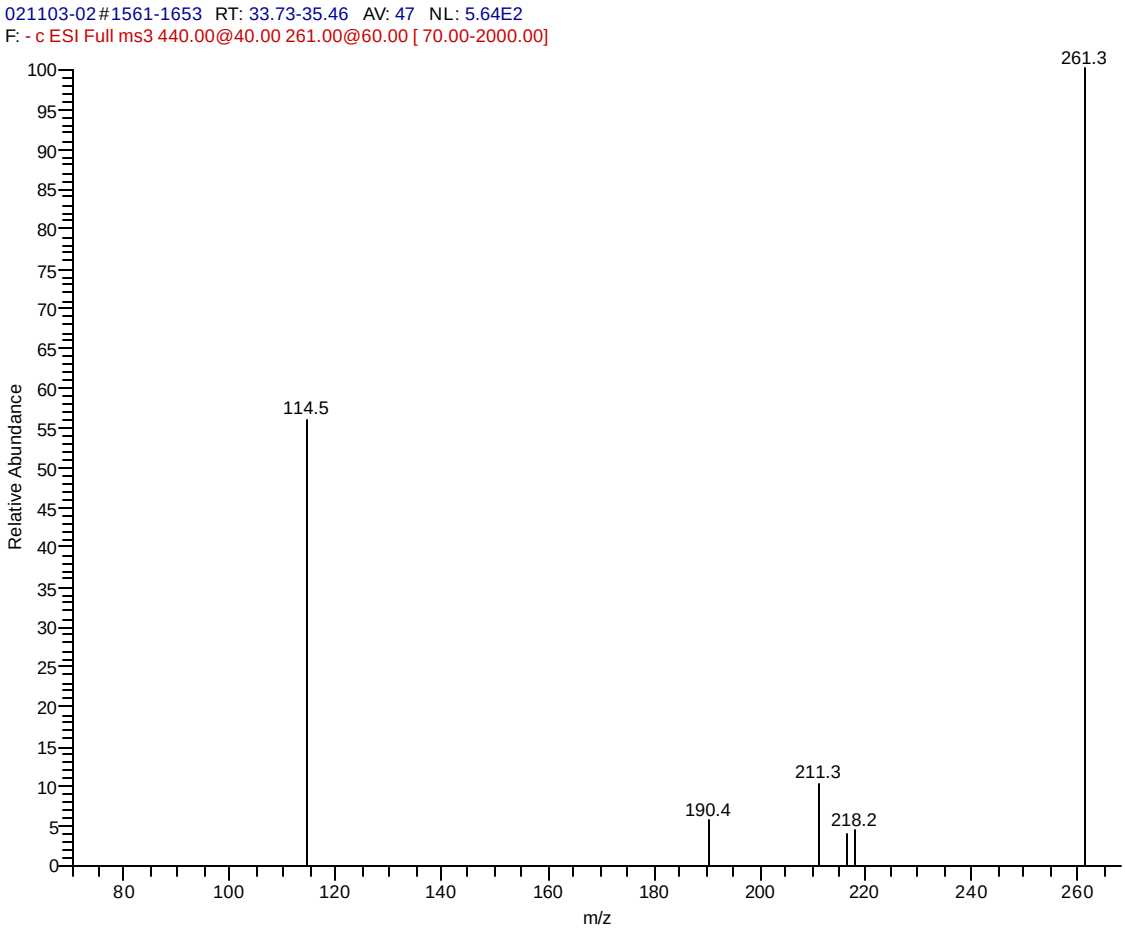

C.4. LC/MS^3 spectra of S-4 daughter ion at m/z 261.

The major daughter ion of S-4 (m/z 261) was fragmented. The resulting spectra showed granddaughter ion at m/z 190, 218, and 233. These ions confirm the structure of S-4 and were used to determine the structure of the metabolite of S-4.

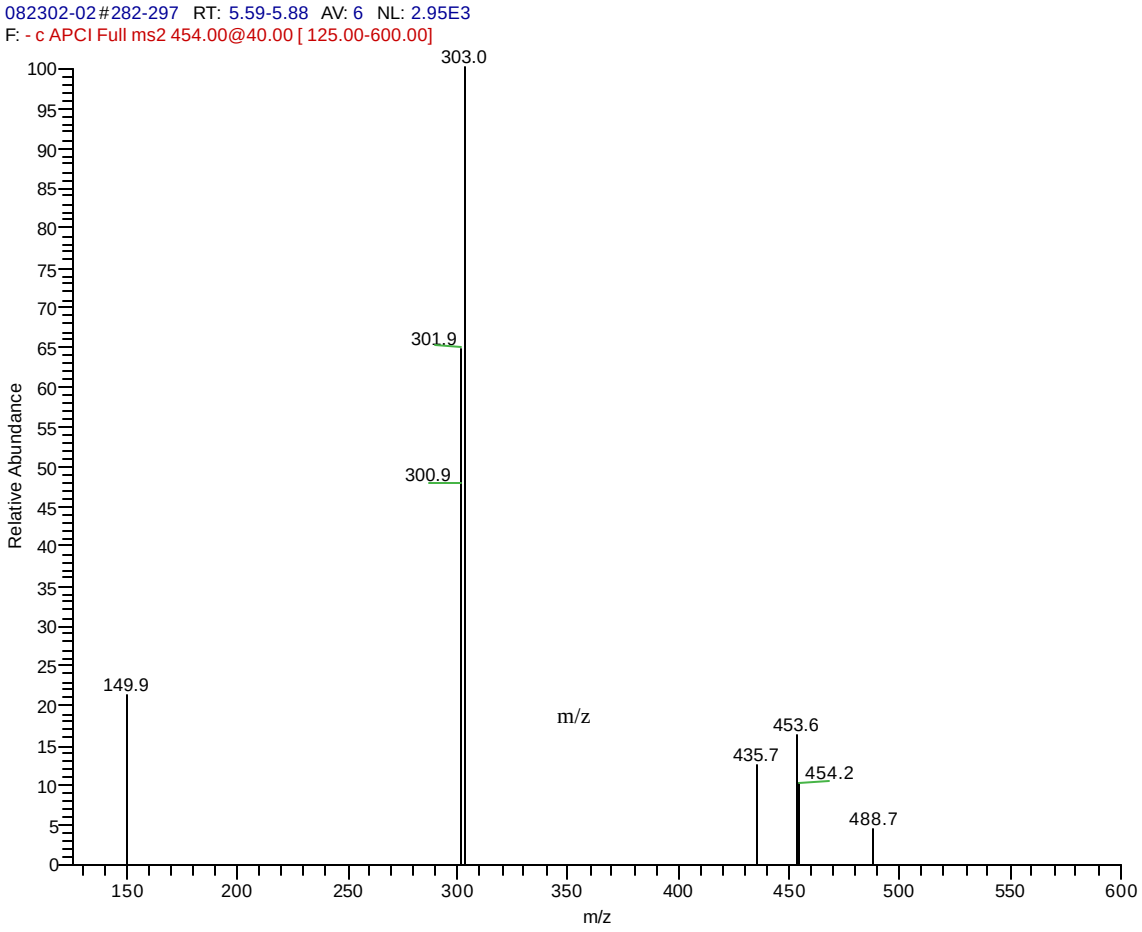

C.5. LC/MS^2 Spectra of Metabolite M1 (m/z/ 454).

The mass of metabolite M1 corresponds to the addition of a methyl group to the parent compound, S-4. Fragmentation of this molecular ion produced daughter ions at m/z 150 and 303. This shows an addition of 14 Da. to the daughter ion 289 found in the parent compound.

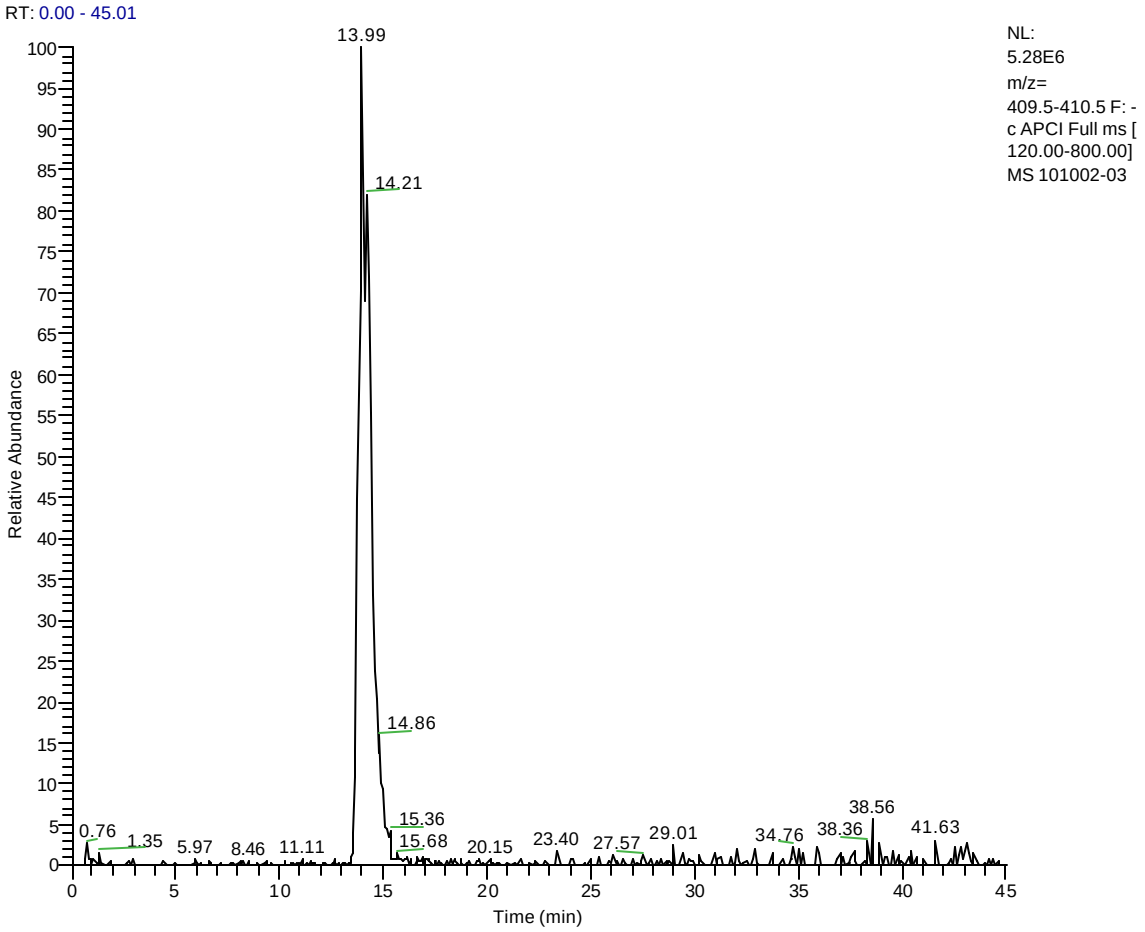

C.6. Chromatograph of Metabolite M2 (m/z 410)

Dog and rat urine were separated on a reverse phase column and the resulting chromatograph showed the parent drug peak eluting at 13.9 minutes.

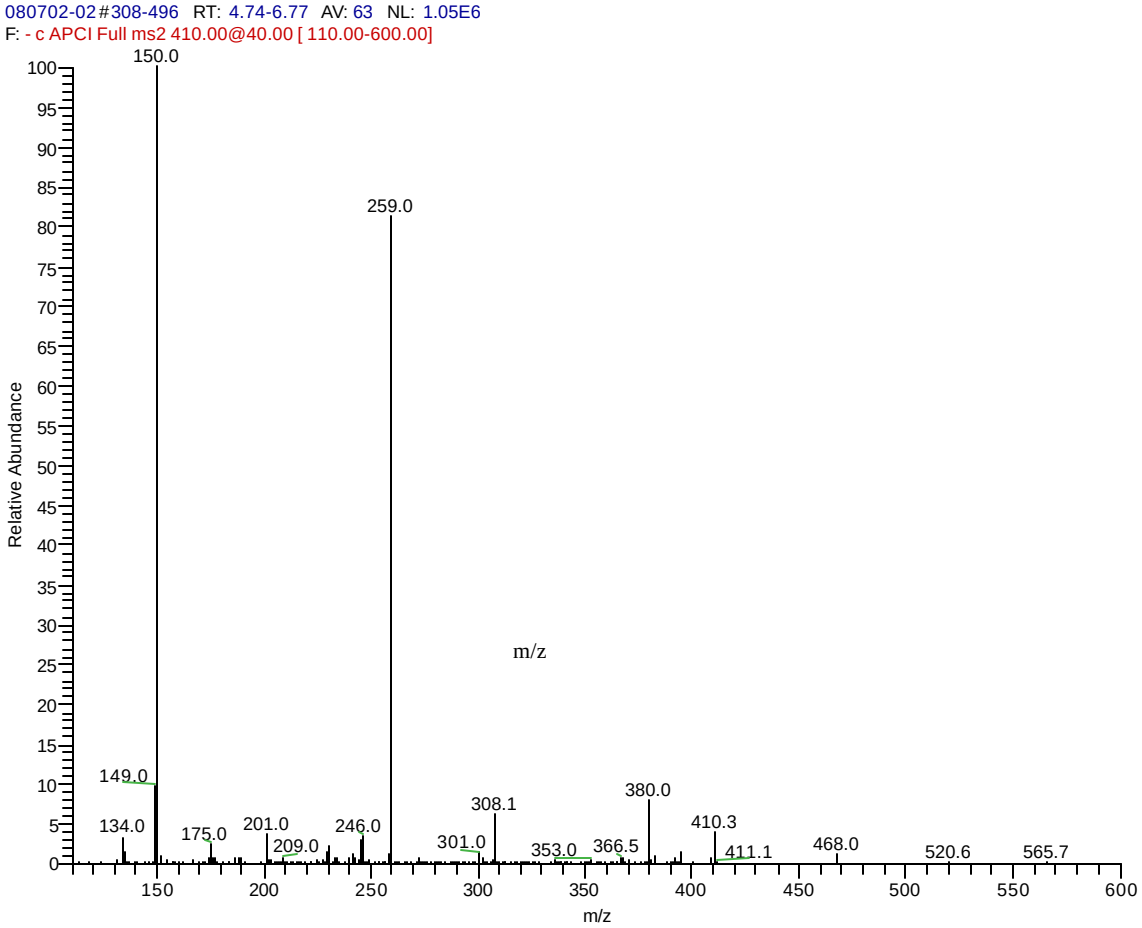

C.7. LC/MS^2 Spectra of Metabolite M2 (m/z 410).

The mass of metabolite M2 corresponds to the reduction of the nitro group in the para-position of the A ring to an amine group. Fragmentation produced daughter ion with m/z 150 and 259. This shows the reduction of 30 Da. to the daughter ion 289 found in the parent compound.

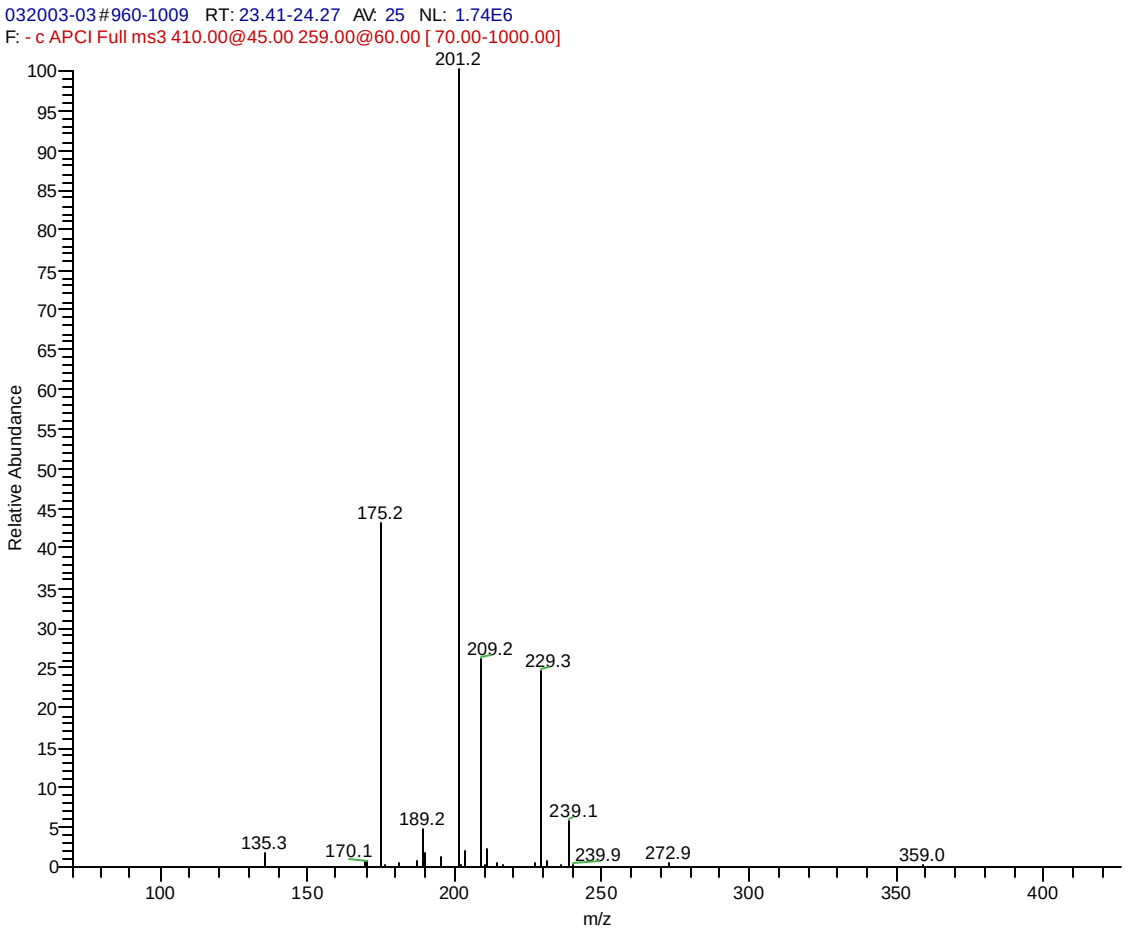

C.8. LC/MS^3 spectra of Metabolite M2 daughter ion at m/z 259.

Fragmentation of the base peak at m/z 259 produced granddaughter ions at 175, 201, and 209. When comparing the granddaughter ion at m/z 175 to that of the granddaughter ion at 205 produced from the fragmentation of daughter ion at m/z 289 of the parent drug, there is a loss of 30 Da. This fragment corresponds to the cleavage of the amide bond. The overall fragmentation pattern confirms that the ion at m/z 410 is the deprotonated molecular anion of the nitro reduced parent compound (amine metabolite).

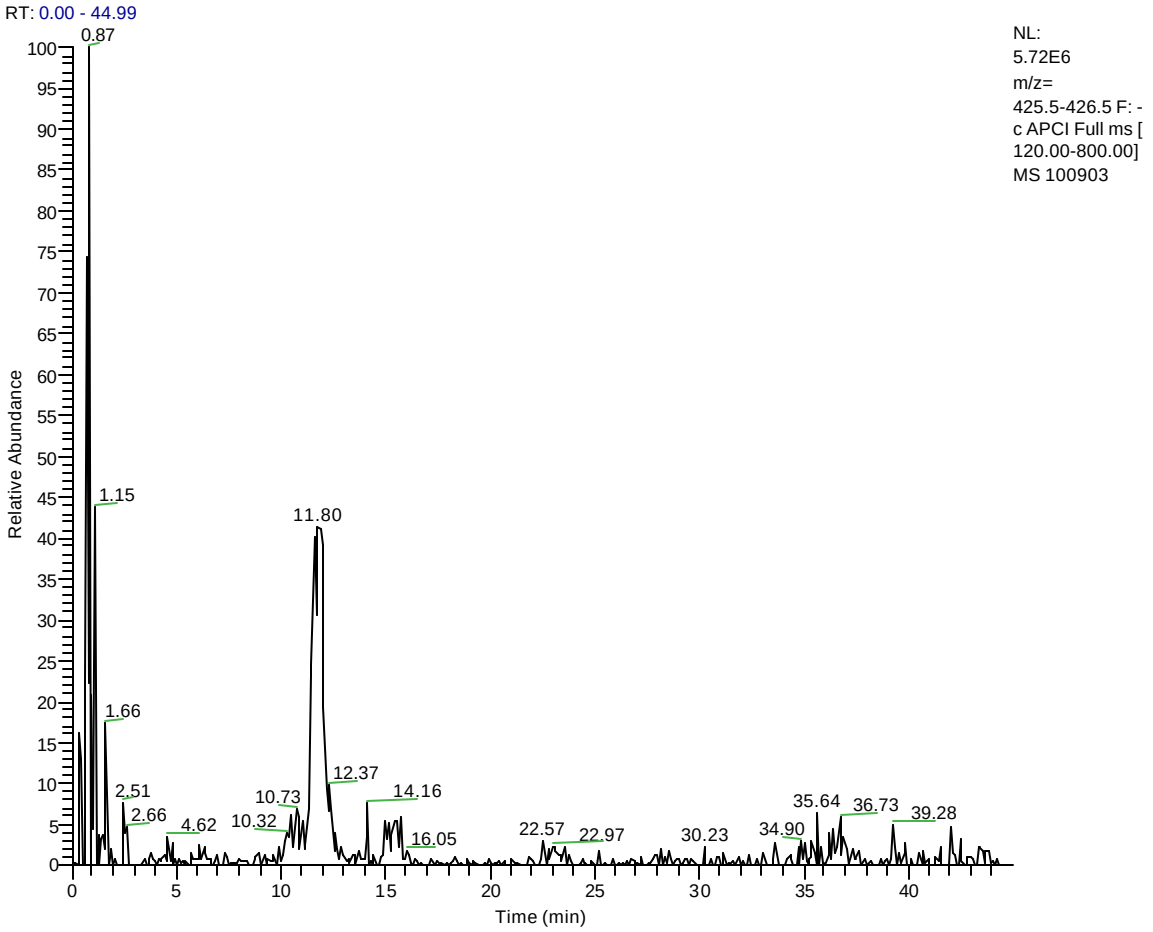

C.9. Chromatograph of Metabolite M3 (m/z 426)

Rat urine was separated on a reverse phase column and the resulting chromatograph showed the parent drug peak eluting at 11.8 minutes.

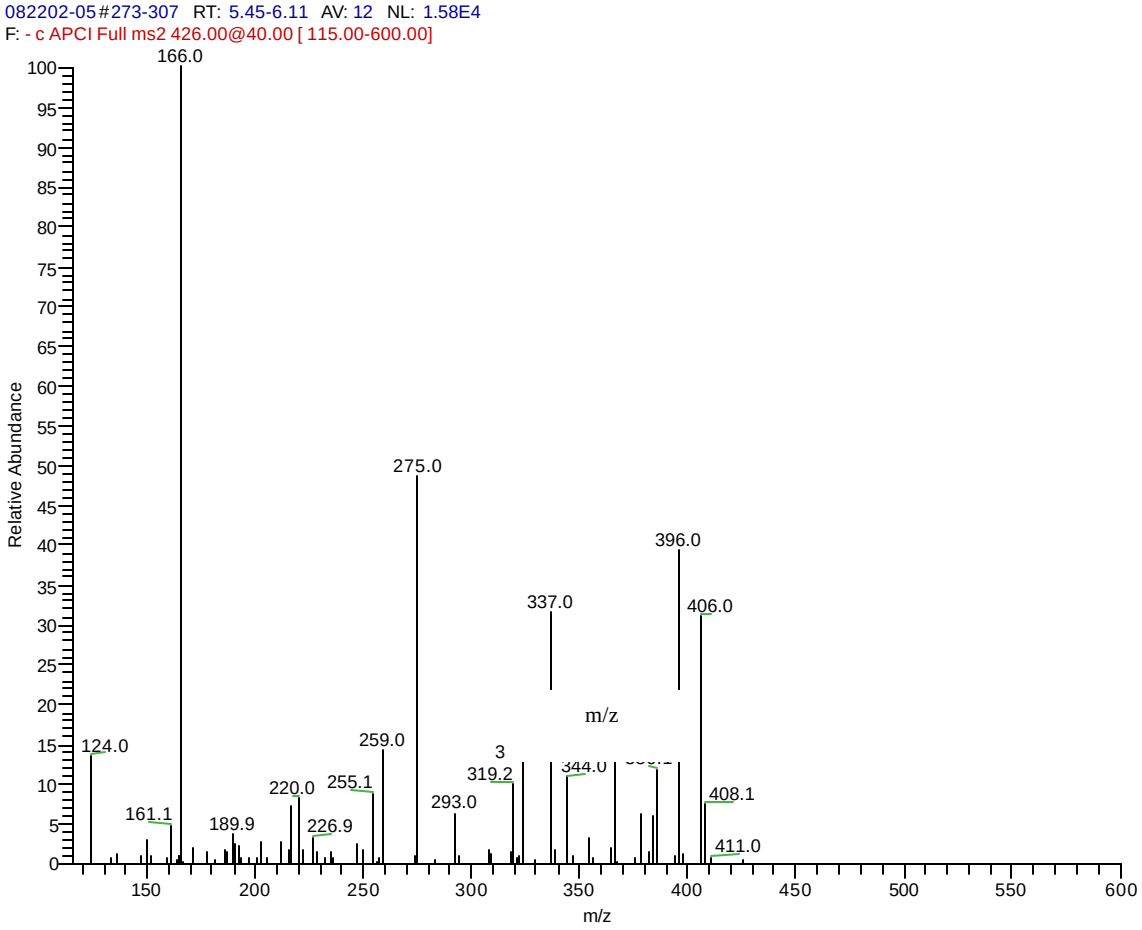

C.10. LC/MS^2 of Metabolite M3 (m/z 426).

The mass of metabolite M3 corresponds to the addition of an oxygen atom to the nitro reduced metabolite M2 (m/z 410). The present of the fragment at m/z 166 suggest that the oxygen is associated with the B ring of the compound.

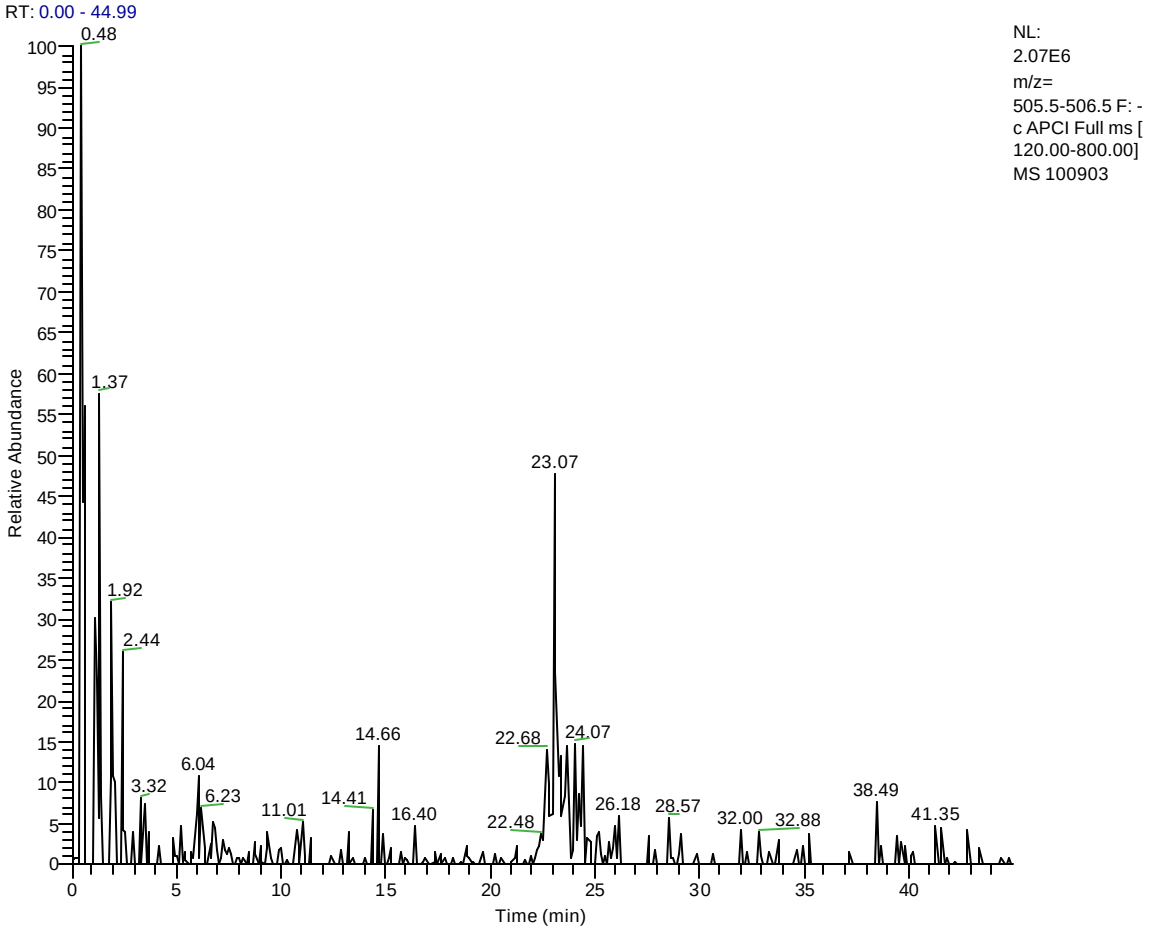

C.11. Chromatograph of Metabolite M4 (m/z 506)

Rat urine was separated on a reverse phase column and the resulting chromatograph showed the parent drug peak eluting at 23 minutes.

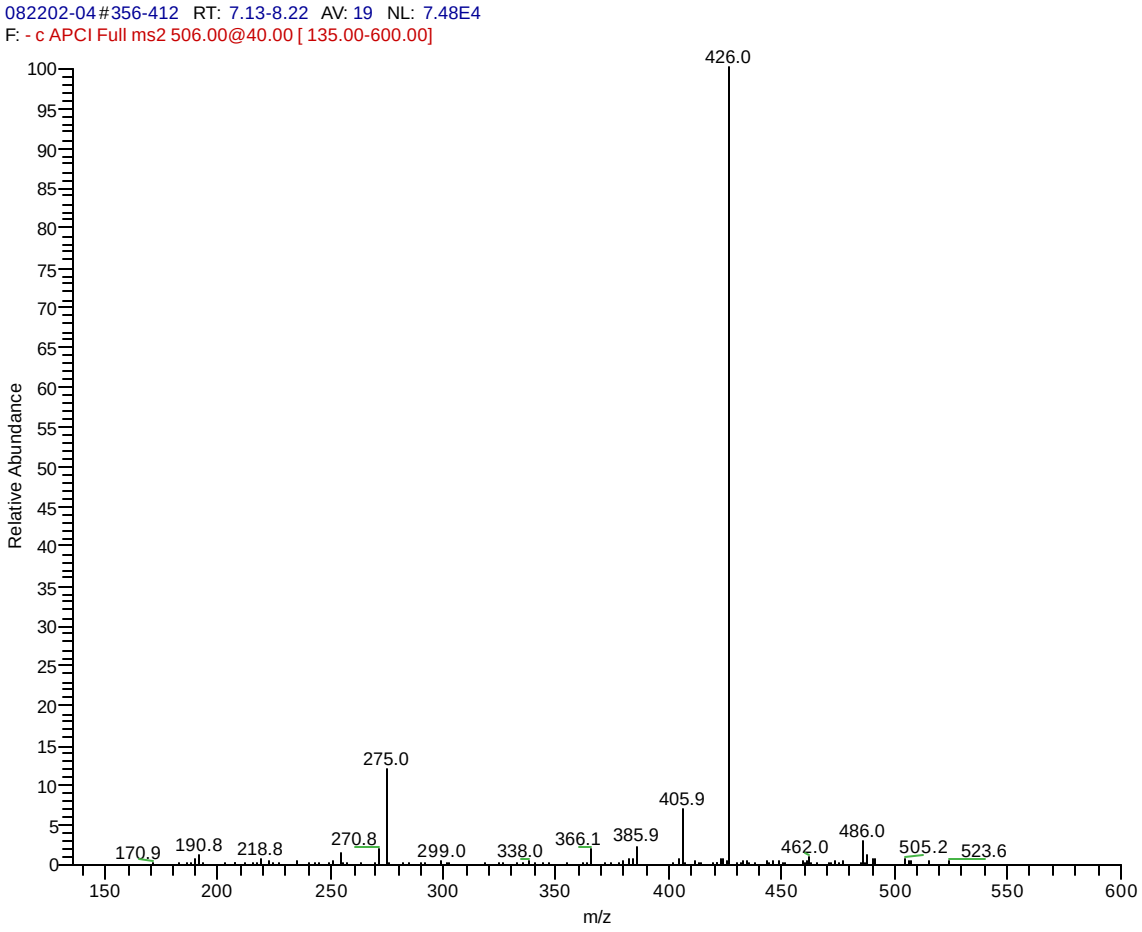

C.12. LC/MS^2 Spectra of Metabolite M4 (m/z 506).

The mass of metabolite M4 corresponds to the sulfation product of the nitro-reduced metabolite (m/z 410). Fragmentation produced daughter ions at m/z 426 and 275. The daughter ion at m/z 426 is form by the loss of 80 Da., which corresponds to the loss of the sulfate moiety (SO_3).

.

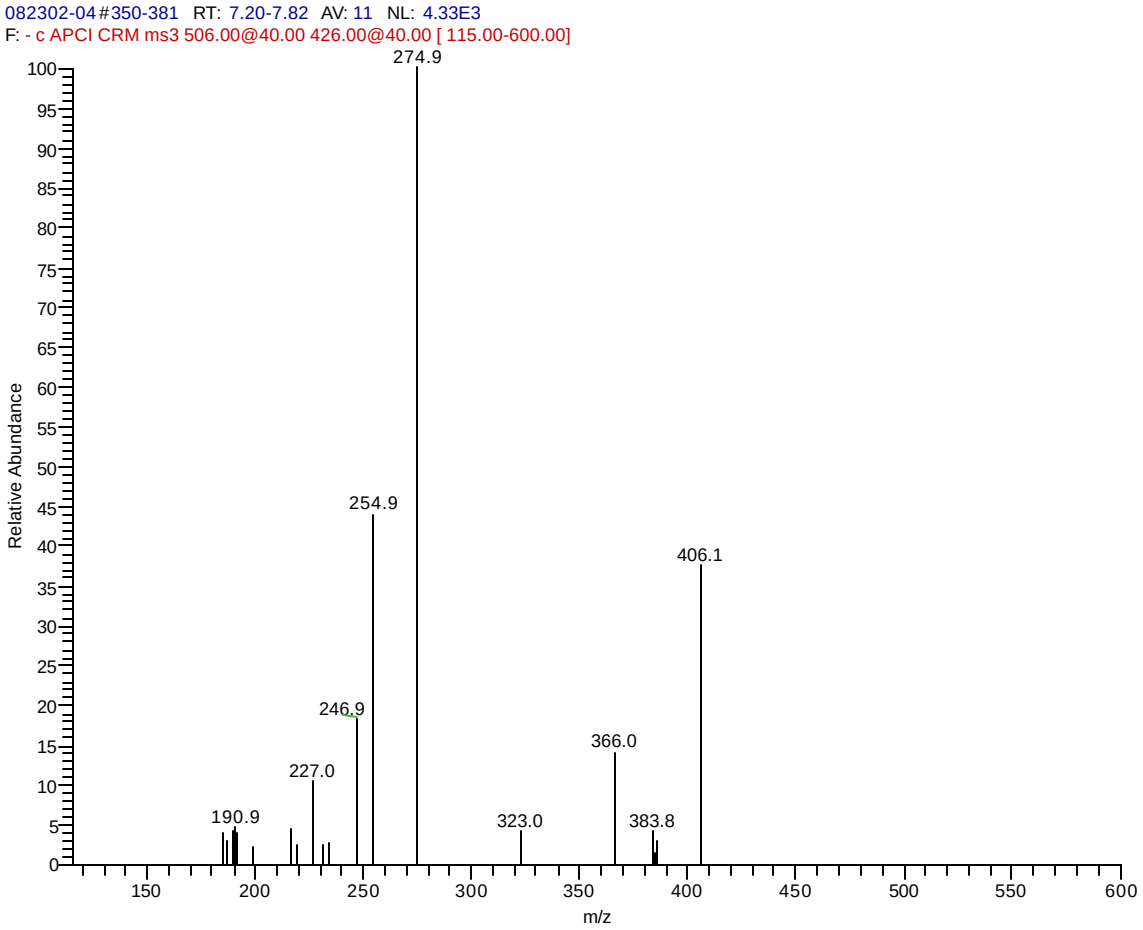

C.13. LC/MS^3 Spectra of Metabolite M4 daughter ion at m/z 426.

Fragmentation of the base peak at m/z 426 produced granddaughter ions at 255, 275, 366, and 406

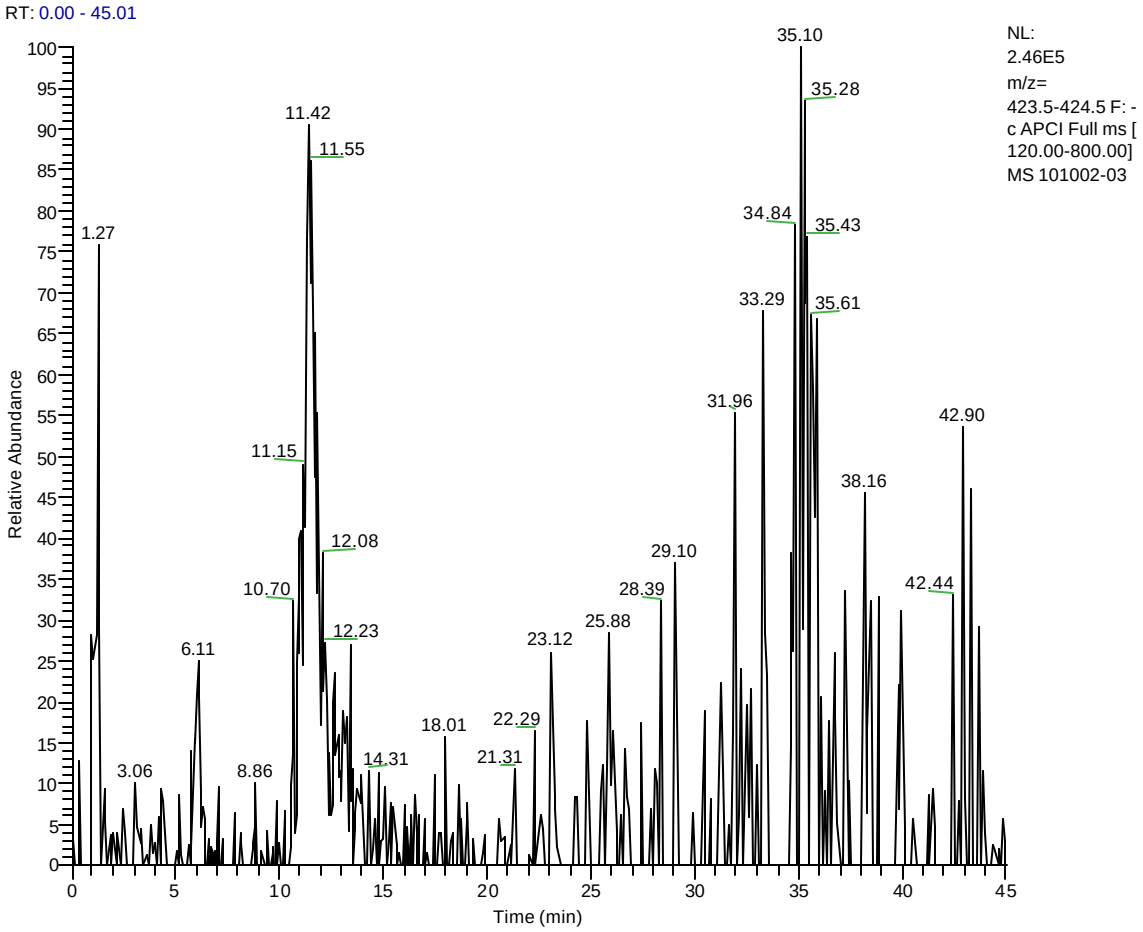

C.14. Chromatograph of metabolite M5.
Dog urine was separated on a reverse phase column and the resulting chromatograph showed the parent drug peak eluting at 11.4 minutes.

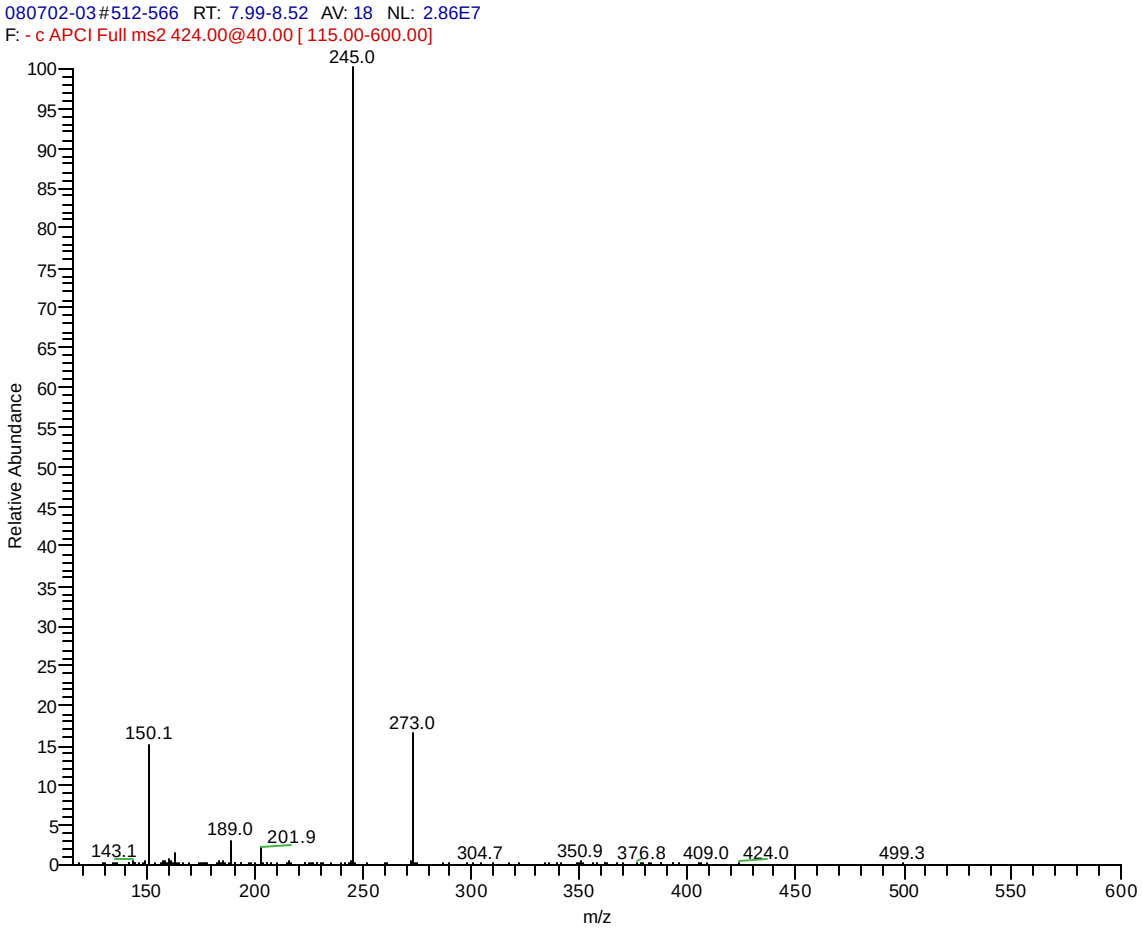

C.15. LC/MS^2 Spectra of Metabolite M5 (m/z 424).

The mass of metabolite M5 corresponds to the loss of an oxygen molecule from the parent compound. Fragmentation of this molecule produced daughter ion at m/z 150, 245, and 273. This shows a decrease f 16 Da. to the daughter ions 289 and 261 found in the parent compound.

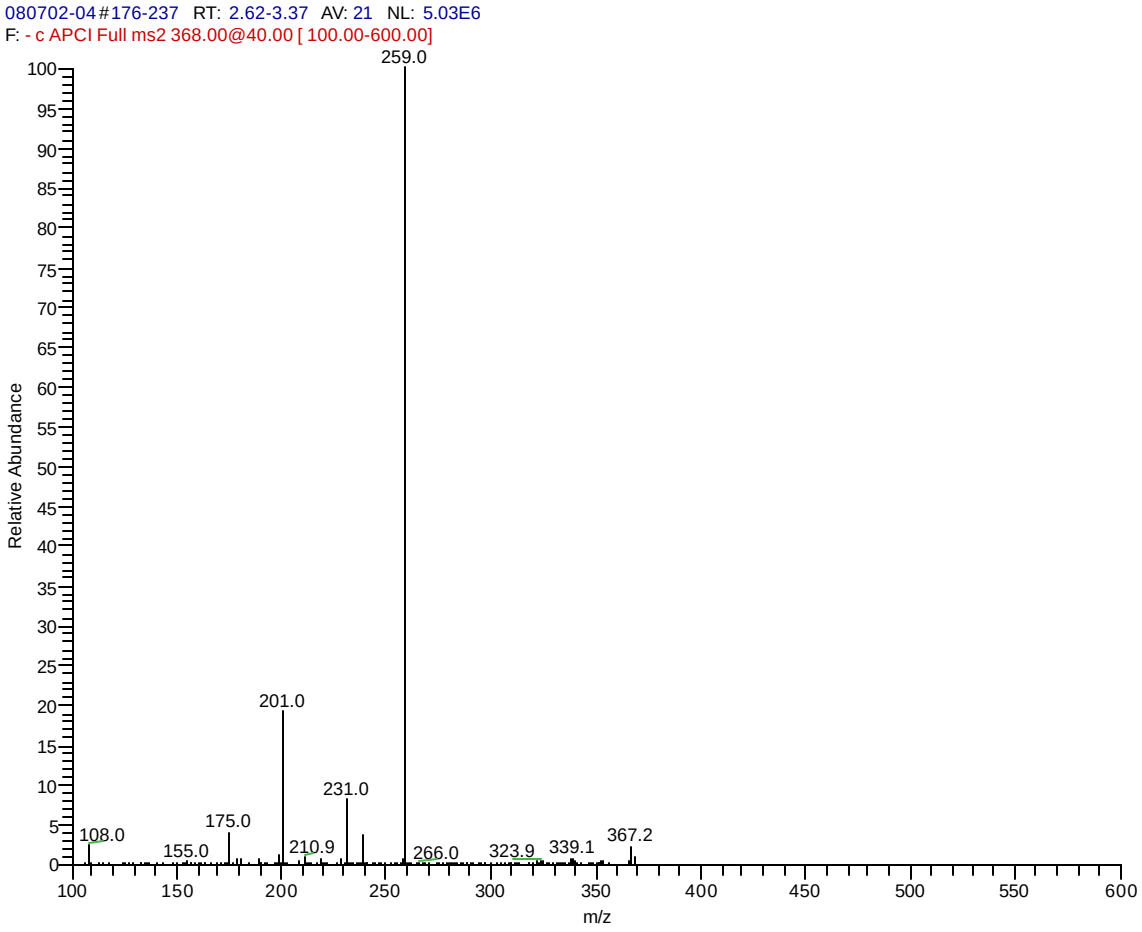

C.16. LC/MS^2 Spectra for Metabolite M6 (m/z 368).

The mass of metabolite M6 corresponds to deacetylation of the amine metabolite (m/z 410). This molecular ion produced daughter ion at m/z 259, 201 and 107. This spectrum shows the decrease of 42 Da. from the daughter ion 150 found in the parent compound. In addition the daughter ion at 259 was also seen in the LC/MS^2 spectra of the amine metabolite.

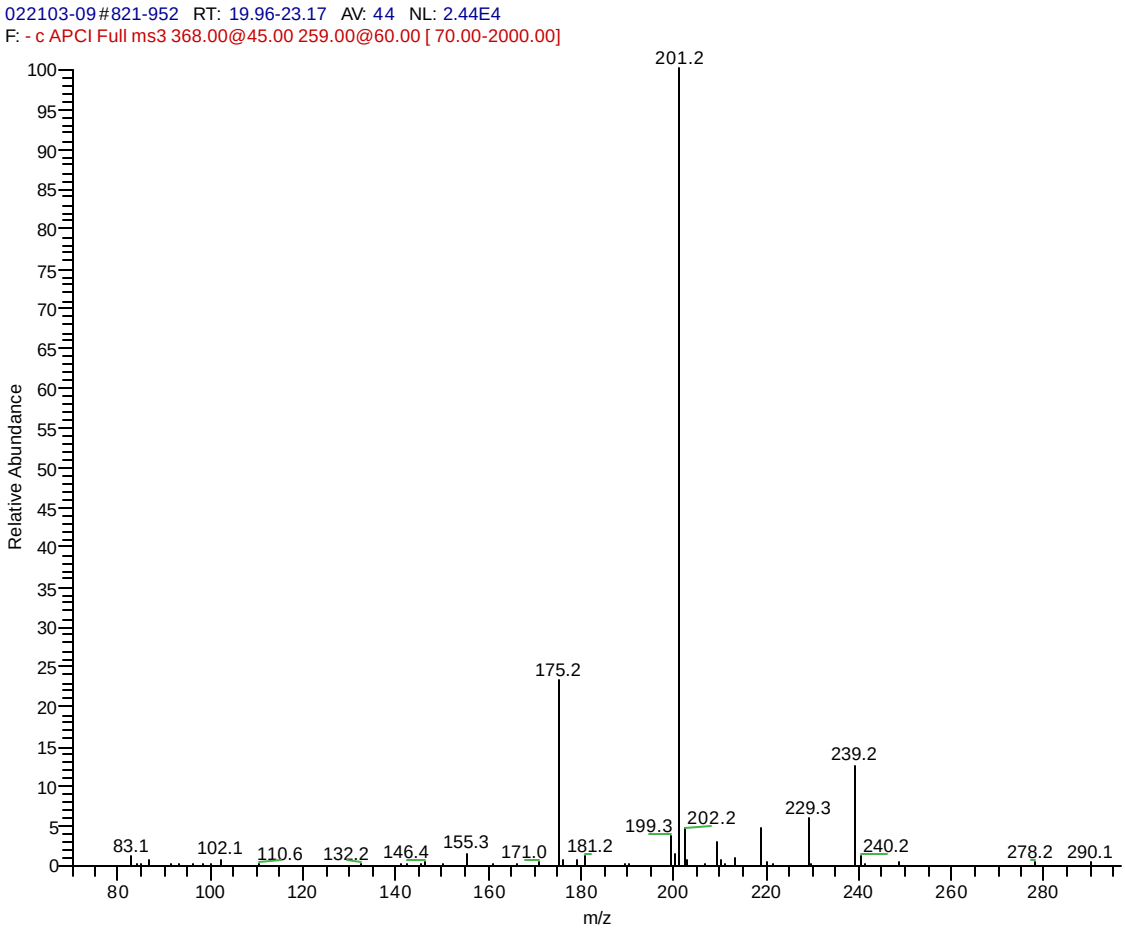

C.17. LC/MS^3 Spectra of Metabolite M6 daughter ion at m/z 386.

The fragmentation of base peak 259 produced the same fragmentation pattern seen with the amine metabolite.

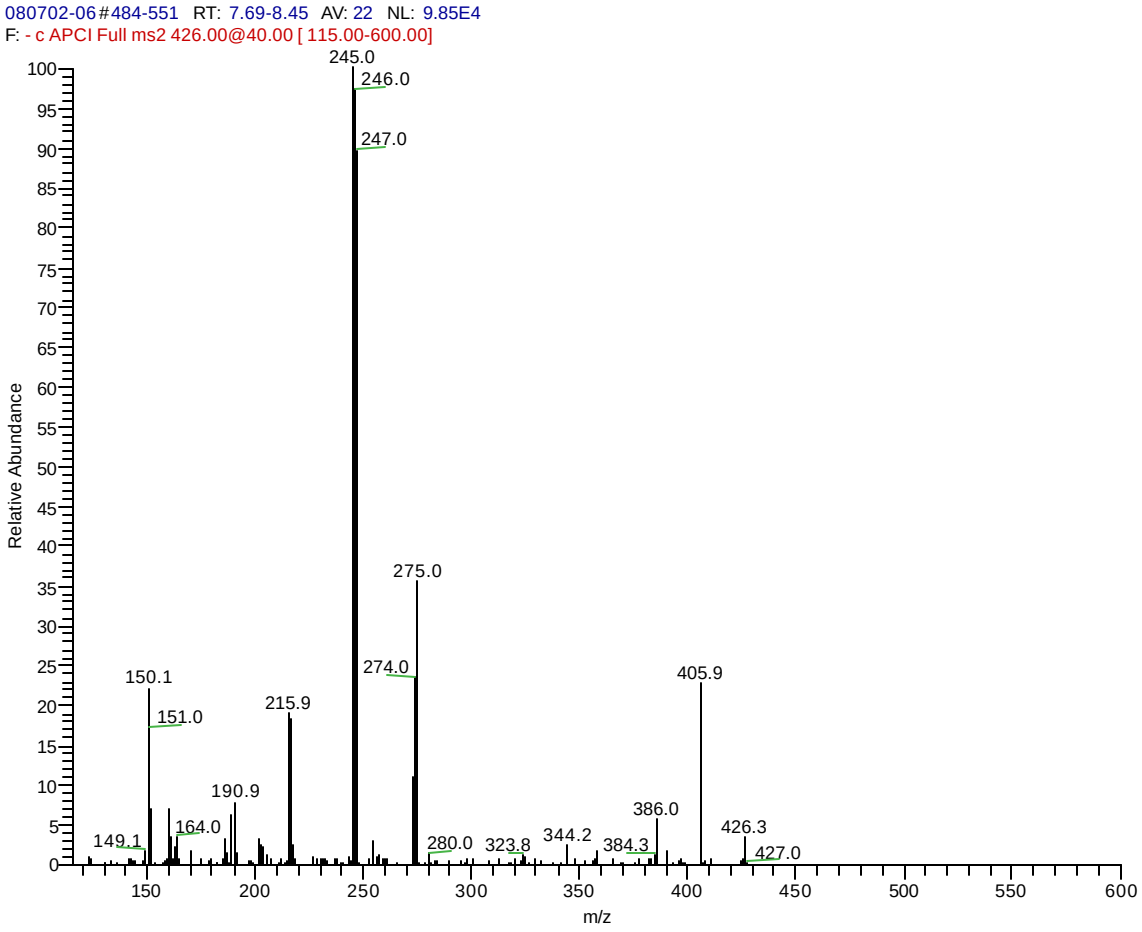

C.18. LC/MS^2 spectra of Metabolite M7 (m/z 426).

The mass of metabolite M7 corresponds to oxidatation of the amine metabolite (m/z 410). This molecular ion produced daughter ion at m/z 150, 245, 275, and 406. This spectrum shows the increase of 16 Da. from the daughter ion 259 found in the spectra of the amine metabolite. In addition the presence of the daughter ion at m/z 150 suggests that no oxidation occurred on the B-ring of the molecule.

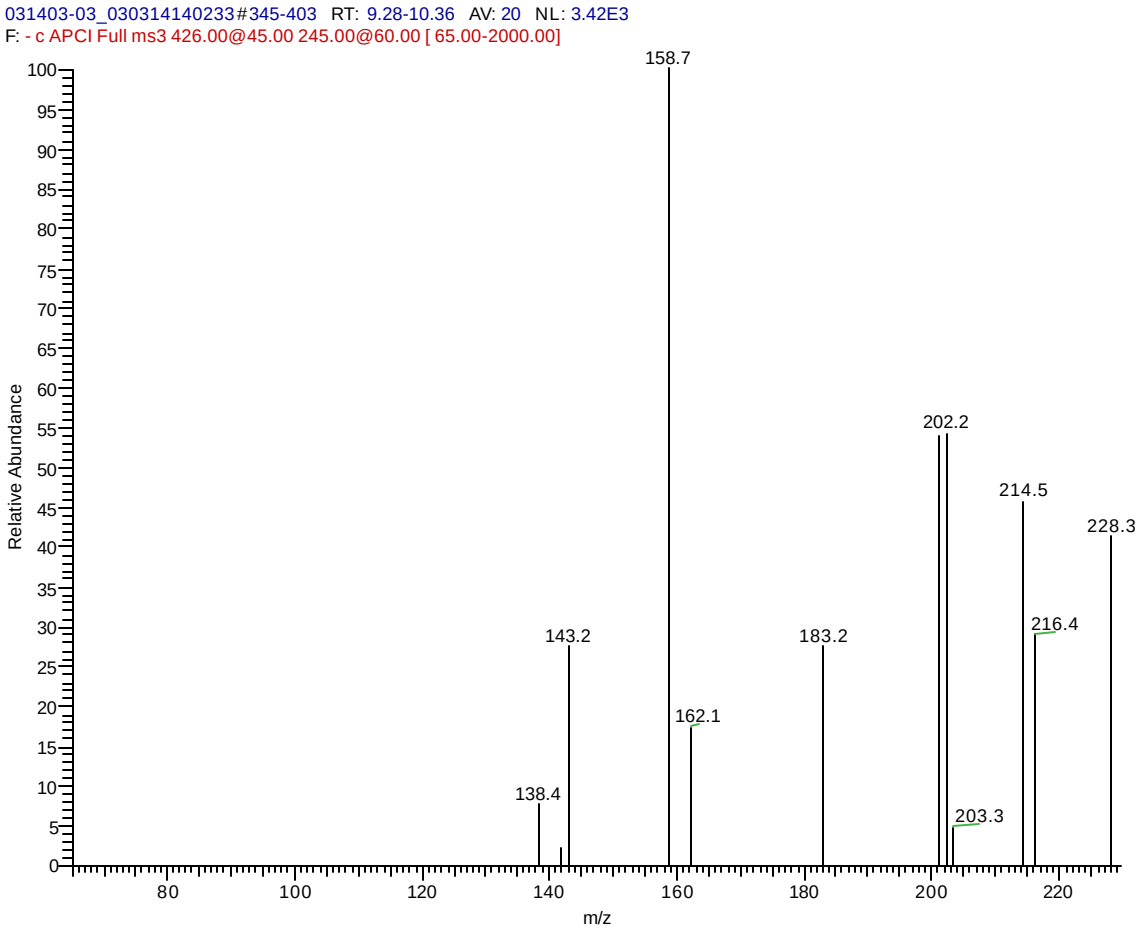

C.19. LC/MS^3 Spectra of Metabolite M7 daughter ion at m/z 245.

The fragmentation of base peak 245 produced the granddaughter ion at m/z 159. This ion was produced by the fragmentation of the hydroxyl group from the amine on the para position of the A ring. These findings suggest that oxidation occurred on the amine group of the A ring.

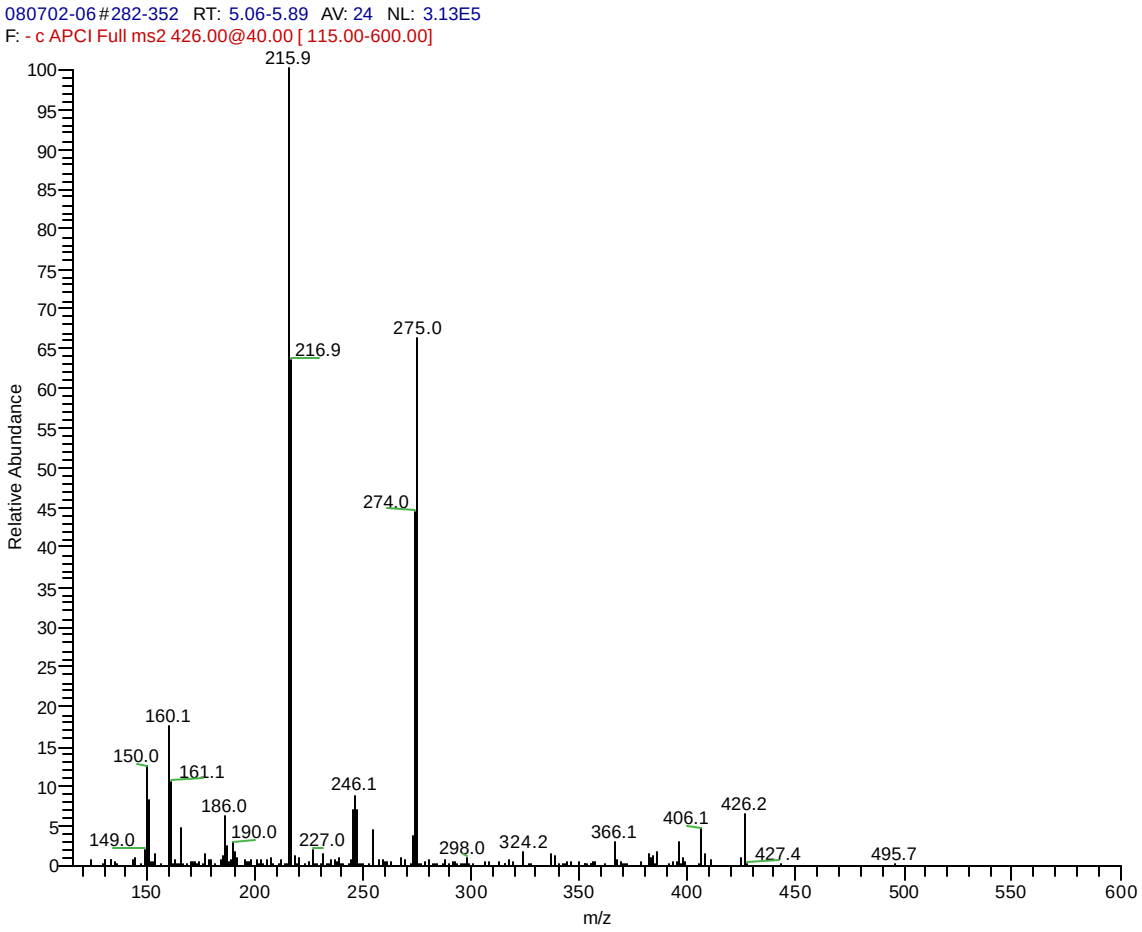

C.20. LC/MS^2 spectra of Metabolite M8 (m/z 426).

The mass of metabolite M8 corresponds to oxidatation of the amine metabolite (m/z 410). This molecular ion produced daughter ion at m/z 160, 215, and 275. This spectra showed the increase of 16 Da. from the daughter ion 259 found in the spectra of the amine metabolite. The presence of a daughter ion at m/z 275 corresponds to the addition of an oxygen molecule at either the aromatic A ring, the amine group at the para-position of the A ring, or the methylene carbon.

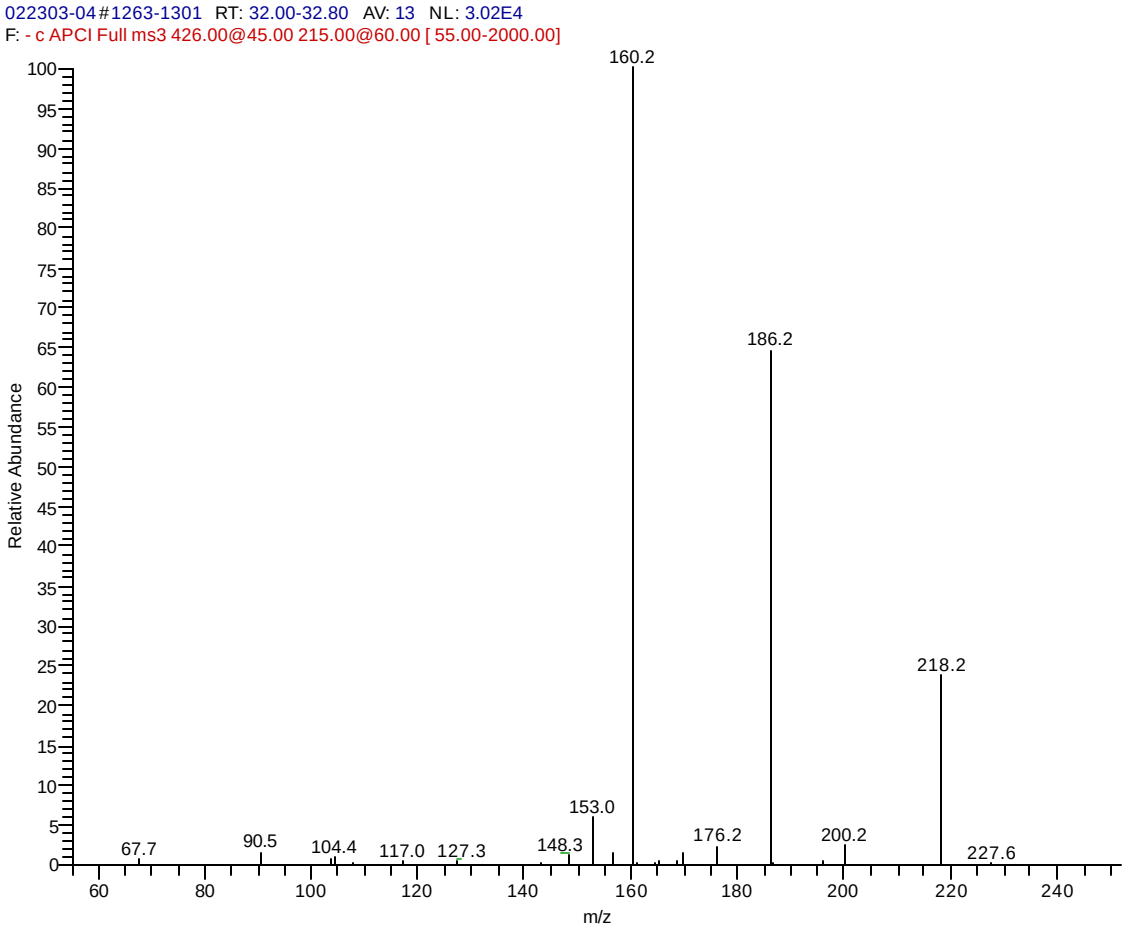

C.21. LC/MS^3 Spectra of Metabolite M8 Daughter Ion at m/z 216.

The fragmentation of base peak 216 produced the granddaughter ion at m/z 160, 186, and 218. The presence of these ions and the absence of their corresponding oxidated ions demonstrates that there was no addition of an oxygen atom to the amine on the on the para-position of the A ring or the A ring itself. Therefore, these findings suggest the oxidation occurred at the methylene carbon.

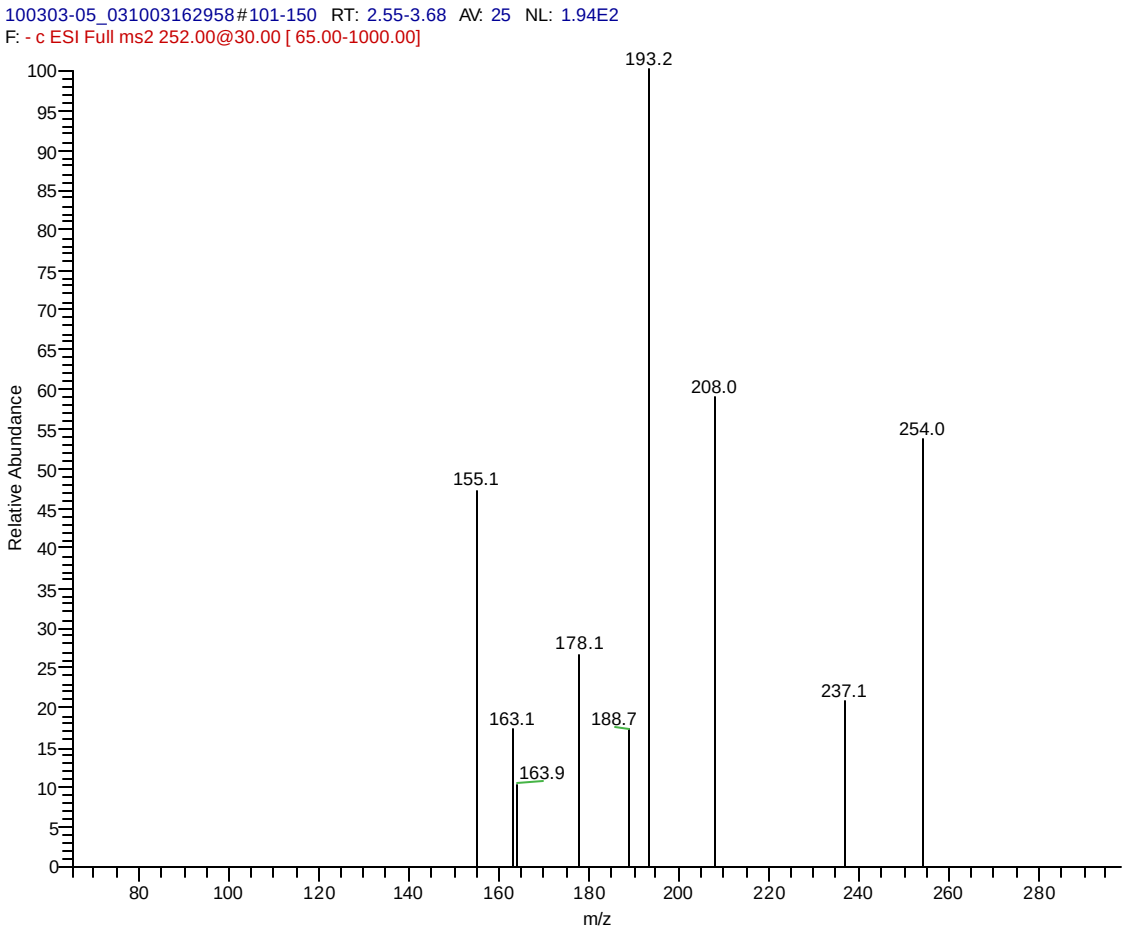

C.22. LC/MS^2 Spectra of Metabolite M9 (m/z 252).

The mass of metabolite M9 corresponds to the hydrolysis of the parent compound, S-4, at the amide bond. Fragmentation of this molecular ion produced daughter ions at m/z 155, 193, and 208.

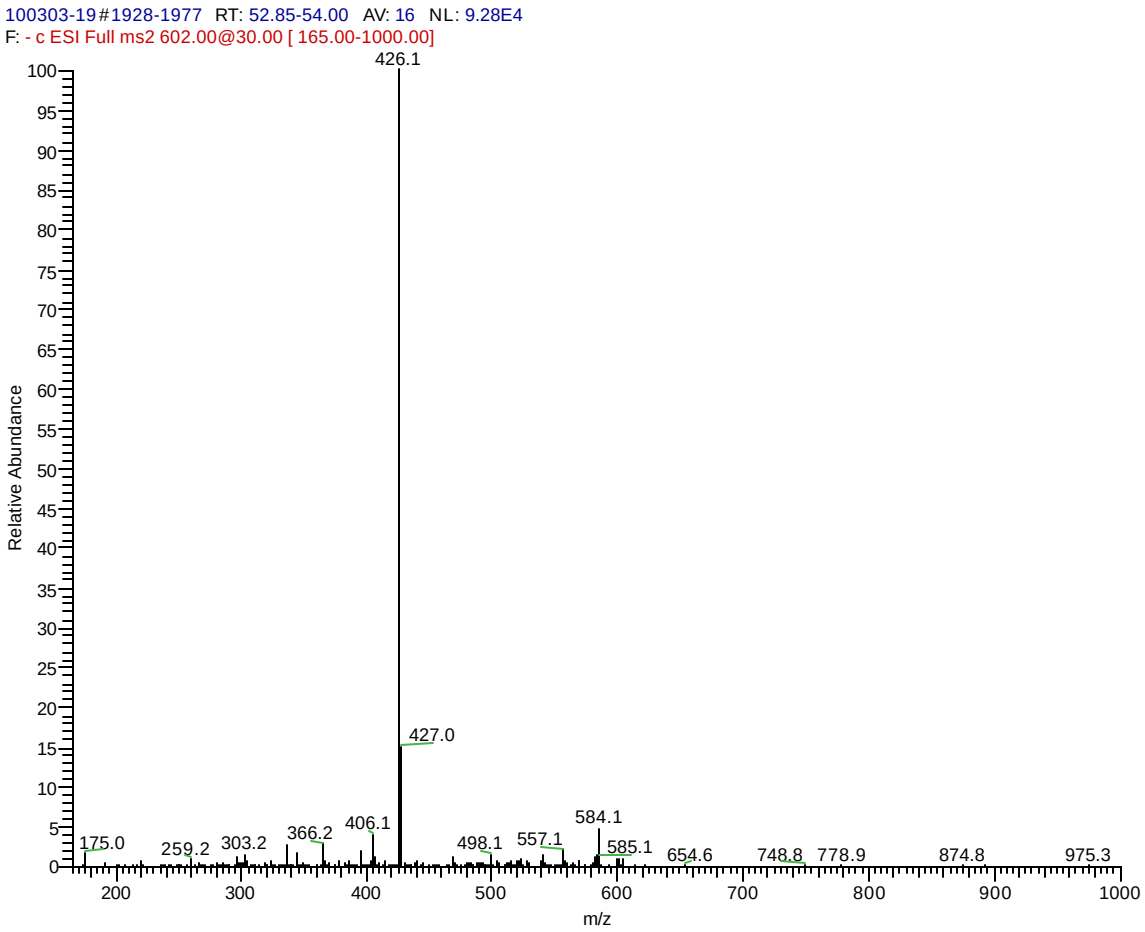

C.23. LC/MS^2 Spectra of Metabolite M10 (m/z 602).

The mass of metabolite M10 corresponded to the glucuronidated hydroxylated amine metabolite. Fragmentation produced the daughter ions at m/z 426, which is produced by the loss of the glucuronide conjugate (176 Da.).

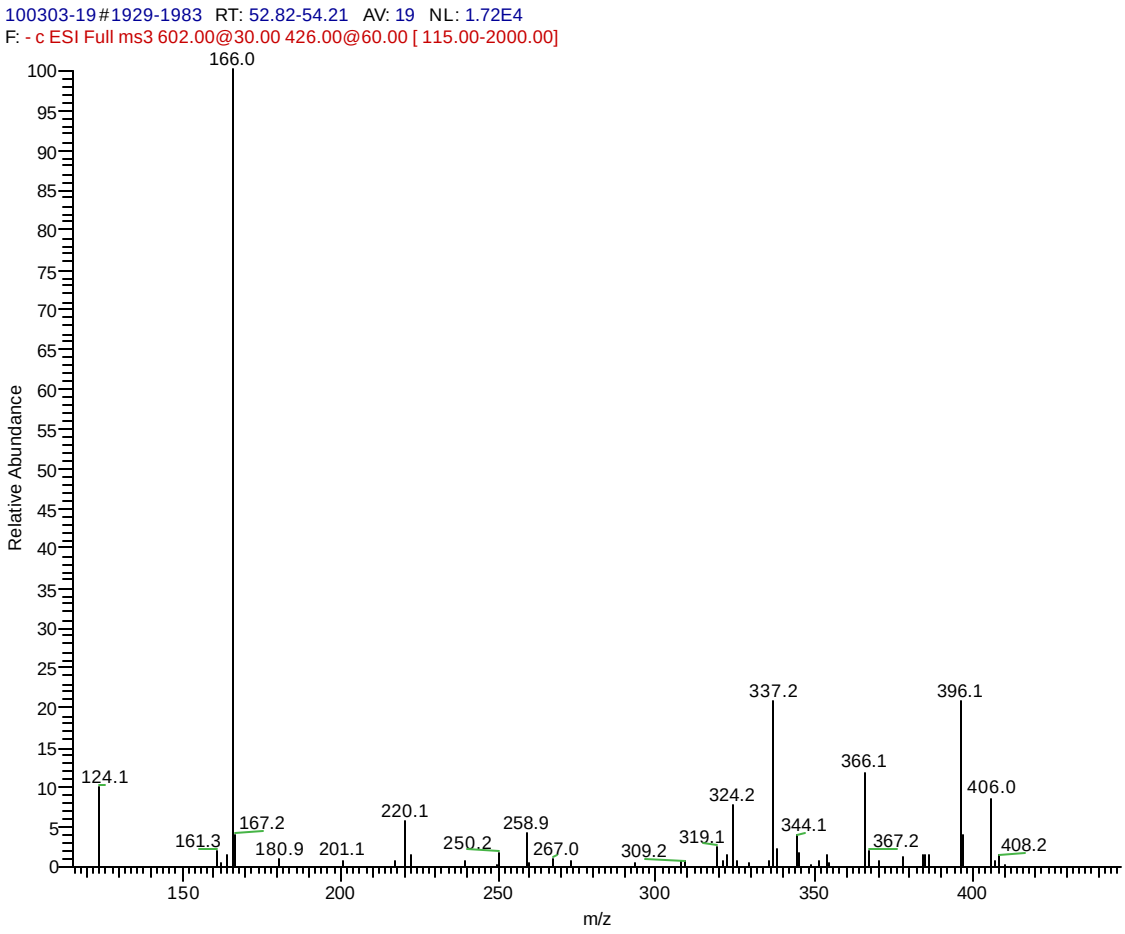

C.24. LC/MS^3 Spectra of Metabolite M10 Daughter Ion at m/z 426.

Fragmentation of the daughter ion at m/z 426 produced granddaughter ions at 166, 337, and 396. The presence of the fragment at m/z 166 (similar to metabolite M3) suggests that the metabolite was hydroxylated and then glucuronidated on the B ring.

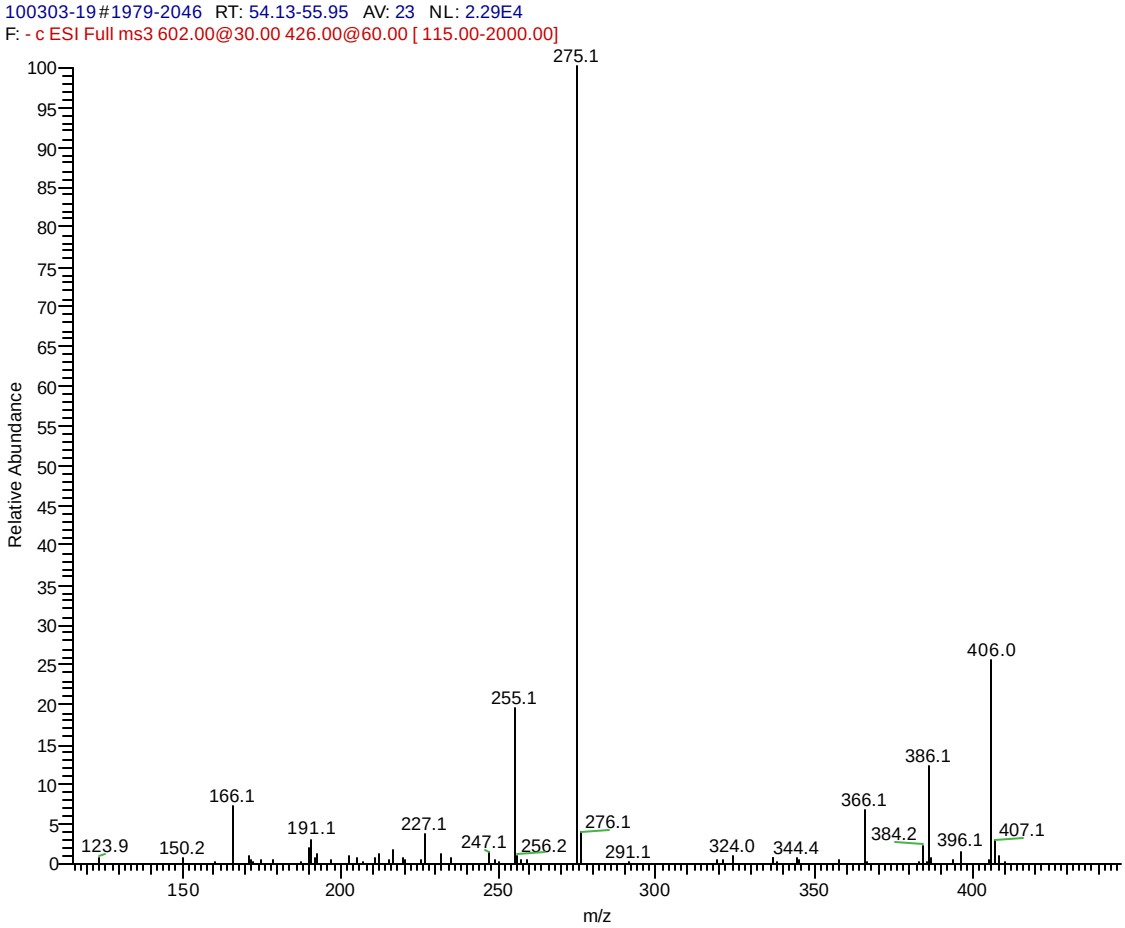

C.25. LC/MS^3 Spectra of Metabolite M11 Daughter ion at m/z 426.

Fragmentation of the second peak produced granddaughter fragments at m/z 255, 275, and 406. The presence of the fragment at m/z 275 suggests that the metabolite was hydroxylated and then glucuronidated on either the A ring, of the amine on the para position of the A ring. The fragmentation pattern was similar to that of metabolite M7.

Sample	DPM in Sample	% of Injected Dose
Liver	4285486	3.25
Intestines	11690121	8.88
Kidney	18197	0.014
Pancreas	60540	0.046
Muscle	60	0.00004
Heart	33112	0.025
Intestinal Content	10651136	8.09
Spleen	1101	0.0008
0-8 hr Feces	525367	0.40
8-24 hr Feces	46358623	35.2
0-8 hr Urine	16887732	12.82
8-24 hr Urine	36995976	28.09

Table C.26. Final Disposition of [C^{14}]S-4 in Rats after 24 hours.
Total radioactivity of selected organs, feces and urine sample were determined by liquid scintillation counting. Approximately 97% of the injected dose was recovered.

Sample	DPM in Sample	% of Injected Dose
Heart	11782	0.008
Muscle	1020	0.0007
Spleen	15678	0.011
Pancreas	8184	0.006
Intestines	966112	0.70
Liver	2258339	1.63
Kidney	66182	0.05
Prostate	2195	0.002
Stomach Wall	48691	0.035
Fat	10073	0.007
Stomach Content	2307571	1.66
Intestinal Content	8212016	5.92
0-8 hr Feces	118204	0.09
8-24 hr Feces	42798292	30.85
24-48 hr Feces	8458155	6.10
0-8 hr Urine	7189691	5.18
8-24 hr Urine	29056378	20.94
24-48 hr Urine	13312800	9.60

Table C.27. Final Disposition of [C^{14}]S-4 in Rats after 48 hours.
Total radioactivity of selected organs, feces and urine sample were determined by liquid scintillation counting. Approximately 83% of the injected dose was recovered

Time (min)	DPM
1	42.31
3	70.44
5	28705.93
7	312.75
9	145.1
11	66.51
13	61.92
15	48.95
17	43.48
19	40.48
21	31.89
23	36.42
25	36.37
27	44.57
29	81.17
31	98.34
33	136.27
35	131.92
37	128.27
39	218.35
41	394.7
43	654.16
45	1369.47
47	5250.09
49	3855.1
51	80.81
53	50.59
55	54.06
57	41.83
59	35.19
61	38.39
63	35.17
65	35.39
67	32.81
69	35.55
71	32.12

Table C.28. Radioactive Fraction Collection in 24 Hour Urine Samples of Rats. Fractions were collected every 2 minutes and the radioactivity determine by liquid scintillation counting.

Time (min)	DPM
1	30.69
3	52.94
5	176.41
7	670.25
9	151.5
11	75.21
13	269.28
15	607.39
17	238.46
19	231.31
21	184.85
23	151.03
25	71.82
27	339.74
29	534.94
31	395.34
33	219.97
35	201.34
37	222.34
39	351.37
41	539.55
43	4273.12
45	711.17
47	751.41
49	1082.35
51	17216.23
53	449.51
55	146.11
57	76.69
59	61.5
61	62.76
63	66.19
65	61.69
67	48.19
69	43.64
71	41.5

Table C.29. Radioactive Fraction Collection in 24 Hour Aqueous Fecal Samples of Rats. Fractions were collected every 2 minutes and the radioactivity determine by liquid scintillation counting.

Time (min)	DPM
1	31.4
3	63.43
5	269.75
7	130.51
9	356.93
11	224.85
13	95.9
15	67.88
17	59.35
19	47.7
21	47.27
23	41.64
25	42.13
27	57.15
29	100.67
31	120.42
33	158.07
35	129.01
37	166.08
39	213.86
41	2828.83
43	223.08
45	219.32
47	297.26
49	478.05
51	3561.62
53	28992.93
55	1456.03
57	593.35
59	334.88
61	154.37
63	91.71
65	67.55
67	52.11
69	49.04
71	52.06

Table C.30. Radioactive Fraction Collection in 24 Hour Organic Fecal Samples of Rats. Fractions were collected every 2 minutes and the radioactivity determine by liquid scintillation counting.